

Cryopreservation of mesenchymal stromal cells within tissue engineering approaches

**A thesis submitted for the degree of
Doctor of Natural Sciences (Dr. rer. nat.)**

in the subject of *Cryotechnology*

by

Vitalii Mutsenko, M.Sc. Biochemistry

December 2018

**Hannover Medical School
International PhD Program ‘Regenerative Sciences’
in Hannover Biomedical Research School (HBRS)**

Institute for Multiphase Processes,

Leibniz University Hannover

Acknowledged by the PhD committee and head of Hannover Medical School

President:	Prof. Dr. Christopher Baum (until 31 st December 2018) Prof. Dr. Michael Manns (as of 1st January 2019)
Supervisors:	Prof. Prof. h. c. Dr.-Ing. Birgit Glasmacher, M.Sc., Dr. Oleksandr Gryshkov, Institute for Multiphase Processes, Leibniz University Hannover, Germany
Co-Supervisors:	Prof. Dr.rer.nat. Thomas Illig, Hannover Unified Biobank, Hannover Medical School, Germany Prof. Dr.-Ing. Stephan Kabelac, Institute for Thermodynamics, Leibniz University Hannover, Germany
External expert:	Prof. Dr. Barry Fuller, Department of Surgical Biotechnology Faculty of Medical Sciences University College London, United Kingdom
Internal expert:	Prof. Dr. Boris Chichkov, Institute of Quantum Optics, Leibniz University Hannover, Germany
Day of public defence:	25 th January 2019

PhD project funded by:

The Federal Ministry of Education and Research as well as the Deutsche Forschungsgemeinschaft (DFG, German Research Foundation) for the Cluster of Excellence REBIRTH (EXC 62/3 valid until Dec 2017, EXC 62/4 valid until Oct 2019).

IP@Leibniz of Leibniz University Hannover promoted by the German Academic Exchange Service (DAAD) during the study - project code 57156199.

Contents

Contents.....	i
Abbreviations.....	iv
List of Figures and Tables	vi
Abstract.....	viii
1. Introduction	1
1.1. Basic principles of cryopreservation.....	1
1.1.1. Cryoprotective agents	1
1.1.2. Slow freezing and vitrification.....	2
1.2. Challenges in cryopreservation of multidimensional structures	4
1.2.1. Cryopreservation of cell monolayers and 2D tissue-engineered constructs	5
1.2.2. Challenges in cryopreservation of 3D TEPs	8
1.2.3. State of the art in TEPs' cryopreservation	9
1.3. Sugars as alternatives to DMSO and electroporation as a method for sugar delivery.....	13
1.3.1. Application of sugars as non-toxic CPAs	15
1.3.2. Methods of sugar delivery through cell membrane	16
1.3.3. Electroporation of cells for sugar delivery.....	17
1.4. Aims and the outline of the study	18
2. Materials and methods.....	20
2.1. Chemicals.....	20
2.2. Cell culture.....	20
2.2.1. Cells	20
2.2.2. General cell culture	20
2.2.3. Culture of cells on cover slips for cryomicroscopy	21
2.2.4. Seeding of cells onto scaffolds.....	21
2.3. Cell manipulation and analysis	21
2.3.1. Electroporation for permeabilization and recovery assays	21
2.3.2. Assessment of post-thaw survival of cells loaded with sugars after electroporation	23
2.3.3. Visualization of Lucifer Yellow uptake in suspension cells.....	24
2.3.4. Resazurin reduction test.....	25
2.3.5. Visualization of Lucifer Yellow uptake in adherent cells.....	26

2.3.6. Cell volume measurements	26
2.3.7. Stereomicroscopy and scanning electron microscopy of scaffolds	26
2.3.8. Cytoskeleton integrity	27
2.3.9. Viability assay of cells seeded in scaffolds	27
2.4. Scaffold preparation	28
2.5. Cryopreservation of cells and scaffolds	28
2.5.1. Cryopreservation of scaffolds using conventional protocol	28
2.5.2. Cryopreservation of cells after electroporation	29
2.5.3. Cryopreservation of scaffolds using modified protocol	29
2.6. Cryomicroscopy	30
2.6.1. Freezing and thawing behavior of adherent cells	30
2.6.2. Evaluation of scaffolds using cryomicroscopy	31
2.6.3. Influence of sugars on recrystallization behavior	31
2.7. Evaluation of physico-chemical and mechanical properties of scaffolds after modified cryopreservation	31
2.7.1. Raman microscopy	32
2.7.2. Fourier transform infrared spectroscopy	32
2.7.3. Biomechanical testing	33
2.7.4. Mercury intrusion porosimetry	33
2.7.5. Swelling test	34
2.7.6. Differential scanning calorimetry	34
2.7.7. Determination of thawing rate	35
2.7.8. Osmolality measurements	35
2.8. Western blotting	36
2.9. Statistics	36
3. Results	38
3.1. Cryopreservation of <i>cj</i> MSCs on 2D carriers and the effect of sucrose	38
3.1.1. The effect of sucrose loading on cell viability, attachment and response to hyperosmolar stress	38
3.1.2. The effect of combined application of intra- and extracellular sucrose on DMSO- based cryopreservation of <i>cj</i> MSCs in adherent state	45
3.2. Effect of freezing on cells seeded onto 3D collagen-HAP scaffolds	48
3.2.1. Appearance and cytocompatibility of collagen-HAP scaffolds	48
3.2.2. Conventional cryopreservation of 3D collagen-HAP scaffolds seeded with <i>cj</i> MSCs	49

3.2.3. Effect of freezing on ice formation and its impact on the collagen-HAP scaffolds	50
3.2.4. Impact of modified cryopreservation on physico-chemical and mechanical properties of cell-free scaffolds.....	51
3.2.5. Impact of modified cryopreservation on viability of <i>cj</i> MSCs frozen in 3D scaffolds	58
3.2.6. Comparison of recrystallization behavior of DMSO vs. DMSO with sucrose...	60
3.3. Effect of cell electroporation with sugars on cryopreservation outcome.....	61
3.3.1. Evaluation of cell permeabilization and recovery.....	61
3.3.2. Evaluation of electroporation-assisted cryopreservation on post-thaw cell survival.....	64
3.4. Evaluation of some physical properties of sugar-containing electroporation buffers relevant to cryopreservation.....	69
3.4.1. Determination of glass transition and melting temperatures in electroporation buffers used for cryopreservation	69
3.4.2. Ice formation and recrystallization behavior	70
4. Discussion.....	73
4.1. Cryopreservation of cells on 2D carriers and the effect of sucrose on <i>cj</i> MSCs	73
4.2. Effect freezing on cells seeded into collagen-HAP scaffolds	79
4.3. Evaluation of electroporation for the delivery of cell impermeable sugars and their effect on cryopreservation outcome	89
5. Summary	94
6. Outlook.....	97
6.1. Sucrose, antifreeze proteins and directional freezing as means to improve the cryopreservation outcome of adherent cells.....	97
6.2. Optimization and further characterization of ‘in air’ freezing and translation to other TEPs and cell types	98
6.3. Electroporation of stem cells in TEPs to establish their DMSO- and serum-free cryopreservation.....	100
7. References	102
Acknowledgments.....	116
List of own publications.....	117
Curriculum Vitae	120
Statement of Contribution.....	123
Declaration	125

Abbreviations

Symbol	Description
2D	two-dimensional
3D	three-dimensional
ANOVA	Analysis of variance
CAC	cacodylate buffer
<i>cj</i> MSCs	<i>Callithrix jacchus</i> mesenchymal stromal cells
CPA(s)	cryoprotective agent(s)
dimethyl sulfoxide	DMSO
DMEM	Dulbecco's modified eagle medium
DSC	differential scanning calorimetry
EDC	N-(3-dime-thylaminopropyl)-N-ethylcarbodiimide hydrochloride
EDTA	trypsin-ethylenediaminetetraacetic acid
EF2	elongation factor
Ethidium Homodimer-1	EthD-1
European Medicines Agency	EMA
FACS	Fluorescence-activated cell sorting
FBS	fetal bovine serum
Food and Drug Administration	FDA
FTIR	Fourier transform infrared spectrometer
GMP	Good Manufacturing Practice
HAP	hydroxyapatite
HES	hydroxyethyl starch
hESCs	human embryonic stem cells
HMDS	hexamethyldisilazane
hMSCs	human mesenchymal stromal cells
Hoechst	bisbenzimidazole H 33342 trihydrochloride
hUCMSCs	human umbilical cord mesenchymal stem cells

IBPs	ice-binding proteins
IIF	intracellular ice formation
iPSCs	induced pluripotent stem cells
IQR	interquartile range
IRI	ice recrystallization inhibition
LY	Lucifer Yellow
MAPK-kinase	mitogen-activated protein kinase
PBS	phosphate-buffered saline
PI	propidium iodide
PVP	polyvinylpyrrolidone
SD	standard deviation
SDS	sodium dodecyl sulfate
SEM	scanning electron microscopy
TE	tissue-engineered
TEPs	tissue-engineered products

List of Figures and Tables

Figure 1.1 Physical events and cryoinjury of cells during freezing and thawing.	4
Figure 1.2 Methods for delivery of trehalose into mammalian cells.....	7
Figure 2.1 Electroporation set up used for the controlled electroporation of hUCMSCs with sugars.....	23
Figure 2.2 Representative photo of the electrodes used in this work.....	25
Figure 2.3 Schematic of conventional and modified freezing-thawing procedures.....	30
Figure 3.1 Influence of 24 h incubation with different sucrose concentration on cell viability.....	39
Figure 3.2 Influence of sucrose concentration on cell morphology	40
Figure 3.3 Influence of 24 h incubation with sucrose on cytoskeleton	41
Figure 3.4 Effect of invertase on sucrosomes	41
Figure 3.5 Impact of LY and sucrose on sucrosome formation	42
Figure 3.6 Effect of pretreatment on IIF	43
Figure 3.7 Volumetric change in <i>cj</i> MSCs when they were loaded with 100 mM sucrose	44
Figure 3.8 Western blot of phosphorylated form of MAPK p38	44
Figure 3.9 Impact of sucrose containing medium on adherent cell cryopreservation.....	46
Figure 3.10 Analysis of ice formation in adherent cells.....	47
Figure 3.11 Size and structure of collagen-HAP scaffolds	48
Figure 3.12 Attachment and spreading cells within 3D scaffolds.....	49
Figure 3.13 Effect of conventional cryopreservation on scaffolds and cells	50
Figure 3.14 Cryomicroscopic analysis of scaffolds during freezing and isothermal annealing	51
Figure 3.15 Raman analysis of scaffolds frozen vs. fresh	52
Figure 3.16 FTIR profiles of collagen-HAP scaffolds before and after cryopreservation.....	53
Figure 3.17 Mechanical properties of scaffolds before and after cryopreservation.....	54
Figure 3.18 Representative pore size distribution plots	55
Figure 3.19 Specific heat capacity for collagen-HAP scaffolds with and without CPAs.....	56
Figure 3.20 Representative warming curves for conventional and modified thawing.....	57
Figure 3.21 Attachment and spreading of MSCs after cryopreservation	58
Figure 3.22 Live dead staining of cells in collagen -HAP scaffolds after cryopreservation...	59
Figure 3.23 Quantitative assessment of post-thaw cryopreservation outcome	60
Figure 3.24 Cryomicroscopic pictures illustrating the impact of sucrose on recrystallization of DMSO solution	61

Figure 3.25 Viability and efficiency of PI uptake during electroporation	63
Figure 3.26 Influence of electrical field and sugar type on cell morphology	64
Figure 3.27 Post thaw viability of hUCMSCs using different sugar concentrations	65
Figure 3.28 Detection of electroporation of hUCMSCs by Lucifer Yellow uptake	66
Figure 3.29 Post thaw viability of hUCMSCs after cryopreservation for loaded or non-loaded cells	68
Figure 3.30 Morphology of cells 24h after cryopreservation using either sugars or DMSO compared to non-cryopreserved cells.....	69
Figure 3.31 Thermogram of different sugars analyzed with DSC	70
Figure 3.32 Cryomicroscopic analysis of ice crystal growth using cryomicroscopy.....	72
Figure 6.1 Results on design and cryopreservation of PCL200/PLA100 electrospun fiber mats seeded with HeLa cells.....	98
Figure 6.2 Results on translation of modified protocol to cryopreservation of tissue-like structures formed by <i>cj</i> MSCs within coaxial alginate beads.	99
Figure 6.3 Still frame from a thermal video recorded by μ -Thermalyzer software.	100
Figure 6.4 Electrode assembly for electroporation of electrospun fiber mats (A).	101
Table 1.1 Short summary on the current success in the cryopreservation of TEPs.	9
Table 1.2 Short summary on the application of sugars to decrease DMSO concentration.	16
Table 2.1 The molar extinction coefficients for resazurin.....	26
Table 3.1 Osmolality of freezing solutions containing 10% DMSO/20% FBS supplemented with 0-500 mM sucrose.....	47
Table 3.2 Raman spectral assignments for collagen and HAP.....	52
Table 3.3 Summary with representative values used to characterize pore size distribution. ..	54
Table 3.4 Thawing rates and time intervals determined for conventional and modified cryopreservation.	57
Table 3.5 Characteristics of hyperosmolar buffers and results after electroporation.....	67
Table 3.6 Characteristics of hyperosmolar buffers and results after electroporation.....	70
Table 3.7 Mean projected area of ice crystals during isothermal annealing.	72

Abstract

The role of cryopreservation in the improvement of quality of life of human beings is undisputable because of remarkable progress in long-term storage of diverse cells and tissues in biobanks around the world. This is dictated by a need for immediate availability of clinically relevant cells and tissues for the use in assisted reproductive technology, regenerative and transfusion medicine. The further advancements in the field are linked with improvements of safety, storage logistics and shipment services where in addition to cells frozen in suspension, successful cryopreservation of cells in adherent state would have significant commercial benefits associated with the ‘ready-to-use’ delivery of cell products on demand. The latter still remains elusive today due to high susceptibility of adherent cells to osmotic stress and toxicity of cryoprotective agents augmented by massive cryodamage and detachment dictated by their firm fixation to the substrate. Conventional slow-freezing using dimethyl sulfoxide (DMSO) and thawing in a water bath developed for suspended cells do not provide sufficient protection of stem cells frozen on two-dimensional (2D) or three-dimensional (3D) substrates. Therefore, the first part of the current thesis work deals with the development of cryopreservation strategy for long term storage of stem cells in adherent state. This was first studied on 2D model (cell monolayer frozen on glass coverslips) using combined pre-freeze treatment of cells with sucrose and its addition to DMSO-based freezing solution. The optimal combination was further transferred to 3D model (cells frozen on porous collagen-hydroxyapatite (HAP) scaffolds) and was enhanced by implementing of ‘in air’ freezing and modified thawing approaches. The highest cell viability achieved for cells frozen in 3D scaffolds was around 80%.

The motivation for the second part of the thesis’ work was dictated by current considerations in regenerative medicine towards DMSO- and serum-free biopreservation in GMP-compliant manufacturing of cells and tissue-engineered products (TEPs). This was studied on cell suspension to establish biopreservation of stem cells using electroporation-assisted intracellular delivery of sugars. The maximum cell viability achieved using electroporation of cells with sucrose, trehalose and raffinose was also around 80% but in this case without any DMSO and xenogenic serum.

Thus, this methodological work successfully addressed several cryobiological challenges and envisages the translation of the latter electroporation-based approach to DMSO- and serum-

free biopreservation of ‘ready-to-use’ TEPs to provide their off-the-shelf availability for research and clinical applications.

1. Introduction

1.1. Basic principles of cryopreservation

Cryopreservation is a technological process directed towards ensuring stable long-term storage of cells, tissues, organs or artificial TEPs and genetic biodiversity. It comprises a number of steps such as equilibration with a cryoprotective agent (CPA), freezing using temperature control equipment, subsequent storage at cryogenic temperatures and warming of a biospecimen before application in a clinical practice (for review see Jang et al., 2017).

Cryopreservation considerably increases the potential shelf-life of biomaterials because metabolic processes at cryogenic temperatures are suspended. Living cells are only stable and functional in a narrow temperature and hydration range. According to classical two-factor hypothesis developed by Peter Mazur, at high cooling rates, losses in cell viability can be attributed to intracellular ice formation (IIF), whereas at low cooling rates, cells are subject to excessive dehydration and cryodamage resulting from ‘solution effects’ (Mazur et al., 1972). Typically, there is a critical cooling rate where damage due to IIF and solution effects injury is minimal and survival is maximal (Mazur, 1984). This optimal cooling rate varies greatly depending upon the cell type and is related to the cell’s membrane permeability to water and cryoprotective agent. Extracellular ice formation results in an increase of the solute concentration in the non-frozen water fraction surrounding the cells causing cells to dehydrate. The extent and rate of freezing-induced dehydration is dependent on the cooling velocity and the cell-specific membrane permeability to water and cryoprotective agents as described in the water transport model (Levin et al., 1976).

1.1.1. Cryoprotective agents

Cryopreservation requires not only use of cell-specific optimal cooling rates but also CPA to reduce the damaging impact of ice formation. Means of cellular cryoprotection include control over cooling process and application CPAs. CPAs are substances that can prevent the development of cryoinjury of biological objects and preserve their structural and functional characteristics after thawing. All CPAs could be divided into 2 major classes: intracellular (permeating) and extracellular (non-permeating). The classical examples of penetrating CPAs are glycerol and DMSO discovered by Polge et al., 1949 and Lovelock and Bishop, 1959, respectively. Since then the list of CPAs has included new permeable CPAs such as ethylene

glycol, propylene glycol, dimethyl formamide and membrane-impermeable CPAs such as sucrose, trehalose, hydroxyethyl starch (HES), polyvinylpyrrolidone (PVP) and ficoll (for review, see Elliott et al., 2017). Intracellular CPAs are thought to be the most effective due to their high penetrating capability but they are also characterized by the highest toxicity (for review see Best, 2015). Therefore, actual issue remains the elimination or at least reduction of toxic concentrations and search for new non-toxic compounds with cryoprotective properties.

CPAs decrease the ice nucleation temperature and the amount of ice formed during freezing. In addition, CPAs modulate the rate of cell and membrane dehydration and allow dehydration to continue at low subzero temperatures thereby decreasing the incidence of IIF (Prickett et al., 2015). CPAs immobilize cells in a highly viscous glassy state in which damaging degradation reactions are inhibited. Cell permeating cryoprotective agents can be used in combination with high molecular weight membrane-impermeable macromolecules to increase the glass transition temperature of the cryopreservation. Proteins are stabilized by cryoprotective agents because cryoprotective agents are preferentially excluded from the protein surface, which increases the barrier for protein unfolding and denaturation (Lee and Timasheff, 1981).

1.1.2. Slow freezing and vitrification

Slow-freezing cryopreservation is the method that requires gradual cooling of a biological material and relatively low concentrations of CPAs. When an aqueous solution freezes, phase change from water to ice occurs. As a consequence, the concentration of the solute in the remaining unfrozen fraction increases until remaining maximally freeze-concentrated liquid converts into a glass at so called glass transition temperature (T_g'). After reaching this temperature a sample can be safely stored in the liquid nitrogen until later use.

Since ice nucleation during cooling is a stochastic event, in nature freeze-tolerant organisms developed a strategies to prevent or promote supercooling and ice formation by producing antifreeze or ice-nucleating proteins, respectively (reviewed in Davies, 2014). Cryobiologists, in turn, developed a range of methods to be able to actively induce ice formation which is beneficial for cell recovery as reviewed in Morris and Acton, 2013.

Another breakthrough reported in the 1980s by Fahy et al. was the discovery of a novel cryopreservation strategy known as vitrification for cell and tissue preservation in which high concentrations CPAs and high cooling rates are used to absolutely avoid ice formation (Fahy

et al., 1984). Vitrification (*vitreous* in Latin means *glass*), or ice-free cryopreservation, is an alternative approach to ‘normal’ cryopreservation that enables cells or tissues to be cooled to cryogenic temperatures in the absence of ice. Vitrification simplifies and may improve cryopreservation because it eliminates i) mechanical injury from ice, ii) the need to find optimal cooling and warming rates, and iii) the importance of differing optimal cooling and warming rates for cells in mixed cell type populations (Fahy and Wowk, 2015). However, it introduces a greater risk of cryoprotectant toxicity during the addition and removal of cryoprotectants. Vitrification of larger tissues remains a great challenge, since the cooling rate that can be applied to ensure homogeneous freezing decreases with increasing sample size (Giwa et al., 2017). In reproductive medicine, vitrification has proven its great potential, i.e. for female cancer patients. Cryopreservation of patients’ own ovarian cortex tissue allows women to become pregnant again after cancer treatment (for review see Silber, 2016). However, successful vitrification of other complex large-size tissues remains elusive due to inhomogeneous delivery of highly concentrated CPAs into a tissue and development of increased thermo-mechanical stresses.

Both slow-rate freezing and vitrification are equally effective cryopreservation tools and both are associated with many challenges dictated by physical events which could cause cryoinjury of cells as can be seen from the **Fig. 1.1**. Among them are recrystallization of ice and devitrification of glass during warming. Recrystallization involves the conversion of small ice crystals formed during cooling into large crystals as a result of differences in surface free energy. Devitrification is the conversion of amorphous solid also formed during cooling to ultraviscous water followed by the conversion of this water to ice (Seki and Mazur, 2008).

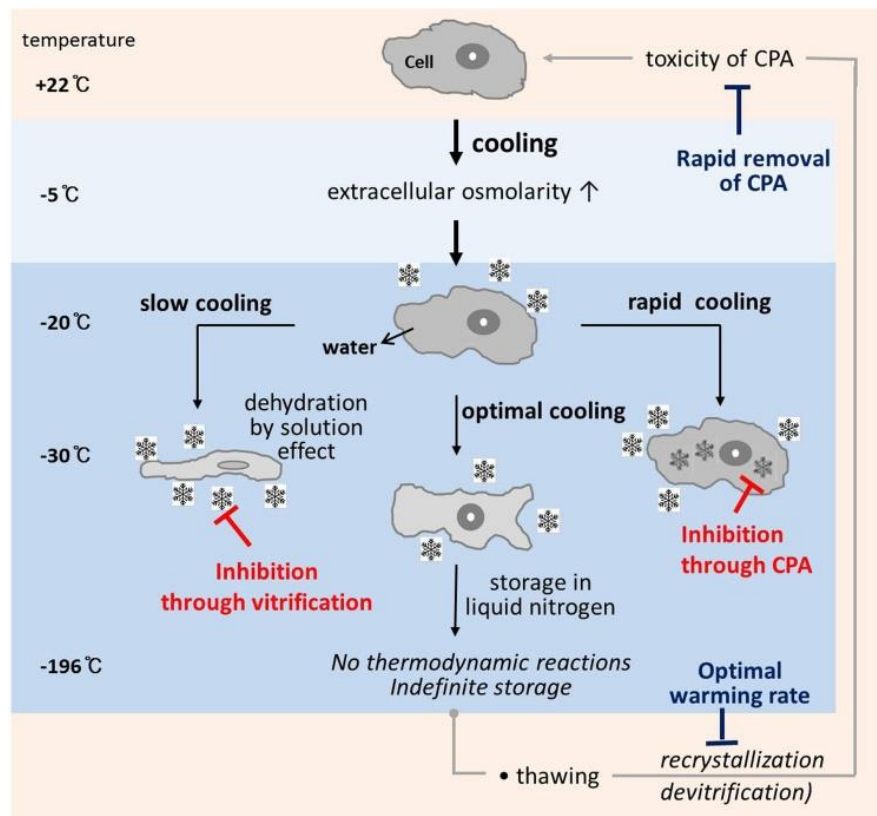


Figure 1.1 Physical events and cryoinjury of cells during freezing and thawing.

Jang, T.H., Park, S.C., Yang, J.H., Kim, J.Y., Seok, J.H., Park, U.S., Choi, C.W., Lee, S.R., Han, J., 2017. Cryopreservation and its clinical applications. *Integr. Med. Res.* 6, 12–18. (CC BY-NC-ND license, <https://www.elsevier.com/about/policies/open-access-licenses>).

1.2. Challenges in cryopreservation of multidimensional structures

Stem cell cryobanking is the long-term storage of stem cells and their derivatives, or biological samples containing stem cell populations, for later use in regenerative cell therapy. Cryopreservation of dissociated stem cells is commonplace in biobanking practice. A great variety of cell types such as mesenchymal (Yong et al., 2016), human embryonic (Holm, 2015) and hematopoietic (Daniele and Zinno, 2015) stem cell lines are stored in biobanks worldwide for immediate availability for research, regenerative medicine, biotechnology and transplantology. Establishment of European Bank for induced pluripotent stem cells (iPSCs) (De Sousa et al., 2017) provides a great opportunity for world-wide distribution of established iPSCs lines to enable their translation from clinical trials to personalized medicine (for review see Ntai et al., 2017). In spite of several decades of research, a simple, effective and safe method to cryopreserve cells in adherent state is still unavailable. What is rapidly becoming

apparent is that the development of such method would facilitate numerous applications in the field of drug or cosmetics testing, cell-based therapies and fundamental biomedical research. For instance, successful cryopreservation of 2D skin (Pasch et al., 2000) or cornea (Routledge and Armitage, 2003) constructs would provide robust engineered tissue supply and transplantation for patients in need in a ready-to-use format. From another perspective, such 2D systems may serve as models to uncover the specifics and improve the cryopreservation efficiency for more complex 3D systems, e.g., TEPs. However, high variability of available data regarding approaches and post-thaw survival rates of cell monolayers indicates that their cryopreservation is technically demanding and requires further integration of multidisciplinary research in the cryobiology field.

1.2.1. Cryopreservation of cell monolayers and 2D tissue-engineered constructs

Cryopreserved cell monolayers offer also practical benefits to routine diagnostics making large shipment of samples with reduced lot-to-lot variations possible, by providing time for their evaluation before clinical use and tighter inventory control (Huang et al., 2002). To date, cryopreservation of cell monolayers is gaining increased commercial attention due to evident benefits offered by its ready-to-use format (Bahari et al., 2018; Pless-Petig et al., 2018). For example, successful cryopreservation of cell types vulnerable to enzyme dissociation such as iPSCs in cell plates pioneered by Katkov et al., 2011 would substantially improve banking and shipment of this highly promising cell type. However, there are multiple challenges to establish stable storage and shipment of cells frozen in adherent cells before it will reach widespread clinical application and commercialization. First of all, isolated cells and cells fixed to a substrate differently respond to cryopreservation-related stresses. Cells attached to a substrate undergo more severe osmotic shock as compared to spherical cells able to reach minimum cell volume upon CPA addition and removal according to classical theory postulated by Meryman, 1971. As a result, cytoskeleton of attached cells becomes strained which makes them more prone to detachment on propagation of ice front when ‘solution effect’ occurs (Meryman et al., 1977). Liu and McGrath, 2005 showed that freezing induces distortion of F-actin, the disassembly of connexin-43 and vinculin in osteoblast cells attached to hydroxyapatite discs presumably due to mechanical forces exerted by extracellular ice and differential thermal contraction. However, the exact mechanisms of cryodamage during cell monolayer cryopreservation are still not fully understood.

A growing number of scientific articles reporting on achievements and challenges associated with the cryopreservation of cell monolayers primarily suggest that conventional freezing protocol requires modifications to successfully protect adherent cells. In this context, a nature of a substrate (Xu et al., 2012) and particularly its thermal expansion characteristics (Rutt et al., 2018) play a crucial role in post-thaw recovery of adherent cells. Miyamoto et al., 2009 compared cryopreservation of rat primary hepatocytes and mouse embryonic stem cells on conventional plastic dish and collagen vitrigel membranes with univocally better cell post-thaw recovery reported for the membranes. The other crucial process parameter for adherent cells, as showed by Pegg, 2002, is an application of slow cooling rates. In this study, the maximum recovery for vascular endothelial cells frozen as a confluent layer on microcarrier beads at 0.3 K/min was reported to be 85%. Extensive evidence on other improvements include directional freezing (Bahari et al., 2018), alginate-entrapment (Malpique et al., 2009), preincubation with trehalose (Stokich et al., 2014), application of ice crystallization (Matsumura et al., 2016) or recrystallisation (Graham et al., 2017) inhibitors and ice nucleants (Kilbride et al., 2016). In particular, CryoPlate™ concept for high throughput cryopreservation of adherent cells on plates deserves particular attention due to its potential practical utility (Campbell and Brockbank, 2014). This system utilizes nucleation step at -6°C and two-step thawing comprising intermediate equilibration for 30 min at -20°C in a freezer followed by rapid thawing in a water bath at 37°C. For certain cell types, such as adherent colonies of human embryonic stem cells, vitrification was shown to be a superior to conventional freezing (Beier et al., 2011). In another study, myoblast cell sheets were successfully vitrified in thin polyethylene films and thawed directly on hot plate pre-warmed to 37 °C (Ohkawara et al., 2018). In the study by Ma et al., 2006 combination of DMSO, collagen gel entrapment and trehalose loading was collectively used for efficient cryopreservation of adherent neuronal networks. Some cell types such as human embryonic stem cells (hESCs) are very sensitive to cryoinjury and difficult to cryopreserve in suspension. Ji et al., 2004 developed a cryopreservation technique based on stabilizing of hESCs colonies attached to Matrigel™ matrix by loading of cells with trehalose prior to cryopreserving in a DMSO-based CPA with high post-thaw cell with viability much higher compared with cryopreservation in suspension. The practice of sugar loading for cryopreservation and freeze-drying purposes (mostly sucrose and trehalose) achieved increased attention due to extraordinary protection they provide to cells when being present intracellularly. As summarized by Acker, 2006, the mechanisms of intracellular protection provided by intracellular sugars could be attributed to:

1. Reduction of the magnitude of volumetric change upon freezing by increasing intracellular osmolarity and osmotically inactive volume;
2. Stabilization of biomolecules;
3. Destructuring effect on water;
4. Formation of an intracellular glassy state.

Among methods for intracellular delivery of disaccharides, the simplest one which does not require any complicated equipment and take advantage of the natural cell ability to internalize extracellular molecules is fluid-phase endocytosis. It is a time- and temperature-dependent physiological process which was shown to be responsible for transient permeabilization and loading of membrane-impermeable trehalose into mammalian cells upon prolonged *in vitro* culture (Miao Zhang, et al., 2016; Oliver et al., 2004). Other alternative innovative approaches developed for introduction of protective disaccharides into mammalian cells are presented in the **Fig. 1.2**.

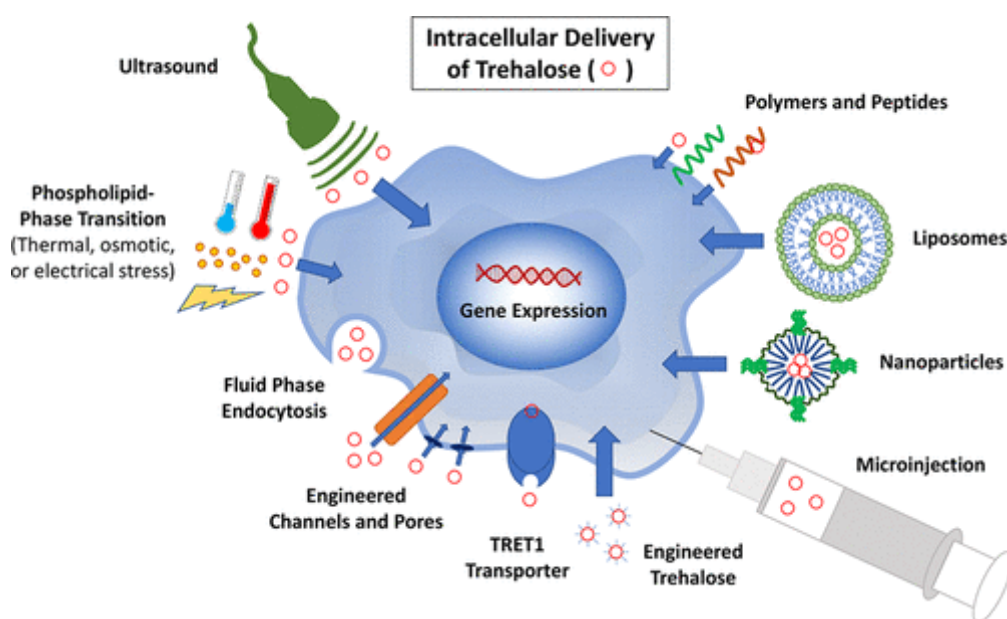


Figure 1.2 Methods for delivery of trehalose into mammalian cells.

Reprinted with permission from Stewart, S., He, X., 2018. Intracellular Delivery of Trehalose for Cell Banking. *Langmuir*. Copyright © 2018, American Chemical Society.

Apart from trehalose, another protective disaccharide sucrose, ubiquitously known as common table sugar, is mostly used as a non-penetrating CPA to dehydrate and stabilize cells and tissues in the course of dry and cryopreservation. The main advantage of sucrose in comparison to trehalose is its low production costs and availability. Interestingly, stimulating studies utilizing sucrose for pre-freeze treatment of human mesenchymal stromal cells

(hMSCs) showed that sucrose can be used for their DMSO-free cryopreservation in suspension with equally good survival rates compared to trehalose (Petrenko et al., 2014; Rogulska et al., 2017). These studies also demonstrated that the highest level of protection is provided when along with pre-freeze treatment sucrose is used as an extracellular CPA. In general, osmotic preconditioning of cells with sucrose was demonstrated to cause its endocytotic uptake (Bright et al., 2016) with formation of osmotically swollen late endosomes referred to as sucrosomes (Bright et al., 1997; Helip-Wooley and Thoene, 2004).

1.2.2. Challenges in cryopreservation of 3D TEPs

One of the leading technologies to enable rapid translation and commercialization of regenerative medicine research is cryopreservation of cells, tissues and organs (Giwa et al., 2017). A growing demand worldwide in functional tissue substitutes requires application of tissue engineering approaches to meet clinical needs. In turn, tremendous advancements in this field in the 21st century actualizes the need for synergistic co-development of preservation methodologies for TEPs including organs-on-a-chip (for review see Wang and Elliott, 2017), since the production cycle of TEPs is a time consuming, multi-step technological process. This involves scaffold fabrication and sterilization, cell isolation, seeding onto scaffolds at dynamic conditions (e.g. in a bioreactor) and long-term testing *in vitro* as well as transplantation *in vivo*. In this regard, the novel concept of establishment of biobanking of ready-to-use potentially marketable TEPs led to intensification of multidisciplinary research increasing the role of cryobiology in personalized tissue engineering therapies (Neves et al., 2016). Cryopreservation of TEPs could reduce the time expenditure associated with a routine manufacturing process and increase its economic efficiency. As a result, shortening of processing time and improvement of sample logistics enabled by cryopreservation is linked with apparent benefits for patients by ensuring ‘off-the-shelf’ availability of transplants for regeneration of damaged tissues (Sarangi and Pramanik, 2010). This innovative strategy could also streamline routine laboratory production of TEPs for research needs and make experimental scheduling more flexible. Fahy et al., 2006 convincingly showed how regenerative medicine can benefit from cryobiology research efforts to optimize supply chain management issues through cryopreservation of complex systems. Although cell biobanking is a well-established procedure due to recent achievements in cryopreservation of suspended cells, efficacious long-term storage of 3D TEPs for tissue regeneration meets a number of challenges. First of all, the problem of hampered mass and

heat transfer causing large thermal gradients and unequal CPA loading additionally rises. Development of cryopreservation protocols for TEPs requires a careful consideration of complex spatial cell-cell and cell-substrate interactions for delicate CPA loading, exposure and removal as well as information on thermal properties of a substrate such as its thermal conductivity, expansion and specific heat. Not less crucial and problematic is a selection of an appropriate thawing method since the conventional thawing in a water bath developed also for suspended cells causes formation of fractures in 3D TEPs as a consequence of mechanical stresses and requires further optimizations. One of the most currently discussed rewarming procedures for tissues is based on inductive heating of magnetic nanoparticles (Manuchehrabadi et al., 2017).

1.2.3. State of the art in TEPs' cryopreservation

Structural complexity of TEPs and immense diversity of biomaterials and cell types used for their preparation impose high requirements for their efficient cryopreservation and may account for variable and conflicting data available in scientific publications on this topic (summarized in the **Table 1.1**). Along with slow cooling, vitrification is increasingly considered as a highly promising technology for cryopreservation of TEPs (Wu et al., 2015). Additional challenges and advantages associated with vitrification of 3D TEPs are reviewed elsewhere (Kuleshova et al., 2007; Wang, 2012).

Table 1.1 Short summary on the current success in the cryopreservation of TEPs.

Preservation modality	Cell and scaffold type	CPAs	Viability (%)	Reference
Vitrification	Tissue-engineered (TE) cartilage: calf articular chondrocytes on poly-l-lactic acid scaffolds	3.97 M DMSO, 3.97 M formamide, 2.83 M 1,2-propanediol	56	Farooque et al., 2009
Vitrification	porcine MSCs on polycaprolactone-gelatin nanofibrous scaffolds	40% ethylene glycol (EG), 0.6 M sucrose	level of control	Wen et al., 2009
Programmable slow freezing	TE skin: fibroblasts on sponge made out of hyaluronic acid and atelo-collagen	10% DMSO, 20% fetal bovine serum (FBS)	50	Kubo and Kuroyanagi, 2004
Vitrification	TE bone: mouse calvaria-derived osteoblasts cell line MC3T3-E1 on	3.1 M DMSO, 3.1 M formamide, 2.71 M EG with ice blocker	43	Liu and McGrath, 2005

	hydroxyapatite discs	SuperCool Z-1000		
Slow freezing	hMSCs on alginate-gelatin cryogel scaffolds	10% DMSO in culture medium	around 80	Katsen-Globa et al., 2014
Slow freezing	hMSCs on chitin scaffolds	10% DMSO, 10% FBS	54	Mutsenko et al., 2017
Slow freezing	goat bone marrow stem cells on corn starch and polycaprolactone scaffolds	10% DMSO	54	Costa et al., 2012
Slow freezing	Mouse C2C12 myoblast cells on electrospun polyurethane scaffolds	10 % DMSO in culture medium	55	Batnyam et al., 2017
Programmable slow freezing	hMSCs on silk nanofibrous scaffolds	Trehalose 40 mM, ectoin 40 mM, catalase 100 µg, DMSO 2.5%	73	Bissoyi et al., 2014
Slow freezing	hMSCs on bioscaffold based on platelet rich plasma and synovial fluid	10% DMSO and 10% DMSO + 0.2 M Sucrose	70	Gurruchaga et al., 2017
Slow freezing	hMSCs on collagen scaffolds	10% DMSO/ 20% FBS	59	Petrenko et al., 2017
Slow freezing	<i>Callithrix jacchus</i> MSCs in alginate hydrogel	10% DMSO/17.5% FBS	62	Gryshkov et al., 2014
Direct placing into LN ₂	TE epidermal membranes: human keratinocytes on chitosan-gelatin membranes	0.4 M trehalose, 10% DMSO, 50% FBS	68	Chen et al., 2011
Slow freezing with ice seeding	TE skin: human dermal fibroblasts on polyglycolic acid scaffolds	1.4M DMSO	81	Wang , 2004
Slow freezing	goat bone marrow-derived MSCs; mouse MC3T3-E1 cell line on gelatin-based CultiSpher-S microcarrier beads	10% DMSO, with or without 200 µM ascorbic acid, 90% FBS or goat serum, respectively	52 and 42, respectively	Lippens and Cornelissen, 2010
Slow freezing	SaOS-2 cells attached to 2D and 3D poly(lactide-co-glycolide) scaffolds	10% DMSO	around 80	Kofron et al., 2003
Slow freezing	mouse fibroblasts NIH/3T3 on 3D scaffolds made of reticulated polyvinyl formal resin	10% DMSO, 15% FBS	65	Miyoshi et al., 2010

From the above table it is apparent that there is some progress in cryopreservation of 3D TEPs with respect to cell viability levels but their safe and effective low-temperature maintenance over prolonged periods of time remains arduous and involves complex phenomena and issues to be addressed. For every composite tissue optimal conditions must be individually defined taking into considerations freezing resistance of a cell to much extent dictated by material properties of a scaffold. For example, post-thaw fate of cells frozen in a hydrogel, fibrous or microsphere scaffold (depending on a target tissue engineering application) even being frozen in a similar manner in 10% DMSO and thawed at 37°C water bath may considerably vary. For example, as the recent study by Pogozhykh et al., 2018 on the cryopreservation of bioengineered multicellular placental constructs implies, tolerance limits to cryodamage depends on the structure of the studied object, intercellular bonds, as well as interaction of its components with cryoprotective agents. This reflects a need for establishment of experimental models to understand fundamental factors of cryodamage and improve freeze-thaw protocols for preservation of 3D TEPs. Interestingly, a comparative study on freezing of rabbit cornea done by Fong et al., 1987 showed that the least degree of damage was observed when corneas were equilibrated with 1M DMSO and frozen ‘in air’ (i. e. in the absence of any extracellular medium) compared to bulk medium. The related theoretical study by Zhang et al., 2005 subsequently demonstrated that i) the thermal stresses occurring in the process of cryopreservation ‘in air’ are much smaller than that of in a bulk medium and ii) the thermal stresses during thawing are much higher than those of freezing. In cryopreservation of isolated (Ozawa et al., 2014) and adherent cells (Bahari et al., 2018; Bissoyi et al., 2016) in reduced volumes of CPAs other thawing approach were assessed involving addition of 37°C pre-warmed media to samples or direct placement of frozen samples into a pre-warmed media. This provides fast thawing and simultaneous dilution of CPAs and potentially could be combined with ‘in air’ freezing to reduce cracking associated with much more pronounced thermo-mechanical stresses developing upon thawing in a bulk medium. Given that high-quality cryopreservation of 3D TEPs has not yet been achieved, enrichment of DMSO-based freezing solutions with other CPAs may favor better protection while decreasing the overall toxicity of multicomponent CPA cocktails (Elliott et al., 2017) by reducing the absolute amount of DMSO. Disaccharides such as trehalose and sucrose are recognized as toxicity minimizing extracellular CPAs and were shown to be effective for cryopreservation of rare cell types such as spermatogonial stem cells (Lee et al., 2014), primary human hepatocytes (Katenz et al., 2007), adherent neuroblastoma cells (Bailey et al., 2015) and human fetal liver

hematopoietic stem/progenitor cells (Petrenko et al., 2008) in combination with DMSO. In this context, Solocinski et al., 2017 showed that addition of trehalose to DMSO-based CPAs dramatically reduces the area per ice crystals while increasing the number of ice crystals which correlates with increased cell viability.

Intriguingly, loading of acellular heart valves with sucrose prior to freeze-drying has been associated with diminished pore formation (Vásquez-Rivera et al., 2018) and excellent in vivo performance after implantation into juvenile sheep (Goecke et al., 2017). It must be stressed that in freeze-drying procedure samples are first subjected to slow freezing which implies that highly concentrated sucrose effectively protects acellular scaffolds against cryoinjury. However, scaffolds populated with cells represent much more complex and cryosensitive system and require application of moderate amounts of not only non-penetrating but also penetrating CPAs to warrant sufficient protection of both a scaffold and cellular component. In this context, Gurruchaga et al., 2017 in cryopreservation of hMSCs on 3D allogeneic bioscaffold showed that application of sucrose alone is suboptimal, unless it is combined with a DMSO. In our work with chitin scaffolds, we observed 15% increase in cell viability provided by sucrose-pretreatment and addition of sucrose into DMSO-based medium (Mutsenko et al., 2016). Moreover, as have been recently demonstrated by Sydykov et al., 2018, supplementation of DMSO-containing cryoprotective formulations with sucrose is promising for stable storage of biological objects since it increases glass transition temperature and decrease molecular mobility in the glassy state. Raman studies by Yu et al., 2018 have recently shown strengthened intermolecular hydrogen bonding in a binary system sucrose-water at -50°C. It could be assumed that in a ternary system water-sucrose-DMSO sucrose with its eight hydroxyl groups present on the molecule would act as a hydrogen bond donor to both DMSO and water while preserving its ‘destructuring’ effect on the water network. In the study by Heng et al., 2004 addition of 0.25 M sucrose to 20% DMSO significantly enhanced viability of primate CV-1 cell line frozen in microcapsules after slow-rate freezing presumably due to alleviation of DMSO toxicity by reducing its absolute amount.

1.3. Sugars as alternatives to DMSO and electroporation as a method for sugar delivery

Stem-cell therapy is one of the most promising strategies in the modern medicine for treatment of patients suffering from diverse disabilities or chronic diseases. The sector of stem cell-based therapy is part of rapidly developing healthcare industry and attracted a lot of attention to the scientific community. A number of cell therapy products such as for example Holoclar® based on limbal stem cells registered as a product for eye burns in Europe or MSCs approved for pediatric patients with graft versus host disease in Canada and New Zealand offer great promise and benefits to patients in clinical trials (Trounson and McDonald, 2015). Manufacture of such products have to follow Good Manufacturing Practice (GMP) standards to ensure safety and high reproducibility which is required by governmental institutions such as Food and Drug Administration (FDA, United States) or European Medicines Agency (EMA, Europe) (Bedford et al., 2018). In the mentioned context, important role plays the cryopreservation of cellular products and it is an inevitable step of the production chain. In clinical settings, repeated transplantations and flexible treatment scheduling are needed or unavoidable (Hunt, 2011). Apart from transplantation value, efficient long-term storage of cell products in hospital-integrated biobanks would play a leading role for advancement of precision medicine research (Zatloukal et al., 2018). There are conflicting reports on the impact of cryopreservation procedures on cell functionality in clinical settings. For example, Peters et al., 2008 highlighted the impaired suppressive capacity of cryopreserved regulatory T cells. François et al., 2012 and Moll et al., 2014 showed compromised immunomodulatory profile of frozen-thawed mesenchymal stromal cells (MSCs). Chinnadurai et al., 2017 reported on susceptibility of frozen MSCs to T-cell mediated apoptosis. In contrast, in the work by Luetzkendorf et al., 2015, no negative impact of cryopreservation on immunomodulating potential of GMP-grade human MSCs was shown. Moll et al., 2016 provided broad overview of the current status in the clinical use of fresh and cryopreserved MSCs with the general conclusion that there are limited but significant differences between these two groups. Most clinical applications use frozen stocks of cells and this requires the detailed phenotypic characterization of fresh and cryopreserved cells (Cathery et al., 2018). In practice, the most frequently used freezing media in cell banking comprises the cryoprotective agent DMSO and FBS. However, GMP-grade cryopreservation media must be animal-component free and provide high batch-to-batch consistency and

quality of cell products stored under deep cryogenic temperatures. This is because of high immunogenicity, lot-to-lot variability, risk of contamination and bioethical issues associated with application of FBS. Therefore, there is much ongoing research into replacement of FBS with different non-animal components. An often used example is human platelet lysate in both cell expansion (Bieback, 2013) and cryopreservation media with (Rogulska et al., 2017; Tolosa et al., 2011; Wang et al., 2017) or without DMSO (Rogulska et al., 2017). DMSO was first synthesized in 1866 by the Russian scientist Alexander Zaytsev and first used for cryopreservation purposes by Lovelock and Bishop, 1959 against freezing damage to human and bovine red blood cells as well as bull spermatozoa. Since that time until present moment, DMSO is an indispensable component of main freezing solutions. Despite widespread use of DMSO, it may cause adverse effects after transplantation (Shu et al., 2014), alter cell pluripotency (Katkov et al., 2006) and epigenetic profile (Chatterjee et al., 2017, 2016; Iwatani et al., 2006). In recent years, the trend towards GMP-compliant cryopreservation led to development and commercialization of next generation cryopreservation media without DMSO and FBS such as BambankerTM DMSO Free or CryoSOfreeTM. However, lack of long-term studies, narrow spectrum of tested cell lines and potential risks associated with undisclosed components substituting DMSO or FBS raise safety concerns. Thus, search for new non-toxic cryopreservation formulations which would minimize or completely eliminate DMSO and animal serum while maintaining high cryopreservation efficiency is rationally justified. Another hot topic and point of discussion is which DMSO concentration is considered optimal before the infusion into patients. Unfortunately, no consensus has been reached on which DMSO concentration is considered safe for the infusion into patients and the issue of its depletion before infusion is still debated (Morris et al., 2014). One strategy for mitigating DMSO-related complications after transplantation is direct reduction of its concentration from routinely used 10% to 5% or lower as it is suggested in some comparative studies such as by Bakken, 2006 and Mitrus et al., 2018. Alternatively, the replacement of DMSO could be achieved by combining CPAs from different classes (penetrating, non-penetrating, sugars, alcohols) with various modes of action (Best, 2015; Lauterboeck et al., 2016). In this respect, it is of great importance to select the proper process parameters such as CPA concentration, temperature and time of exposure, cooling/heating rate, ice crystallization temperature and CPA addition/removal procedure. This could unlock the full potential of the cryoprotective agents without using animal substances or DMSO.

1.3.1. Application of sugars as non-toxic CPAs

Among nature inspired, non-toxic CPAs are sugars, polyols and ice-binding proteins (IBPs). The latter are a part of natural protective mechanism used in cold-adapted organisms such as fish, bacteria, algae, diatoms, fungi, insects, and plants and have been evolved from natural selection and adaption (Dolev et al., 2016). IBPs possess many appealing properties such as ice shaping, freezing point depression in a non-colligative manner and ice recrystallization inhibition (IRI). These proteins are xenogenic and the immunogenicity issue remains actual (Crevel et al., 2007).

In this context, sugars are accumulated in some extremophile species of fungi (Robinson, 2001), plants (Tarkowski and Ende, 2015), invertebrates (Everatt et al., 2015), poikilothermic vertebrates such as frogs, reptiles and fishes (Costanzo and Lee, 2013) tolerating subzero temperatures. Some sugars and sugar alcohols possess numerous protective benefits which were explored to reduce DMSO and FBS concentrations. The exceptional protein stabilization by sugars is well known and for this reason they have routinely been used as excipients in pharmaceutical (reviewed in Mensink et al., 2017) and food (Soltanizadeh et al., 2014) industries. For medical purposes, sugars were used as additives in dry preservation of red blood cells (Yu et al., 2004) and platelets (Zhou et al., 2007). It has recently become feasible to lyophilize decellularized heart valves using sucrose (Vásquez-Rivera et al., 2018) without damaging the ultrastructure of the tissue. The developments in the area of fertility cryopreservation indicate that sugars are essential for successful recovery of oocytes (Wright et al., 2004) and sperm (Sieme et al., 2016) after returning back to physiological conditions.

Hence, sugars are being increasingly considered for reduction of toxic concentration of DMSO as shortly summarized in the **Table 1.2** or another widely used penetrating CPA such as glycerol (Koshimoto and Mazur, 2002).

Table 1.2 Short summary on the application of sugars to decrease DMSO concentration.

The most effective CPA combinations reported	Cell type	Maximal post-thaw viability	Reference
5% DMSO, 0.3 M sucrose	human fetal liver hematopoietic stem/progenitor cells	over 70%	Petrenko et al., 2008
0.05 M glucose, 0.05 M sucrose and 1.5 M EG	human dental follicle tissue	over 70%	Park et al., 2017
5% DMSO, 60 mM trehalose, 100 µg/ml catalase and 30 µM zVAD-fmk (in post-thaw culture medium)	human amniotic fluid-derived stem cells	over 80%	Cho et al., 2014
2.5% DMSO, 30 mM trehalose, or 5% DMSO, 60 mM sucrose	human hematopoietic stem cells	over 85% and over 90, respectively	Rodrigues et al., 2008
2.5% DMSO, 40 mM trehalose, 40 mM ectoine, 100 µg catalase and 30% FBS	human adherent MSCs	up to 70%	Bissoyi et al., 2016
2.5% DMSO, 30 mM trehalose	human stem cells from umbilical cord blood	over 90%	Chen et al., 2016
0.5 M DMSO, 0.1 M trehalose + 0.3 M raffinose, (intra- and extracellular respectively)	human oocytes	up to 90%	Younis et al., 2009
0.2 M trehalose alone	rat hepatocytes	over 90%	Cardoso et al., 2017
2% DMSO, 0.2 M trehalose	human umbilical cord blood stem cells	over 70%	Mantri et al., 2015
5% DMSO, 2% polyethylene glycol, 3% trehalose and 2% bovine serum albumin	mouse MSCs and bovine MSCs	over 90% and over 80%, respectively	Liu et al., 2011

Another study has recently shown that combination of sugars, sugar alcohols and small-molecule additives to be superior to DMSO in terms of post-thaw cell attachment, alignment of the actin cytoskeleton and epigenetic stability (Pollock et al., 2017).

1.3.2. Methods of sugar delivery through cell membrane

Some sugars with cryoprotective properties became much more attractive as CPAs after overcoming permeability barrier to them. A big number and variety of methods of trehalose delivery for cryopreservation is summarized in a recent review by Stewart and He, 2018 (see **Fig. 1.2**) with their advantages and drawbacks. Supported by numerous publications, the concept of establishing controlled and non-toxic cryopreservation technologies using

trehalose is of high multidisciplinary interest. Nanoparticle-mediated delivery of trehalose (Rao et al., 2015) or its co-delivery of with antioxidants (Chen et al., 2017) using synthetic polymer PVitE-25 are interesting and novel approaches to load cells with this disaccharide. Although being encouraging and effective, these methods require a better understanding of intracellular trafficking of trehalose-bearing transporters. Apart from trehalose, other sugars such as sucrose and raffinose possess excellent cryoprotective properties and are perspective for intracellular delivery. Raffinose was loaded for the first time into mouse oocytes via microinjection in 2010 by Eroglu and this promoted high cryosurvival, fertilization, and development rates (Eroglu, 2010). The incorporation of sucrose into mammalian cells using high intensity femtosecond laser pulses and its applications to biopreservation was investigated by Kohli et al., 2005. In that study, the highest post-laser exposure survival rate was achieved using 200 mM sucrose with 145 mM being delivered inside the cells. Later on, 63.7 mM trehalose from 800 mM extracellular trehalose was loaded into red blood cells at a field strength of 1.5 kV/cm, field strength in combination with 1 ms pulse length and 4 pulses in one minute (Zhou et al., 2010). After freeze-drying and reconstitution the cell recovery was 70%.

1.3.3. Electroporation of cells for sugar delivery

Sucrose was much earlier successfully loaded by electric pulses into different cell types such as mouse erythrocytes (Kinosita and Tsong, 1978) or rat hepatocytes (Gordon et al., 1985). Gordon et al. compared the sucrose uptake using electroporation and natural uptake. In 1997 a group of scientists investigated the effect of the reversible permeabilization with H5 mutant of the *Staphylococcus aureus* α -toxin on the fibroblast line 3T3 (Russo et al., 1997).

In 1978, Igor Katkov was one of the first pioneers who applied electroporation as a tool for cryopreservation (summarized in Katkov, 2003). Thereafter, with implications for dry and cryopreservation of mammalian cells, trehalose was successfully introduced into mouse myeloma Sp2 cell line by means of reversible electroporation by Shirakashi et al., 2002. Using 2 kV/cm electrical field and 20 μ s pulse duration the intracellular trehalose concentration of 100 mM out of 290 mM external concentration was calculated. Campbell and Brockbank, 2011 compared transport peptides and electroporation for delivery of β -galactosidase into smooth muscle cells as a model for introducing disaccharides into mammalian cells for cryopreservation purposes. Using a single pulse with duration 25 ms 33% of cells in adherent state (out of 50% in 10% DMSO) survived after electroporation at 50

V. Nonetheless, the first actual data on high post-thaw survival of human stem cells after electroporation-induced loading of trehalose were published in 2017 by Dovgan et al. 2017.

Electroporation is a physical method for introducing of membrane-impermeable molecules into cells through transient permeabilization of cellular membrane by electric pulses. In the recent comprehensive review by Stewart et al., 2018, electroporation deserves special attention as: *‘the most mature in regard to industrial applications and clinical translation’*. Electroporation gained broad application in transdermal drug delivery (Charoo et al., 2010), electrochemotherapy (Miklavčič et al., 2014), deoxyribonucleic acid (DNA) vaccines (Sardesai and Weiner, 2011) and delivery of genes (Rols, 2017). Taken together, to introduce different sugars into cells, electroporation seems to be the method of choice and this has to be evaluated in the context of cryosurvival on stem cells. In the following subchapter, a detailed description on the aims and outline of the thesis work will be given.

1.4. Aims and the outline of the study

The central aim of this thesis was to study the application of sucrose to improve DMSO-based cryopreservation of cells in 2D and 3D format and to develop DMSO- and serum-free cryopreservation of cells in suspension using electroporation-assisted delivery of sugars.

For clarity purposes, the terms ‘conventional cryopreservation’ or ‘conventional cryopreservation protocol’ are used interchangeably and describe slow-rate freezing of a biological sample with application of 10% DMSO as a CPA and thawing in a water bath.

This thesis is divided into 3 main conceptual blocks logically interconnected with each other according to hypotheses and aims indicated as follows.

It is hypothesized that:

1. Application of sucrose for pre-freeze cell treatment and addition into DMSO-containing freezing solution improves conventional cryopreservation of cell monolayers compared to the application of DMSO alone.
2. Implementation of ‘in air’ freezing, modified thawing protocol and combined application of sucrose improves provides better cryoprotection to cells frozen in 3D scaffolds than conventional cryopreservation.
3. Electroporation of cells with sugars provides effective DMSO- and serum-free cryoprotection to cells.

The specific aims of the current thesis were:

1. To select optimal concentration of sucrose for loading into *Callithrix jacchus* mesenchymal stromal cells (*cj*MSCs) and for addition into DMSO-based freezing solution providing highest cell survival after cryopreservation in adherent state;
2. To evaluate the impact of pre-selected sucrose concentrations, ‘in air’ freezing and optimized thawing procedure on physico-chemical and mechanical properties of 3D porous collagen-HAP scaffolds and post-thaw recovery of *cj*MSCs;
3. To optimize electroporation parameters and select concentrations of sucrose, trehalose and raffinose correlating with high post-thaw survival of umbilical cord mesenchymal stem cells (hUCMSCs) in suspension after freezing in the absence of DMSO and animal serum.

Chapter 2 describes the methods used throughout all experimental work including the rationale behind selecting particular cell types. **Chapter 3** summarizes the results of the experimental work subdivided into respective subchapters in accordance with the set aims.

Specifically, in **Subchapter 3.1** entitled ‘Cryopreservation of *cj*MSCs on 2D carriers and the effect of sucrose’ the results of optimization studies performed to select sucrose concentrations for pre-freeze treatment and addition into DMSO-based media providing high survival of *cj*MSCs monolayers frozen on glass coverslips are set forth.

Subchapter 3.2 entitled ‘Effect of freezing on cells seeded onto 3D collagen-HAP scaffolds’ presents the results on the fabrication and cryopreservation of tissue-engineered constructs based on 3D collagen-HAP scaffolds and *cj*MSCs.

In **Subchapter 3.3** entitled ‘Effect of cell electroporation with sugars on cryopreservation outcome’ results of optimization studies focused on the selection of permeabilization parameters and concentrations of sugars providing high post-electroporation and post-cryopreservation cell survival are described.

Chapter 4 deals with the individual discussion of results from **Subchapters 3.1, 3.2 and 3.3** and mirrors them in the corresponding **Subchapters 4.1, 4.2 and 4.3**.

Chapters 5 and 6 respectively comprise of an overall summary and outlook of the studies presented in this thesis.

2. Materials and methods

2.1. Chemicals

If not specifically mentioned, all chemicals were purchased from Sigma-Aldrich (Germany). Dulbecco's modified eagle medium (DMEM)/ F-12, FBS were obtained from Gibco, USA and potassium phosphate (K_2HPO_4) from Merck-Millipore (Germany).

2.2. Cell culture

2.2.1. Cells

For cryopreservation experiments in 2D and 3D format amnion-derived *cj*MSCs were used. The rationale behind selecting this particular cell type was that this monkey is well established primate preclinical model with high phylogenetic similarity to human. Moreover, cryopreservation of *cj*MSCs has previously been established in a suspension (Lauterboeck et al., 2016) and within alginate beads (Gryshkov et al., 2015). *Cj*MSCs were kindly provided by PD. Dr. Thomas Mueller (Service Unit Embryonic Stem Cells, Institute for Transfusion Medicine, Medical School Hannover, Germany). The cells were initially isolated as described before (Pogozhykh et al., 2015). *Cj*MSCs were cultured in DMEM supplemented with 15% (v/v) FBS, 1% penicillin/streptomycin (Invitrogen, Germany) and 50 μ M ascorbic acid.

Experiments on the electroporation were conducted in the Laboratory of Biocybernetics, Ljubljana, Slovenia, where hUCMSCs were available. HUCMSCs were kindly provided by Dr. Ariana Barlic, Educell Ltd, Slovenia. Cells were cultured in phenol red-free DMEM/F-12 supplemented with 10% FBS, 2 mM L-glutamine, 100 U/ml penicillin/100 μ g/ml streptomycin and 1 ng/ml of recombinant human Basic Fibroblast growth factor (FGF-basic, Peprotech, UK).

2.2.2. General cell culture

Cells were cultured using standard procedures. Briefly, *cj*MSCs and hUCMSCs were cultured in 10 cm petri dishes (TPP, Switzerland) using standard culture conditions (humidified incubator at 37 °C and 5% carbon dioxide (CO_2)). At 70% confluency, cells were washed ones with phosphate buffered saline and detached using 0.05% trypsin-ethylenediaminetetraacetic acid (EDTA). After cells were detached, the reaction was stopped

by addition of culture media. The cell suspension was centrifuged (200 xg, 8 min), supernatant aspirated and re-suspended in culture medium. *Cj*MSCs were counted using an automatic cell counter (ViCell, Beckman Coulter GmH, Germany) and either transferred to new culture dishes at a density of 1×10^4 cells/cm² or used for cryopreservation experiments involving cryomicroscopy, scaffolds and post thaw viability assessment described below. Cell passages between 7th-9th (*cj*MSCs) and the 5-7th passages for hUCMSCs were used for the described experiments.

2.2.3. Culture of cells on cover slips for cryomicroscopy

To obtain cell monolayers, 100 µl of cell suspension (1×10^4 cells/cm²) was pipetted on a 12 mm glass coverslip (A. Hartenstein, Germany) followed by 1 h incubation in a humidified incubator at 37°C and 5% CO₂ to allow cells to adhere. Thereafter, fresh culture medium was added, and cells were cultivated until about 70% confluency before any tests were performed.

For experiments involving sucrose uptake, cells were incubated for 24 h in culture medium with 1 mg/ml invertase from baker's yeast (approx. 300 units/mg solid, Sigma, Germany). Bright field images were acquired using Axio Vert.A1 microscope (Zeiss, Germany) and processed with Zen 2 blue edition software.

2.2.4. Seeding of cells onto scaffolds

*Cj*MSCs were seeded into the scaffolds using the following procedure. First, scaffolds were presoaked with culture medium for 30 min and placed on a sterile filter paper to remove excess liquid. Subsequently, for one scaffold 4×10^5 cells were resuspended in 60 µl and pipetted on top of the scaffolds. Afterwards, the scaffolds were incubated for 30 min at 37°C in a humidified incubator to allow cell attachment. The next step was to cover the scaffolds with culture medium for further culturing for 24 h at static conditions. As controls, scaffolds treated the same way, but without cells were used.

2.3. Cell manipulation and analysis

2.3.1. Electroporation for permeabilization and recovery assays

Low-conductive electroporation buffers were prepared from 10 mM K₂HPO₄, 10 mM KH₂PO₄ and 1 mM magnesium chloride (MgCl₂) including 250 mM of sucrose, trehalose or raffinose, respectively. To achieve the physiological pH of 7.4, K₂HPO₄ and KH₂PO₄ were

mixed in the ratio of 40.5 to 9.5. A 1×10^6 cells per 100 μ l cell suspension of hUCMSCs was prepared in the electroporation buffer supplemented with 150 μ M propidium iodide (PI, Life Technologies, USA). Cells were transferred to disposable electroporation cuvettes (VWR International, Radnor, PA, USA) with a 2 mm gap size between the electrodes. By using the BTX™ Gemini X2 Electroporation System (Harvard Apparatus, USA) 8 pulses (0.1 ms and 1 Hz) were generated at 0-2.5 kV/cm electric field. All electroporation experiments were conducted under sterile conditions. The pulse parameters were controlled using an AP015 current probe and an ADP305 high-voltage differential voltage probe connected to the oscilloscope (WaveSurfer 422, 200 MHz, all from LeCroy, USA). The respective experimental set up is shown in the **Fig. 2.1**. Following incubation for 2 min at room temperature, samples were washed by centrifugation to remove extracellular PI. The resulting cell pellet was resuspended in electroporation buffer containing respective sugar and seeded at the density of 2.5×10^5 cells/well into a 96-well plate (TPP, Switzerland). Fluorescence intensity of PI-loaded and non-electroporated cells were read at 535/617 nm using an Infinite M200 plate reader (Tecan Austria GmbH). For cell recovery assay, electroporated and non-electroporated cells were seeded at a density of 5×10^3 cells/well into 96-well culture plates and cultivated overnight. To test the viability of the cells, they were incubated with 44 μ M of resazurin dissolved in culture medium for 2 h and fluorescence was measured using the plate reader at 550/590 nm (Ex/Em). All experiments were performed at room temperature at least in four independent repetitions.

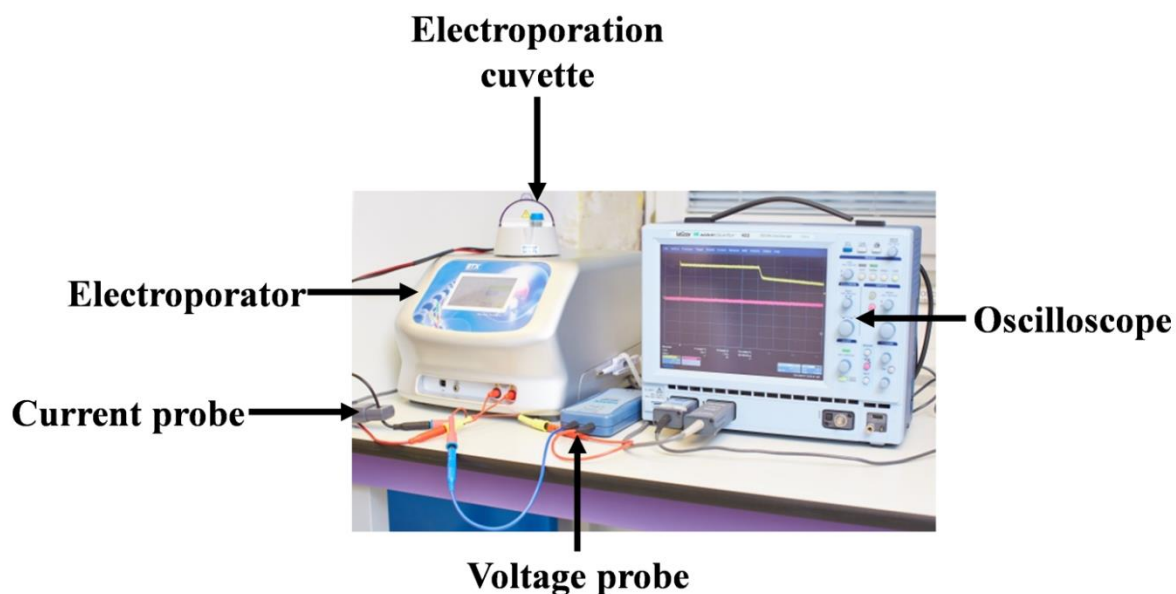


Figure 2.1 Electroporation set up used for the controlled electroporation of hUCMSCs with sugars.

The system consists of the electroporator, a current and voltage probe, the electroporation cuvette and an oscilloscope. The whole system easily fitted into a cell culture hood for working under sterile conditions.

2.3.2. Assessment of post-thaw survival of cells loaded with sugars after electroporation

Before and directly after electroporation and cryopreservation cell survival was assessed using trypan blue exclusion assay and fluorescence-activated cell sorting (FACS). For the first assay, an aliquot of cell suspension was mixed with equal amount of 0.4% trypan blue stain (Invitrogen, USA) and incubated for 2 min at a room temperature. Cells were counted using hemocytometer and the percent of live cells was calculated as the number of live cells/total number of cells.

In the next step, after cryopreservation cell survival was analyzed using FACS. Briefly, 100 μ l cell aliquot was resuspended in sample buffer supplemented with 100 μ g/ml PI. After incubation for 3 min at a room temperature samples were run on flow cytometer (Attune NxT; Life Technologies, USA) with laser excitation at 488 nm. Emission collected with 574/526 nm band-pass filter. Gating was performed against PI-negative (untreated) cells and the cells frozen in 150 mM high-conductivity electroporation buffer where the majority of cells were PI-positive. The measurement was finished when 10 000 events were acquired. Obtained data

was analyzed using the Attune NxT software, where cell survival was assessed on fluorescence intensity histogram.

2.3.3. Visualization of Lucifer Yellow uptake in suspension cells

Efficiency of electroporation was evaluated using Lucifer Yellow (LY) uptake. In this set of experiments, Lucifer Yellow CH dilithium salt with a molecular weight of 521.6 g/mol was used. Cells were allowed to settle to the bottom of 24-well culture plates for 15 min and electroporated using platinum-iridium wire electrodes with 0.8 mm diameter and 4 mm gap as shown on the Fig. 2.2. Pulses at 1.5 kV/cm were applied to hUCMSCs suspension in buffers containing 400 mM of respective sugars and 0.5 mg/ml of LY using the β tech electroporator (Electro cell B10, Betatech, France). Pulse parameters were monitored with the same probes as indicated in the **Subsection 2.3.1**. Electroporated samples were allowed for resealing for 10 min followed by washing with PBS by centrifugation. Negative control samples were treated in the same manner but without electroporation. The LY dye was excited with 425 nm and emission detected from the band pass filter at 605 nm (D605/55m, Chroma, USA). Bright field and fluorescent images were randomly acquired from at least 10 fields of view in the middle between the electrodes using inverted microscope AxioVert 200 (Zeiss, Germany) equipped with VisiCam 1280 camera (Visitron, Germany) and the MetaMorph 7.1.1 PC software (Molecular Devices, USA). The total number of cells and the number of LY-positive cells were manually counted on each image using cell counter plugin in ImageJ software (U. S. National Institutes of Health, Bethesda, Maryland, USA). The efficiency of electroporation was calculated as the percentage of the LY-positive cells from total number of cells on one image. Solution osmolality was measured by freezing point depression with OSMOMAT 030 osmometer (Gonotec, Germany).



Figure 2.2 Representative photo of the electrodes used in this work.

They were attached to the bottom of 24-well plate which was put under a microscope.

2.3.4. Resazurin reduction test

To select the optimal concentration of sucrose for pre-treatment, cell viability was evaluated using resazurin reduction test. Briefly, cells were seeded in 6-well plates with the density of 1×10^4 cells/cm² and cultured until approximately 70% confluency with the supplements described in the **Subsection 2.2.1**. Cells were incubated in 0-250 mM sucrose for 24 h with 50 mM increment. A 440 μ M (10 \times) stock solution of resazurin sodium salt (Sigma, Germany) was prepared in a culture medium without phenol red (Merck Millipore, Germany). Resazurin solution diluted in a culture medium without phenol red was added to cells at 10% final concentration (v/v), and plates were incubated for 2 h at 37 °C prior to reading of absorbance using a spectrophotometer Biochrom Libra 22 (Biochrom, UK). Absorbance of oxidized form resazurin and reduced form resorufin was measured before and after pre-treatment at 600 nm and 570 nm, respectively. Reduction percentage of resazurin before pre-treatment for corresponding comparison groups was taken as a 100%. Reduction percentage was calculated according to the following equation:

$$\text{Reduction percentage} = \frac{\varepsilon_{OX_600nm} \times A_{570nm} - \varepsilon_{OX_570nm} \times A_{600nm}}{\varepsilon_{RED_570nm} \times A_{600nm} - \varepsilon_{RED_600nm} \times A_{570nm}} \times 100\%, \quad (2.1)$$

where ε is the molar extinction coefficients for resazurin and A is the measured absorbance at a given wavelength. The molar extinction coefficients for the oxidized and reduced forms of resazurin are indicated in the following **Table 2.1**.

Table 2.1 The molar extinction coefficients for resazurin.

Wavelength	Reduced Resazurin (ϵ_{RED})	Oxidized Resazurin (ϵ_{OX})
570 nm	155677	80586
600 nm	14652	117216

2.3.5. Visualization of Lucifer Yellow uptake in adherent cells

To visualize internalization of membrane impermeable compounds in adherent cells, LY uptake was studied. Cell monolayers prepared on glass coverslips as described in the **Subsection 2.2.3** were incubated in culture medium supplemented with 100 mM sucrose and/or 100 $\mu\text{g/ml}$ LY dilithium salt (Sigma, Germany). After washing with PBS, samples were fixed in 3.7% (v/v) formaldehyde solution and analyzed using Axiovert 200M fluorescence microscope (Zeiss, Germany). Images of fluorescence and bright field images of cells were analyzed using AxioVision software (Rel. 4.7).

2.3.6. Cell volume measurements

To evaluate the cellular response to sucrose treatment, changes in cell volume were analyzed. Briefly, cells were trypsinized and 100 μl of cell suspension with the concentration 1×10^6 cells/ml were added to 20 ml of phosphate-buffered saline (PBS) or PBS supplemented with 0.1 M sucrose. Cells were equilibrated for 10 min at a room temperature. Cell volume was measured using Beckman-Coulter Multisizer 3 (Coulter Cooperation, USA) equipped with an aperture of 70 μm . The device was calibrated using polystyrene beads of 15 μm diameter (Sigma-Aldrich, Germany) incubated in respective sucrose-free or sucrose-containing PBS. Isoton II was used as a diluent. Median cell volumes were determined from measuring at least 1×10^4 cells. Three independent experiments were performed.

2.3.7. Stereomicroscopy and scanning electron microscopy of scaffolds

The general view and integrity of scaffolds *per se* prior to and after cryopreservation was investigated using a SteREO Discovery.V12 microscope (Zeiss, Germany).

For scanning electron microscopy (SEM) analysis, scaffolds (with and without cells) were washed 3 times (5 min) with 0.1 M cacodylate buffer (CAC, pH 7.4) and fixed for 2 h in 2.5%

glutaraldehyde prepared on the same buffer. After removing fixative by washing, samples were subjected to secondary fixation with 1% osmium tetroxide for 1 h at room temperature. The dehydration step included treatment in graded series of ethanol (25, 50, 70 and 100%) for 10 min. Samples were dried using chemical agent hexamethyldisilazane (HMDS) (Sigma Aldrich, Germany) in concentrations 33%, 50% (in absolute ethanol) for 20 min and 100% overnight in a laminar flow hood. Subsequently, scaffolds were sputter-coated with gold/palladium for 30 s and visualized at 5/15 kV accelerating high voltage and 10 mm working distance in high vacuum using scanning electron microscope (S3400N, Hitachi, Japan). Except from HMDS all other reagents used in this study were from Carl Roth GmbH, Germany.

2.3.8. Cytoskeleton integrity

To investigate the effect of cryopreservation on the cytoskeleton of cells, cell containing scaffolds were washed three times with warm PBS to remove culture medium and fixed with 4% paraformaldehyde (Merck, Germany). After washing, the cell membrane was permeabilized with a 0.5% Triton X100 solution for 5 min followed by washing with PBS. Scaffolds were stained in the dark with bisbenzimidazole H 33342 trihydrochloride (Hoechst, Ex/Em: 346/460 nm) and phalloidin Atto-488 (Phalloidin, Ex/Em: 501/523 nm) at room temperature for 30 min, washed with PBS and visualized using a confocal laser scanning microscope (Zeiss LSM 510 Meta, Germany).

2.3.9. Viability assay of cells seeded in scaffolds

For viability analysis, thawed scaffolds were carefully washed 3 times with PBS, submerged in culture medium and placed in a humidified incubator at 37°C for recovery within 24 h. After incubation, cells were first washed and then stained with 2 μ M Calcein AM and 4 μ M Ethidium Homodimer-1 (EthD-1) (Sigma, USA; live-dead assay), respectively. Both EthD-1 and Calcein AM were excited using argon laser at 514 and 488 nm, respectively, and emission was collected through LP 615 and LP 505 filters, respectively. After staining, samples were washed three times with PBS and analyzed using confocal microscopy. Non-frozen intact scaffolds were used as positive controls. Samples frozen in culture medium were used as negative controls. For quantitative determination of percent of attached viable cells, at least five images were randomly taken of each scaffold (3 scaffolds per experiment) and three

independent experiments were performed. Acquired images were stacked and analyzed using ImageJ 1.49 software (National Institute of Health, USA).

2.4. Scaffold preparation

Scaffolds were fabricated from mineralized collagen nanocomposite by simultaneous collagen fibril reassembly and mineralization as described previously (Gelinsky et al., 2008). Briefly, 1 g collagen type I, isolated from bovine tendon (kindly provided by Syntacoll, Saal/Donau, Germany) and dissolved in 1 L 10 mM hydrochloric acid (company) was mixed with 180 mL of a 0.1 M calcium chloride solution (Carl Roth GmbH, Germany). The pH was adjusted to 7.0 by addition of 168 ml 0.5 M Tris (pH = 7.4) and 22.6 mL of 0.5 M Sørensen phosphate buffer (pH = 7.4). The mixture was incubated at 37°C for 12 h, while the collagen fibrils reassembled and nanocrystalline HAP precipitation occurred simultaneously. The nanocomposite material of homogenously mineralized collagen fibrils was collected by centrifugation. Afterwards, 14 g of the pellet was resuspended in 9 mL of the supernatant. The suspension was then filled in the wells of a 96-well tissue culture polystyrene plate (TPP, Switzerland), frozen at -18°C and subsequently freeze-dried. The sponge-like 3D scaffolds were then cross-linked with 2% (w/v) N-(3-dimethylaminopropyl)-N-ethylcarbodiimide hydrochloride (EDC) solution (Sigma Aldrich, Germany) in 80% (v/v) ethanol for 1 h. Afterwards, scaffolds were rinsed with distilled water, 1% (w/v) glycine solution (Carl Roth GmbH, Germany) and again in water, and finally freeze-dried a second time. Prior to cell seeding, the scaffolds were sterilized by γ -irradiation at 25 kGy.

2.5. Cryopreservation of cells and scaffolds

2.5.1. Cryopreservation of scaffolds using conventional protocol

For conventional cryopreservation, scaffolds were transferred into 1.8 ml cryovials (TPP, Switzerland) containing 0.5 mL culture medium on ice. Double concentrated cryoprotective solution consisting of DMSO (Carl Roth GmbH, Germany) and FBS was added to the samples in a drop-wise manner to avoid osmotic shock and to obtain a final concentration of 10% DMSO and 20% FBS (both v/v). Samples were equilibrated on ice for 10 min and frozen at a cooling rate of 1 K/min down to -80°C using a Mr. Frosty Freezing Container (Thermo Fisher Scientific, Schwerte, Germany). Frozen scaffolds were transferred to an ultra-low temperature Freezer (SANYO, Japan) and stored at -152 °C for at least 5 days before thawing

at 37 °C in a water bath until only a small ice crystal remained (for approximately 2 min). Afterwards, samples were carefully placed into 24-well plates with forceps and washed 3 times with 1 mL of precooled PBS. After addition of growth medium, cell-seeded scaffolds were re-cultivated for 24 h before using in subsequent analyses.

2.5.2. Cryopreservation of cells after electroporation

For cryopreservation of hUCMSCs, cells pulsed in electroporation buffers containing 50-400 mM of sucrose, trehalose and raffinose, respectively. Cells in the concentration of 0.5×10^6 cells/ml were then resuspended in the electroporation buffers containing the same concentrations of sugars and serving as freezing media. Following incubation on ice for 10 min to allow for membrane resealing and cell dehydration cells were placed in 1.8 ml cryovials (TPP, Switzerland) and transferred to alcohol-free cell freezing container CoolCell (Biocision, USA). After overnight storage at -80 °C the cryotubes were transferred into liquid nitrogen containers and stored there for at least 24 h. Thawing of samples was performed in a water bath prewarmed to 37 °C with gentle agitation. As a positive control, a standard cryopreservation medium composed of 10% DMSO (v/v) and 90% FBS (v/v) was used.

2.5.3. Cryopreservation of scaffolds using modified protocol

To increase the efficiency of the cryopreservation of scaffolds, the following protocol was developed:

Scaffolds were seeded the same as described before. After cells were attached, a 24 h preincubation step with 100 mM sucrose was introduced to preload the cells with this sugar. Then, 300 mM sucrose was added to the DMSO based CPA, and the incubation time was extended to 15 min to allow better diffusion into the scaffold. Before freezing, the medium was removed, and this method will be referred as ‘in air’ freezing. Thawing was also modified by swirling the cryovial for 1 minute in a 37 °C followed by addition of 37 °C warm culture medium. A comprehensive overview over the differences between both methods is illustrated in **Fig. 2.3**.

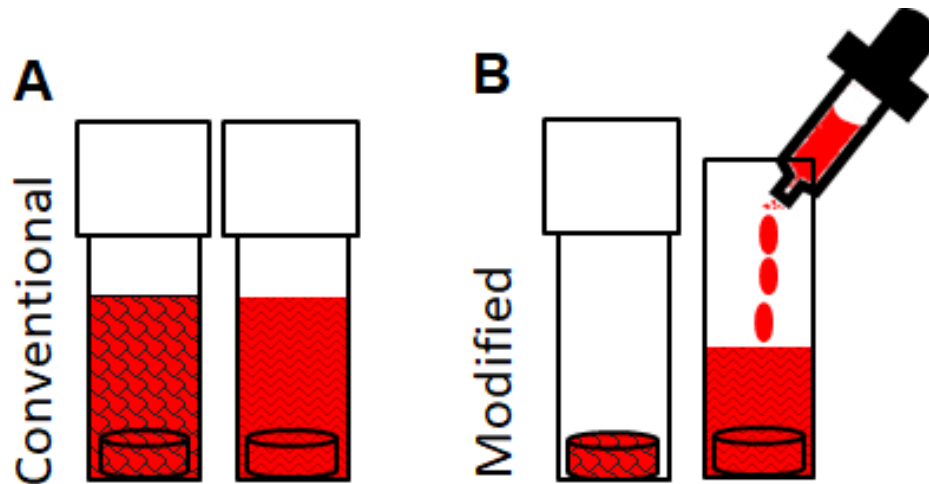


Figure 2.3 Schematic of conventional and modified freezing-thawing procedures.

Conventional cryopreservation implies slow freezing of a sample in 1 ml of CPA and rapid thawing in a water bath (A) until small ice crystals remains. Modified cryopreservation comprises ‘in air’ freezing and thawing for 1 min on a water bath followed by rapid addition of culture medium pre-warmed to 37°C (B).

2.6. Cryomicroscopy

Cryomicroscopy was used to assess the influence of the investigated sugars on the cells, recrystallization and scaffolds. The sample (see below) was placed onto a quartz crucible (Resultec Analytic Equipment, Germany) inside a FDCS196 freeze-drying cryostage (Linkam, UK) which was mounted on an AxioVert M1 m microscope (Carl Zeiss, Germany).

2.6.1. Freezing and thawing behavior of adherent cells

Cryomicroscopy was used for cryopreservation and simultaneous visualization of freezing/thawing process. Briefly, a 5 μ l aliquot of double-concentrated CPAs mixed with trypan blue solution was added to cell monolayers prepared on glass coverslips as described in the **Subsection 2.2.3**. Samples were incubated for 10 min on ice and placed into the quartz crucible.

Cell monolayers were cooled with a ramp of 1 K/min down to -30 °C, held at this temperature for 2 min and rapidly warmed with a ramp of 100 K/min to 4 °C. In order to allow trypan blue to diffuse into cells while not compromising cell survival by CPA after thawing cells were equilibrated at 4 °C for 5 min. Afterwards, multiple images of samples were randomly acquired with Linksys32 software and cell survival was determined by calculating the ratio of

dead cells (trypan blue positive nuclei) to live cells (unstained nuclei) since no detachment in such a closed system was observed.

2.6.2. Evaluation of scaffolds using cryomicroscopy

To better understand the influence of freezing on the scaffold structure and behavior during conventional cryopreservation a cryomicroscopic study using scaffold sections was used. Briefly, paraffin sections of scaffolds with the thickness of 60 μm were prepared using rotary microtome Microm Hm 355S (Microm International GmbH, Germany) and stained with hematoxylin solution modified according to Gill III and 1% eosin Y solution (Merck, Germany). Samples were placed in a quartz crucible (Resultec Analytic Equipment, Germany) and incubated either in PBS or PBS supplemented with 10% DMSO for 5 min at 4°C. The sample was covered with a 12 mm cover glass to prevent evaporation and for transparency. To increase image quality, PBS without FBS was used instead of culture medium. The cryopreservation protocol included the following steps: cooling at 20 K/min to -180 °C, hold at -180 °C for 2 min, thawing at 100 K/min to -10 °C, isothermal annealing at -10 °C for 30 min, secondary cooling at 20 K/min to -50 °C, holding at -50 °C for 1 min and thawing at 100 K/min to 4 °C. The same protocol was used in the analysis of CPA characteristics for modified cryopreservation.

2.6.3. Influence of sugars on recrystallization behavior

To evaluate and understand the ability of sugars (sucrose, trehalose, raffinose) to inhibit ice recrystallization, a cell-free sample aliquot of 2 μl was pipetted on a quartz crucible and covered with a 12-mm cover glass to inhibit evaporation. Samples were incubated at 20 °C for 2 min, cooled with a ramp of 20 K/min down to -180 °C and after holding at -180 °C for 10 min heated with a ramp of 10 K/min to respective annealing temperatures (**Table 3.7**). After isothermal annealing for 30 min the samples were melted with a ramp of 10 K/min back to 20 °C. The projected crystal area was calculated from images using ImageJ software.

2.7. Evaluation of physico-chemical and mechanical properties of scaffolds after modified cryopreservation

All experiments described in this subsection were conducted on cell-free scaffolds. Scaffolds were not pre-treated with 100 mM sucrose before cryopreservation, only experiments with cells involved this step.

2.7.1. Raman microscopy

To investigate the impact of cryopreservation on chemical composition of scaffolds, Raman microscopy was performed. Cell-free scaffolds were frozen in 10% DMSO and 10% DMSO supplemented with 300 mM sucrose prepared on PBS without FBS to reduce background noise from phenol red present in culture media. The respective samples were fixed on a microscope slide with a double-sided glue tape and Raman spectra were acquired using a confocal Raman microscope (Alpha 300 RA, WITec GmbH, Ulm, Germany) in a single point Raman spectrum acquisition mode. The microscope was controlled using a WiTec Control FIVE software (WITec GmbH, Ulm, Germany). Prior to spectral acquisition in a wavenumber range of 200-4000 cm^{-1} , the system was calibrated with Si wafer to achieve the highest intensity at 520 cm^{-1} (crystalline Si-Si bond longitudinal optical phonon vibrations). After calibration the samples were excited using green 532 nm Nd-YAG laser through an optical fiber at 25 mW (accuracy <0.1 mW) as set by TruePower (WITec GmbH, Ulm, Germany) laser power measurement system. The spectral acquisition was conducted at 100x magnification, integration time 10 s and number of accumulations 5. Detection of Raman scattering was performed using a fiber-coupled ultrahigh-throughput UHTS spectrometer with 600 grooves/mm grating. The spectra were then processed using Project FIVE.plus (WITec GmbH, Ulm, Germany) for cosmic ray removal and background subtraction. The spectra were then normalized accordingly to the following equation:

$$I_{norm} = \frac{I_y - I_{min}}{I_{max} - I_{min}}, \quad (2.2)$$

where I_{norm} is normalized intensity (arb. un.), I_y is measured intensity (arb. un.), I_{min} and I_{max} are respective minimum and maximum intensity values.

2.7.2. Fourier transform infrared spectroscopy

Fourier-transform infrared spectroscopy (FTIR) was performed as described in Vásquez-Rivera et al., 2018. Infrared absorption spectra of frozen-thawed and fresh scaffolds were recorded using a FTIR spectrometer (Perkin Elmer, USA), equipped with a triglycine sulfate detector and an attenuated total reflection accessory with pressure arm and diamond/ZnSe crystal. The optical bench was continuously purged with dry air from an FTIR purge gas generator (Whatman, USA). Spectra were acquired at 4 cm^{-1} resolution, 8 co-added interferograms and a wavenumber range of 600-4000 cm^{-1} . An automatic $\text{CO}_2/\text{H}_2\text{O}$ vapor

correction algorithm was used during acquisition of the spectra. Spectral analysis and display was done using Omnic software (Thermo Nicolet, USA). Prior to FTIR measurements, samples were incubated for 1 h in deuterium oxide (D₂O) in order to avoid interference from H₂O absorbance bands in the protein region of the spectrum. To evaluate the overall collagen secondary structure, the amide-I band region (1600–1700 cm⁻¹) was selected. Savitzky-Golay smoothing of second derivative spectra was performed with a 13-point smoothing factor to more clearly resolve contributions from α -helical (~1650 cm⁻¹) and β -sheet (~1630 cm⁻¹) structures of collagen.

2.7.3. Biomechanical testing

In order to investigate the impact of cryopreservation on biomechanical properties of scaffolds, uniaxial compression tests were performed using Instron 5967 Dual Column Testing Machine (Instron, USA). Specifically, fresh and frozen-thawed scaffolds (n = 5) of 5x8 mm (diameter and height, respectively) were analyzed. Under a 50% uniaxial compression the samples were preconditioned with 5 loading cycles at the chart speed 0.3 mm/s in PBS pre-warmed at 37°C. Hence, the correspondent compressive stress at 50% compression, σ (KPa) was calculated, for each time point, according to the equation:

$$\sigma = \frac{F}{A}, \quad (2.3)$$

where F (N) is the recorded force, A (mm²) is the original cross-sectional area of an undeformed scaffold.

2.7.4. Mercury intrusion porosimetry

Pore size analysis experiments were executed using a mercury intrusion porosimeter PoreMaster 60 (Quantachrome GmbH, Germany). Pressures ranging from 1 to 60,000 PSI were applied in a high-pressure station. The pressure was exerted onto the scaffolds using a penetrometer made of glass as a specimen container. A penetrometer with a stem volume of 0.5 cm³ and a sample container of 3.8 cm length was used. In these experiments, the width of the distribution was represented by span calculated as follows:

$$Span = \frac{x_{90} - x_{10}}{x_{50}}, \quad (2.4)$$

where x_{10} , x_{50} and x_{90} are 10, 50, and 90 percentiles of the cumulative percent undersize plot, respectively. Span is the measure of the width of the distribution. The smaller the span is the less pore dispersity is found. In general, x_{90} is the pore diameter for which 90% of the sample pore sizes are below the corresponding measured value, x_{10} is the pore diameter for which 10% of sample pore sizes are below the corresponding measured value and x_{50} is a median diameter.

2.7.5. Swelling test

The effect of cryopreservation procedure on water uptake capacity of scaffolds was determined by performing a swelling test. In tissue engineering, swelling behavior is a crucial parameter for implantation. Briefly, non-frozen and frozen-thawed scaffolds were incubated in water for 24 h at room temperature. A weight of scaffolds before and after placement in water was determined using analytical microbalance Sartorius Quintix 224-1CEU (Sartorius, Germany). Swelling ratio was calculated using the following equation:

$$S = \frac{W_s - W_d}{W_d} \times 100\%, \quad (2.5)$$

whereas W_s is a swollen weight of a scaffold (g) and W_d is a dry weight (g). The values were expressed as mean \pm SD ($n = 5$).

2.7.6. Differential scanning calorimetry

Differential scanning calorimetry (DSC) measurements were performed to determine the heat capacity of dry scaffolds and scaffolds frozen-thawed with CPAs. Samples were analyzed using differential scanning calorimeter with a Netzsch DSC 204F1 Phoenix instrument (Netzsch-Geraetebau GmbH, Selb, Germany). Pulverized samples alone or covered with CPAs with the total mass of approximately 10 mg were added into a 25 μ L aluminum pans. A cooling/heating protocol included the following steps: cooling from 20 $^{\circ}$ C at 20 K/min to -180 $^{\circ}$ C followed by 10 min holding at -180 $^{\circ}$ C and heating at 10 K/min to 30 $^{\circ}$ C. An empty pan was processed in the same way for correction. Data from 3 independent experiments were averaged and correction subtracted.

Specific heat capacity of samples (C_p) was calculated from DSC thermograms recorded using Netzsch software according to the below equation and expressed in J/g \cdot K:

$$C_p = \frac{dQ_{(P+S)} - dQ_{(P)}}{dt} / \left(m \times \frac{dT}{dt} \right), \quad (2.6)$$

where $dQ_{(P+S)}/dt$ is measured heat flow of pan and a sample (J/s) and $dQ_{(P)}/dt$ is measured heat flow of an empty pan (J/s), dT/dt is a heating rate (K/s) and m (g) is the mass of the sample.

In addition, glass transition temperatures of CPAs in the system CPA+scaffold were also calculated.

In order to determine glass transition and melting temperatures of the sugar containing solutions, approximately 10 mg were added into 25 μ L aluminum pans and hermetically sealed whereas an empty pan was used as reference. For DSC measurements, the same cooling/heating protocol was used as in the cryomicroscopy studies for sugars except with no isothermal annealing step. Data were recorded, and thermal events were determined from the obtained DSC thermograms using the software Proteus[®] (Netzsch).

2.7.7. Determination of thawing rate

To experimentally determine thawing rates, two scenarios were compared. In both scenarios, scaffolds were equilibrated for 15 min on ice in the corresponding CPAs: either 10% DMSO/20% FBS or the same with 300 mM sucrose before rapid freezing by immersion into LN. Samples were positioned on the bottom of conventional polypropylene cryovials and thermocouples were inserted approximately into a middle of a sample. Start and end recorded temperatures were -180 °C and 20 °C, respectively. For conventional thawing, scaffolds frozen in 1 ml of CPA solution were rapidly thawed in a 37 °C warm water bath. In modified thawing, scaffolds frozen ‘in air’ were thawed by holding in a water bath for 1 min followed by addition of 1 ml of pre-warmed culture medium. In all cases thawing rates showing linear dependency for two regions of interests (from -180 to -110 °C and -4 to 4 °C) and accordingly time required to reach 4 °C were calculated. Cooling and thawing profile were recorded using an eight-channel RedLab module (Meilhaus Electronic, Germany) with copper-constantan thermocouples and in-house software written with the National Instruments LabVIEW 2007.

2.7.8. Osmolality measurements

The osmolality of sucrose solutions with and without DMSO was measured by an Osmomat 030 cryoscopic osmometer (Gonotec, Germany). After calibration with bidistilled water and

0.3 Osm/kg calibration standard, every test solution was analyzed at least 5 times with a sample volume of 50 μ L.

2.8. Western blotting

To analyze the activation of p38 MAPK-kinase (mitogen-activated protein kinase) in the course of sucrose pre-treatment, western blotting was carried out. Cell lysates were prepared using kinase buffer (50 mM Tris-HCl (pH 7.5), 1 mM EGTA, 1 mM EDTA, 1 mM sodium orthovanadate, 50 mM sodium fluoride, 1 mM sodium pyrophosphate, 0.27 M sucrose, 1% (v/v) Triton X-100, 0.1% (v/v) 2-mercaptoethanol, and complete proteinase inhibitor cocktail). Protein concentration was determined using Bradford assay (Bio-Rad). To equalize amounts of protein 4 \times Laemmli's sodium dodecyl sulfate (SDS) sample buffer (40% glycerol, 4% SDS, 4% β -mercaptoethanol, 0.4 M Tris-HCl, pH 6.7, and 2 mg/ml bromphenol blue) was used. Protein samples (33 μ g) were separated on a 7.5-16% gradient polyacrylamide gradient gel by electrophoresis. As a house-keeping/loading control, elongation factor 2 (EF2) was used. Proteins were transferred from the gels to Hybond ECL membranes (Amersham Pharmacia Biotech). Blots were incubated for 30 min in phosphate buffered saline with Tween-20 (PBS containing 1% Tween-20 and 5% powdered skim milk). After blocking membranes were incubated overnight with the primary antibodies at 4 °C and for 1 h with horseradish peroxidase-conjugated secondary antibodies (diluted 2,000-fold) at room temperature. Anti-phospho-p38 MAPK were from Cell Signaling Technology and anti-EF2 antibodies were from SantaCruz. Blots were developed with self-made ECL detection kit (solution A: 1,2 mM luminol in 0,1 M Tris-HCl (pH 8.6); solution B: 6,7 mM p-coumaric acid in DMSO; solution C: 35% H₂O₂; ratio A : B : C is 3333 : 333 : 1), and the digital chemiluminescence images were taken by a Luminescent Image Analyser LAS-3000 (Fujifilm).

2.9. Statistics

To test the obtained data for normality, a Shapiro–Wilk test was performed. Normally distributed data were reported as mean \pm standard deviation (SD) and analyzed whether using parametric Student t-test or one-way analysis of variance (ANOVA) followed by Tukey's post hoc test for multiple comparisons. Not normally distributed data were reported as median \pm interquartile range (IQR) and analyzed using Kruskal-Wallis test. For representation of quantitative data and their statistical analysis Graph Pad Prism 8.0 (GraphPad Software, USA)

was used. Cut-off p-values less than 0.05 were considered as statistically significant. For convenience of presentation, differences between groups were shown using letters. For all variables with the same letter, the difference between the means is not statistically significant. If two variables have different letters, they are significantly different.

3. Results

3.1. Cryopreservation of *cj*MSCs on 2D carriers and the effect of sucrose

In this subchapter, the effect of sucrose loading, cell attachment on glass and its effect on cryopreservation of attached cells are presented.

3.1.1. The effect of sucrose loading on cell viability, attachment and response to hyperosmolar stress

Cytotoxicity testing of different sucrose concentrations using resazurin reduction assay demonstrated that cell metabolic activity drastically declined by $46.13 \pm 6.70\%$ and $76.36 \pm 5.56\%$ after culturing of cells in the presence of 200 mM and 250 mM sucrose (**Fig. 3.1**). This reduction was correlated with cell detachment and could be in part explained by enhanced osmotic stress which adherent *cj*MSCs could not tolerate over 24 h. The osmolality values of both solutions are 565 mOsm/kg for 200 mM sucrose and 631 mOsm/kg for 250 mM, respectively. Although statistically not significant, slight reduction in cell viability by $5.57 \pm 4.76\%$ in 150 mM group was also observed. Application of 50 mM and 100 mM of sucrose did not cause any toxic effect on cells which is confirmed by slight increase in reduction percent of resazurin in this group compared to corresponding pre-treatment controls by 4.03 ± 1.73 and 4.43 ± 2.77 , respectively (**Fig. 3.1**).

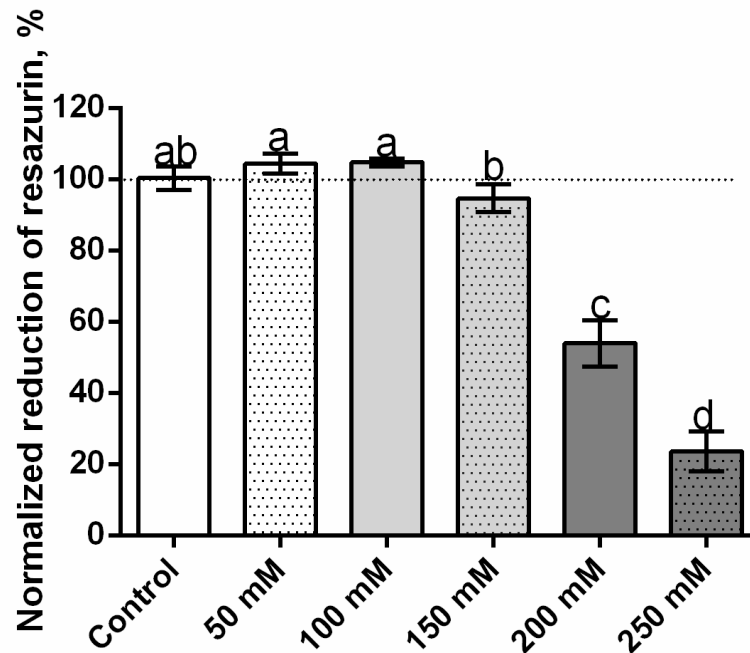


Figure 3.1 Influence of 24 h incubation with different sucrose concentration on cell viability

Results of resazurin reduction assay for different sucrose concentrations used for cell pre-treatment normalized to their respective controls (before pre-treatment). Dotted line indicates a 100 % value for all groups before pre-treatment. Values are shown as mean \pm SD from three independent experiments performed in triplicates. Different letters denote statistically significant differences between groups (One-way ANOVA, $p < 0.05$)

In addition, microscopic examinations revealed altered cell shape and partial cell detachment in the 150 mM (**Fig. 3.2 D**) group probably due to increased stiffness of *cj*MSCs cytoskeleton induced by osmotic imbalance caused by intra- and extracellular sucrose at this concentration (osmolality 505 mOsm/kg). In contrast, cells cultured in the presence of both 50 mM (388 mOsm/kg, **Fig. 3.2 B**) and 100 mM (443 mOsm/kg, **Fig. 3.2 C**) sucrose had similar morphology with control cells (**Fig. 3.2 A**). Unlike control cells, concentration-dependent increase in sucrosome amount and size was observed in all pre-incubated cells, which in case of 150 mM and higher concentrations may also contribute to increased osmotic stress and cell detachment.

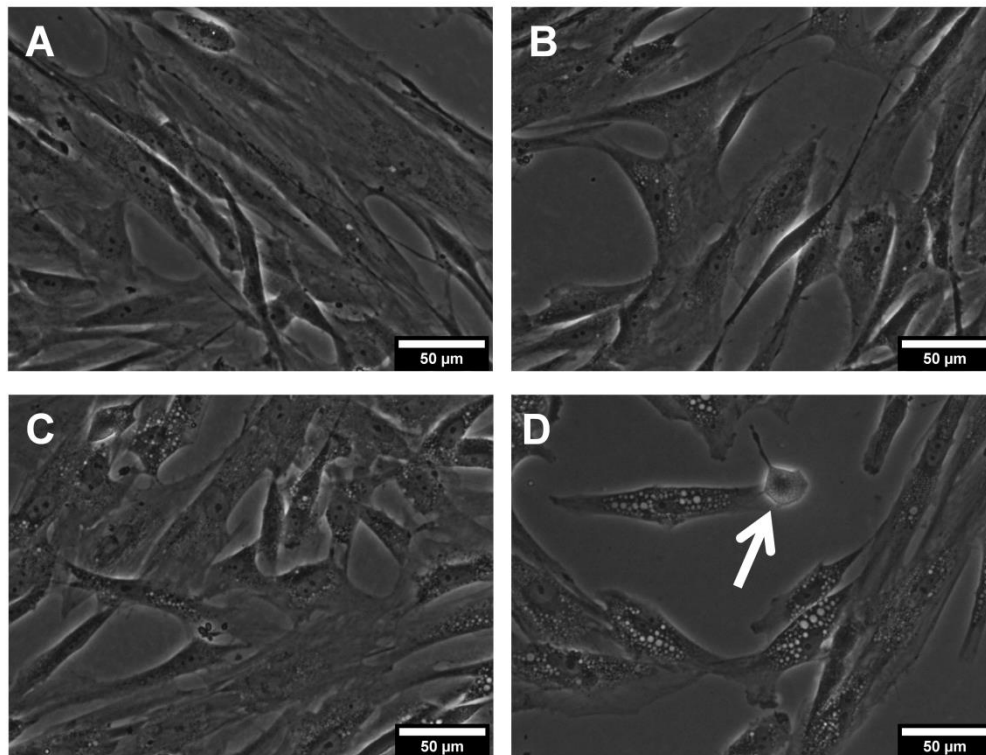


Figure 3.2 Influence of sucrose concentration on cell morphology

Representative bright field pictures of *cj*MSCs: A – control cells; B, C and D – cells pre-incubated for 24 h in 50, 100 and 150 mM of sucrose, respectively. Sucrosomes are seen as phase bright inclusions in cell cytoplasm. The white arrow points to a detaching cell in 150 mM group in which enlarged sucrosomes are clearly discernable.

As a compromise between viability and adverse effects, 100 mM sucrose was chosen for preincubation of cells prior to cryopreservation. Interestingly, in 24 h live cell imaging, *cj*MSCs showed similar movement pattern compared to non-treated cells (data not shown).

Moreover, actin cytoskeleton of *cj*MSCs was not affected by pre-treatment with 100 mM sucrose and no cell detachment was observed (**Fig 3.3**). This suggests the steady-state adaptation dynamics of cells subjected to mild osmotic stress within 24 h.

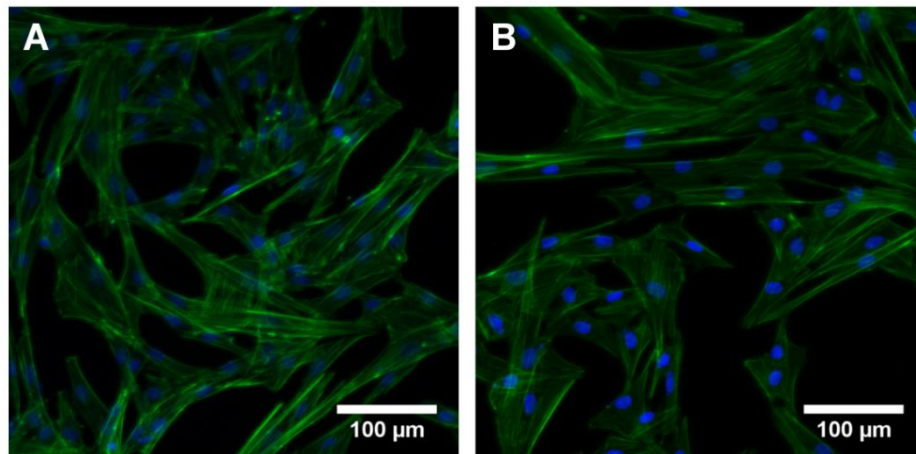


Figure 3.3 Influence of 24 h incubation with sucrose on cytoskeleton
Confocal microscopy images showing phalloidin stained F-actin (green) and DAPI stained (blue) nuclei of control (A) and sucrose-loaded *cj*MSCs (B). No visually detectable changes in cytoskeleton and spreading of cells exposed to 100 mM sucrose were revealed.

To characterize the sucrosomes, sucrose-loaded *cj*MSCs were treated with invertase for 24 h. This enzyme hydrolyzes sucrose to fructose and glucose moieties. As a result, in the invertase-treated cells sucrosomes eventually disappeared (**Fig. 3.4 D vs. B**, respectively) whereas in the culture media group they were still noticeable (**Fig. 3.4 C vs. A**, respectively).

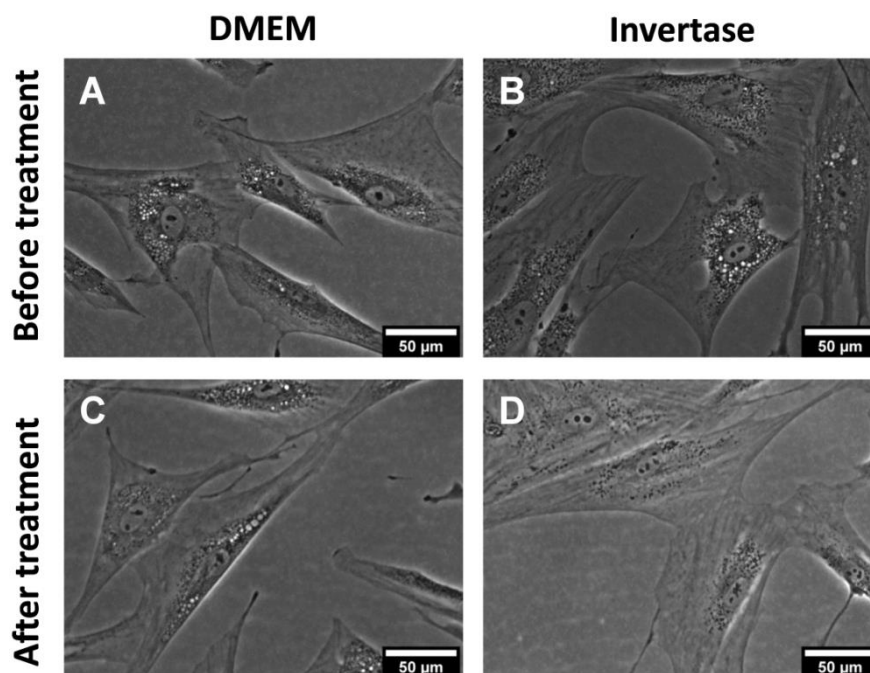


Figure 3.4 Effect of invertase on sucrosomes
Bright field pictures of *cj*MSCs after 24 h preincubation with 100 mM sucrose followed by re-culture in sucrose-free DMEM and treatment with 1 mg/ml invertase from baker's yeasts for additional 24 h, respectively. Presence of sucrosomes in control cells (A, C) and their absence in invertase-treated cells (B, D) suggest efficient invertase-mediated accelerated degradation of sucrose.

Another method to investigate the sucrose uptake is the use of LY which has a molecular weight close to the one of sucrose (457 vs. 342 g/mol, respectively). A 24 h incubation with LY in the presence or absence of sucrose revealed that LY was incorporated into more than 90% of cells regardless of treatment. However, the fluorescent pattern was very different in both experimental groups. Punctate fluorescence bodies distributed throughout the cytoplasm were uncovered in cells cultured in LY alone. Co-culture of LY and sucrose exhibited more diffuse fluorescence located in perinuclear region with no or little punctate bodies.

Of note, cells containing sucrosomes were more spread than control cells. This can be seen on the morphology of the cells as depicted in **Fig. 3.5**. *cj*MSCs are capable of internalizing LY which is roughly the same size as sucrose.

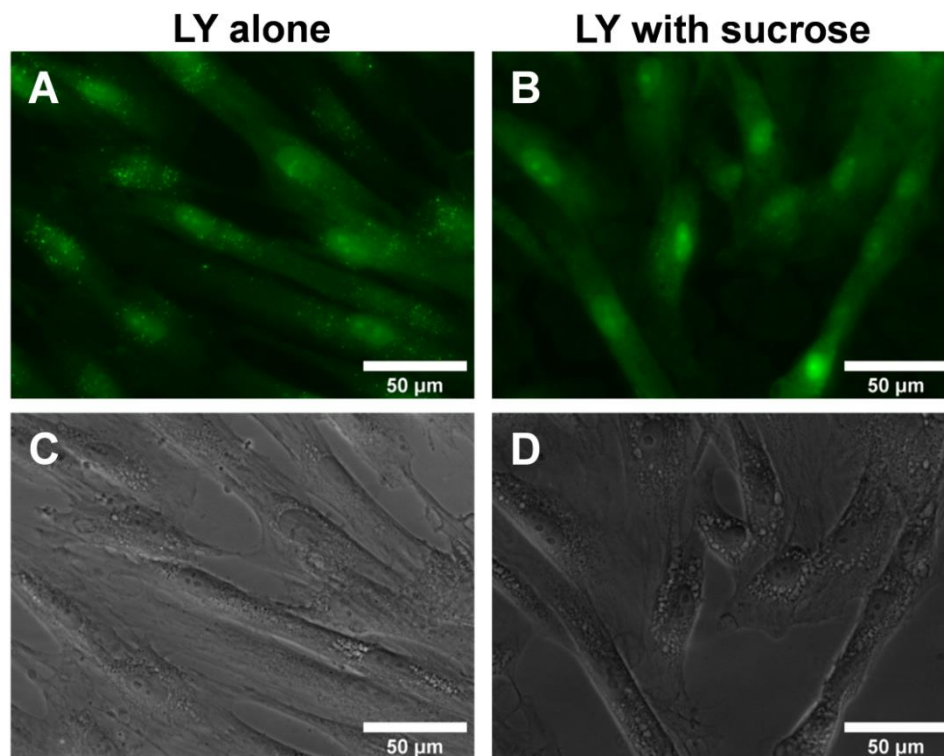


Figure 3.5 Impact of LY and sucrose on sucrosome formation

Fluorescence pictures of *cj*MSCs labeled for 24 h with Lucifer Yellow in the presence or absence of 100 mM sucrose. Cells not exposed to sucrose exhibit typical punctate fluorescence (A) and no sucrosomes (C) whereas cells exposed to sucrose exhibit more diffuse perinuclear fluorescence (B) and sucrosomes (D).

Cryomicroscopy revealed that pretreated suspension cells are more resistant to IIF than non-pretreated and have much bigger size (see **Fig. 3.6 A, B**). The intracellular ice propagation in sucrose-loaded cells (**Fig. 3.6 B and D**) was rather different from that of seen in control cells (**Fig. 3.6 A and C**). The majority of sucrose loaded cells exhibited intracellular ice at the cell

periphery and did not advance further. In contrast, in the control cells ice formation was more observed in the central part of a cell.

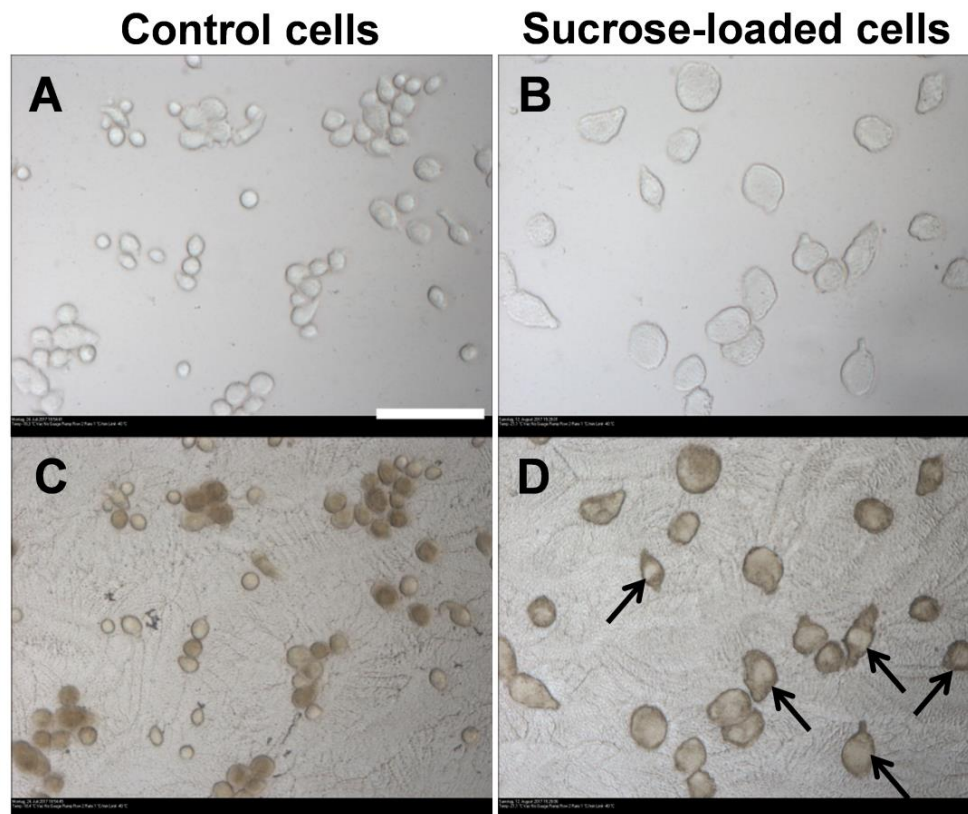


Figure 3.6 Effect of pretreatment on IIF

Cryomicroscopy pictures showing the character of IIF in suspended sucrose-free and loaded cells frozen in culture medium: A and B – control and sucrose-loaded cells before nucleation; C and D – development of IIF in control and sucrose-loaded cells, respectively. Darkening preferentially localized to the peripheral zone in sucrose-loaded cells without its further propagation with lower temperatures may suggest that intracellular sucrose blocks this process. Scale bar represents 100 μm .

The effect of sucrose loading on cell volume changes was evaluated on dissociated *cj*MSCs using Coulter Counter analyzer. Cells treated with 100 mM sucrose significantly increased their cell volume from $3222 \pm 692.0 \mu\text{m}^3$ (control) to $4830 \pm 649.9 \mu\text{m}^3$ (sucrose) which correlates to a 30% increase (**Fig. 3.7**).

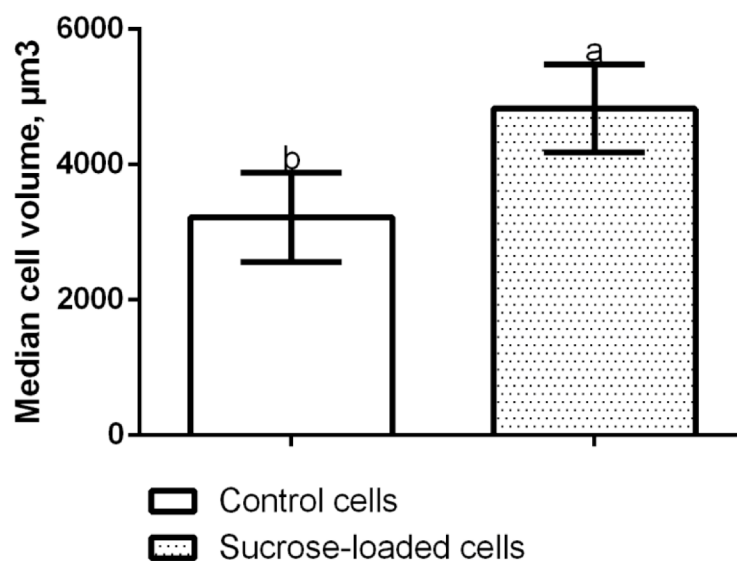


Figure 3.7 Volumetric change in *cj*MSCs when they were loaded with 100 mM sucrose

Graph with the results of volumetric response of *cj*MSCs to sucrose loading. Error bars represent standard deviations. Different letters denote significantly different means of the studied variables according to one-way ANOVA ($p < 0.05$). Cell volume post incubation in 100 mM sucrose significantly increased.

Western blot analysis of the MAPK-kinase p38 showed its increased phosphorylation after 1 h incubation with sucrose and decreased over time to basal level (see **Fig. 3.8**). Although 6h after activation pP38 was still visible, its activity returned to basal levels following 24 h after challenging with sucrose.

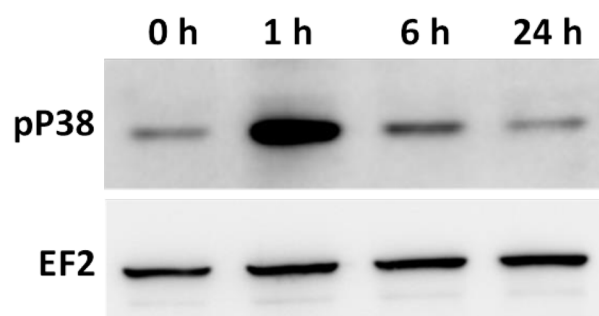


Figure 3.8 Western blot of phosphorylated form of MAPK p38

The results of western blotting showing the effect of sucrose-loading on the dynamics of p38 activation in *cj*MSCs. Upper panel: the expression of phosphorylated form of p38; lower panel: the expression EF2 used as a loading control. The activity of p38 changes over time suggesting compensatory cell adaptation to hyperosmolar sucrose treatment.

To summarize this subchapter, *cj*MSCs could be safely loaded with sucrose for cryopreservation purposes by endocytotic uptake, with optimal sucrose concentration being 50-100 mM. Cell metabolic activity and attachment are not compromised by pre-treatment with chosen sucrose concentrations. The sucrose loading exerted time-dependent change in activation of p38 by phosphorylation and shows it strongest expression after 1 h incubation.

3.1.2. The effect of combined application of intra- and extracellular sucrose on DMSO-based cryopreservation of *cj*MSCs in adherent state

As expected, the viability of suspended *cj*MSCs frozen using slow cooling under the protection of DMSO demonstrated high cell viability at 95.00 ± 1.85 %. However, our preliminary screenings on viability of the same cells but frozen in adherent state showed a drastic decrease in cell viability to 85% for the 10% DMSO/20% FBS group implicating that the adherent *cj*MSCs are more vulnerable to freezing injury than the suspension cells. Instead of raising DMSO concentration (owing to toxicity issues) in further studies the freezing solutions was supplemented with extracellular sucrose. Sucrose is known to have good dehydration, membrane stabilization and glass formation properties. Therefore, in the next steps, 100 mM sucrose was used to pre-treat *cj*MSCs seeded on coverslips. During the freezing experiment the applied CPA was supplemented with sucrose concentrations in the range of 0-500 mM. It was found that supplementation of DMSO with sucrose gave a gradual increase in cell survival from $15.85 \pm 5.78\%$ (DMSO alone) over 28.43 ± 10.84 (100 mM sucrose + DMSO), $41.29 \pm 8.3\%$ (200 mM sucrose + DMSO) and up to $53.00 \pm 8.23\%$ (300 mM sucrose + DMSO) as shown in **Fig. 3.9**. However, higher concentrations of sucrose (400 and 500 mM) not only affected the cryopreservation outcome, but also lead to significant reduction of cell survival ($21.89 \pm 7.25\%$ for 400 mM sucrose and $26.66 \pm 8.16\%$ (500 mM sucrose)).

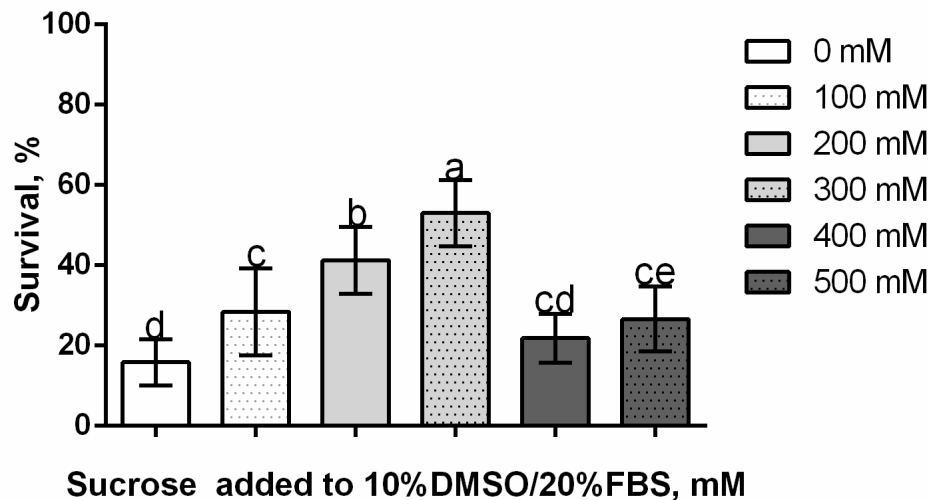


Figure 3.9 Impact of sucrose containing medium on adherent cell cryopreservation

Quantification of cell survival after cryopreservation using DMSO supplemented with 0-500 mM sucrose. Extracellular sucrose increases cell survival with a maximum reached at 300 mM concentration. Different letters denote statistically significant differences between groups (One-way ANOVA, $p < 0.05$).

Adherent cells frozen using the cryomicroscope and slow cooling were also analyzed for IIF. Cells were incubated with either DMEM or a mixture of 10% DMSO and 20% FBS with and without 300 mM sucrose. Since it is still impossible to observe intracellular ice in cells frozen in a 3D scaffold using optical methods, such monolayer models may be informative with the respect to detecting IIF in adherent cells. We observed IIF in *cj*MSCs frozen in the absence of any CPA and in the presence of DMSO with and without sucrose which was manifested as a characteristic cell darkening (**Fig. 3.10**). However, detailed analysis of IIF in adherent cells was not possible due to limited system resolution.

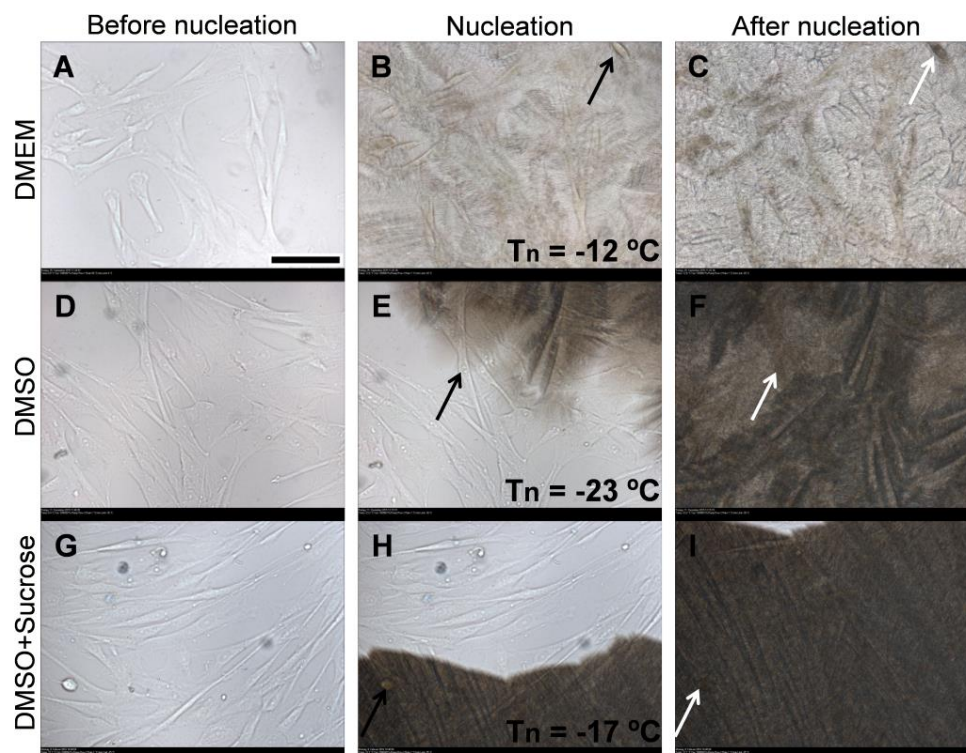


Figure 3.10 Analysis of ice formation in adherent cells

Cryomicroscopic pictures of adherent *cj*MSCs frozen in culture medium or 10% DMSO/20 FBS with and without 300 mM sucrose. Upper panel demonstrates the dynamics of IIF in culture medium: A - before nucleation; B - at nucleation and C – after nucleation. Middle panel shows the same freezing events in DMSO group: D, E and F, respectively. Lower panel indicates the IIF in sucrose group: G, H and I, respectively. Intracellular ice is indicated by transition through black to white arrows and corresponding nucleation temperatures are shown. Scale bar represents 100 μm .

The observed reduction in cells survival could be attributed to detrimental effects of excessive osmotic stress upon exposure to CPA before crystallization and freezing injury due to ‘solution effects’. During slow cooling prolonged exposure to hyperosmolar freeze-concentrated CPAs may result in cell toxicity. As expected, with increasing sucrose content the osmolality increases linearly from 2229 mOsm/kg (10% DMSO only) to 3333 mOsm/kg (10% DMSO in combination with 500 mM sucrose) as summarized in **Table 3.1**.

Table 3.1 Osmolality of freezing solutions containing 10% DMSO/20% FBS supplemented with 0-500 mM sucrose.

Concentration of sucrose, mM	Osmolality, mOsm/kg
0	2229 \pm 102
100	2535 \pm 178
200	2799 \pm 88
300	2968 \pm 62
400	3113 \pm 24
500	3333 \pm 21

3.2. Effect of freezing on cells seeded onto 3D collagen-HAP scaffolds

3.2.1. Appearance and cytocompatibility of collagen-HAP scaffolds

In the present study, using freeze drying 3D porous uniform sized scaffolds having cylindrical shape (5 or 8 mm in diameter and 3 mm in height) were fabricated from mineralized collagen (**Fig. 3.11 A**). A more detailed structural analysis of scaffold structure using SEM revealed interconnected open pores which are preferential for successful cell ingrowth (**Fig. 3.11 B**).

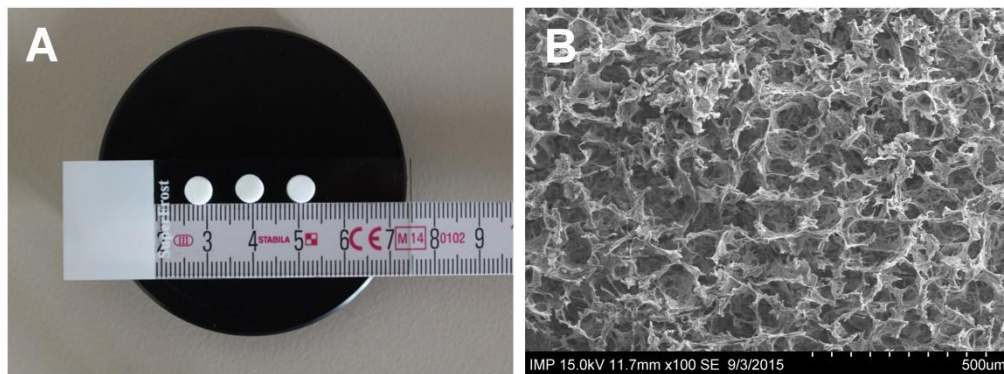


Figure 3.11 Size and structure of collagen-HAP scaffolds

General view of 3D scaffolds having cylindrical shape (A) and SEM picture of porous scaffolds with interconnected pores (B).

Cytocompatibility studies involving *cj*MSCs demonstrated that fabricated scaffolds supported cell attachment and spreading within 3D scaffold environment. **Fig. 3.12 A** demonstrates that *cj*MSCs attached to scaffold surface exhibit characteristic spindle-like shape and filopodia whereas **Fig. 3.12 B** depicts typical arrangement of actin cytoskeletal networks within a 3D scaffold as reconstructed by confocal z-stacks. Cells show that the actin cytoskeleton is intact and spreading of cells in 3D scaffolds is different compared to cells attached to a 2D structure such as glass as was shown on the Fig. 3.3 A.

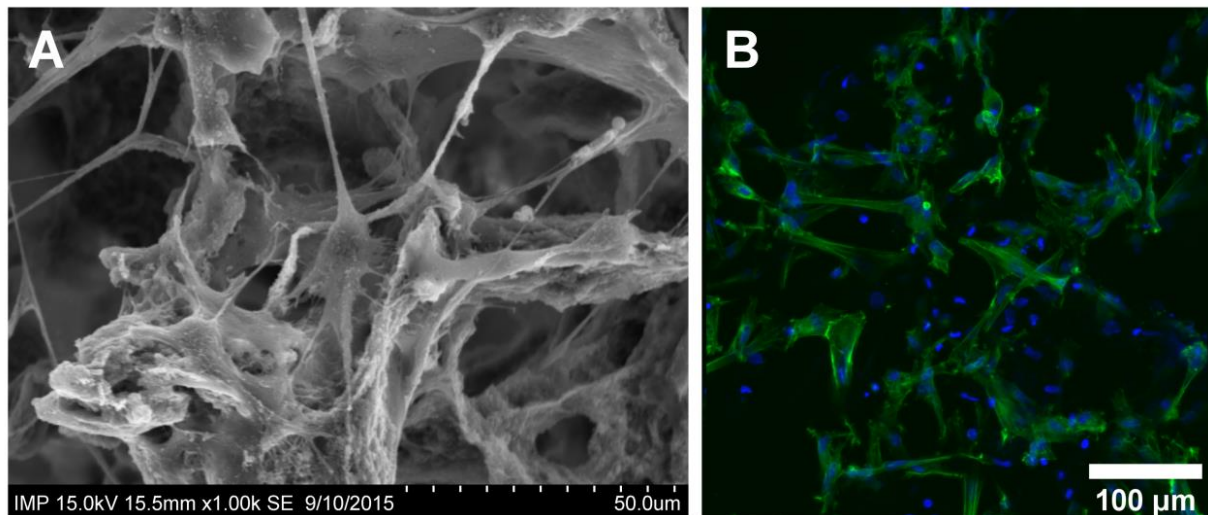


Figure 3.12 Attachment and spreading cells within 3D scaffolds

Representative SEM (A) and confocal microscopy images (B) of *cj*MSCs grown on collagen-HAP scaffolds for 1 day. Actin cytoskeleton (green fluorescence) is stained with phalloidin and nuclei (blue fluorescence) are stained with Hoechst. Both images suggest cell growth and proliferation on the scaffolds.

3.2.2. Conventional cryopreservation of 3D collagen-HAP scaffolds seeded with *cj*MSCs

After confirmation of scaffold cytocompatibility the whole cell-seeded constructs were cryopreserved using standard cryopreservation protocol (slow cooling, application of 10% DMSO/20% FBS, thawing on a water bath). The integrity of scaffolds and attachment of *cj*MSCs in control and frozen groups were studied by stereomicroscopy and confocal microscopy after Hoechst/Phalloidin staining, respectively. Post-preservation assessment revealed different degrees of damage to scaffolds from partial disintegration (**Fig. 3.13 B vs. A**) to complete fragmentation. Second phenomenon observed was massive cell detachment (**Fig. 3.13 D vs. C**) which led to a very low amount of cells and low viability (around 40%, data not shown). Cells inside the damaged scaffolds also show stress fibers and a disrupted cytoskeleton.

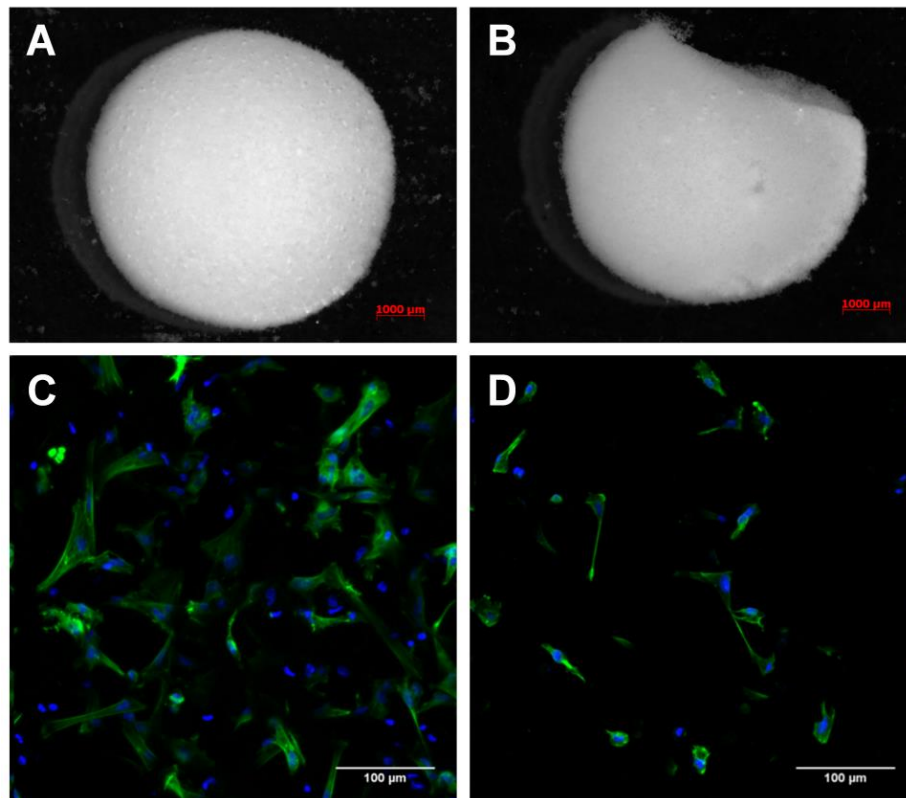


Figure 3.13 Effect of conventional cryopreservation on scaffolds and cells

Stereomicroscopy pictures of collagen-HAP scaffolds before (A) and after (B) conventional cryopreservation. Cryodestruction of a scaffold is clearly visible. Confocal microscopy images of cells stained with Hoechst/Phalloidin before (C) and after (D) conventional cryopreservation. F-actin exhibits green fluorescence and cell nuclei are stained in blue. Fresh cells demonstrate intact cytoskeletal structure whereas frozen cells have strained cell cytoskeleton. Overall decrease in cell number is seen from the representative picture.

3.2.3. Effect of freezing on ice formation and its impact on the collagen-HAP scaffolds

Cryomicroscopic analysis revealed several phenomena happening during freezing which may be associated with the loss of scaffold integrity. First, ice cracking in DMSO and PBS after passing the temperature around -120°C (**Fig. 3.14 C** and **G**, respectively) was found. Second, after reaching the annealing temperature, pronounced recrystallization was seen by time-dependent enlargement of ice crystals (**Fig. 3.14 D** and **H**). In a timeframe of 30 min rapid crystal growth was noticed in both groups with crystals developed in PBS being much larger than that of in DMSO. **Fig. 3.14 A, E** and **B, F** show scaffolds at the equilibration stage with CPA and during nucleation in PBS and 10% DMSO, respectively.

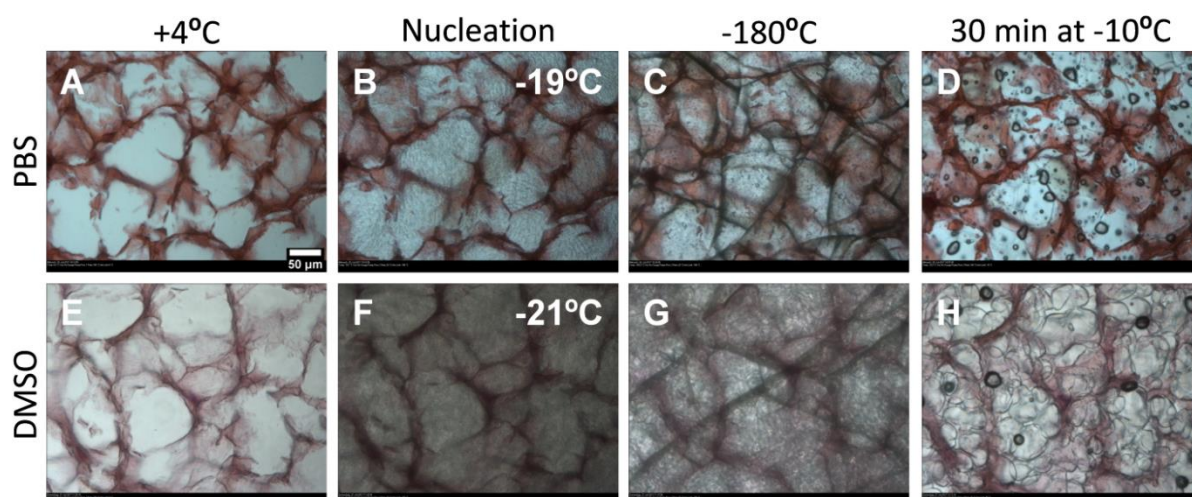


Figure 3.14 Cryomicroscopic analysis of scaffolds during freezing and isothermal annealing

Representative cryomicroscopic images of scaffold sections frozen in PBS (upper panel) and 10% DMSO/20% FBS (lower panel). Images A, E – equilibration with CPA; B, F – nucleation (nucleation temperatures are indicated); C, G – sample cracking; D, H – ice crystals after isothermal annealing for 30 min. Scale bar – 50μm.

To increase the efficiency and decrease the structural damages to the scaffolds a modified cryopreservation protocol was established.

3.2.4. Impact of modified cryopreservation on physico-chemical and mechanical properties of cell-free scaffolds

The effect of cryopreservation on scaffold chemical properties with a focus on the vibrational modes of functional groups characteristic of hydroxyapatite and collagen has been investigated. They appeared to be unaffected by modified cryopreservation both under protection of DMSO alone and with sucrose. For all studied Raman-peaks presented on **Fig. 3.15** and in **Table 3.2** corresponding assignments and wavenumbers are listed. Interestingly, the CH_2 stretching at 3000 cm^{-1} show a reduction in intensity for the cryopreserved scaffolds compared to control.

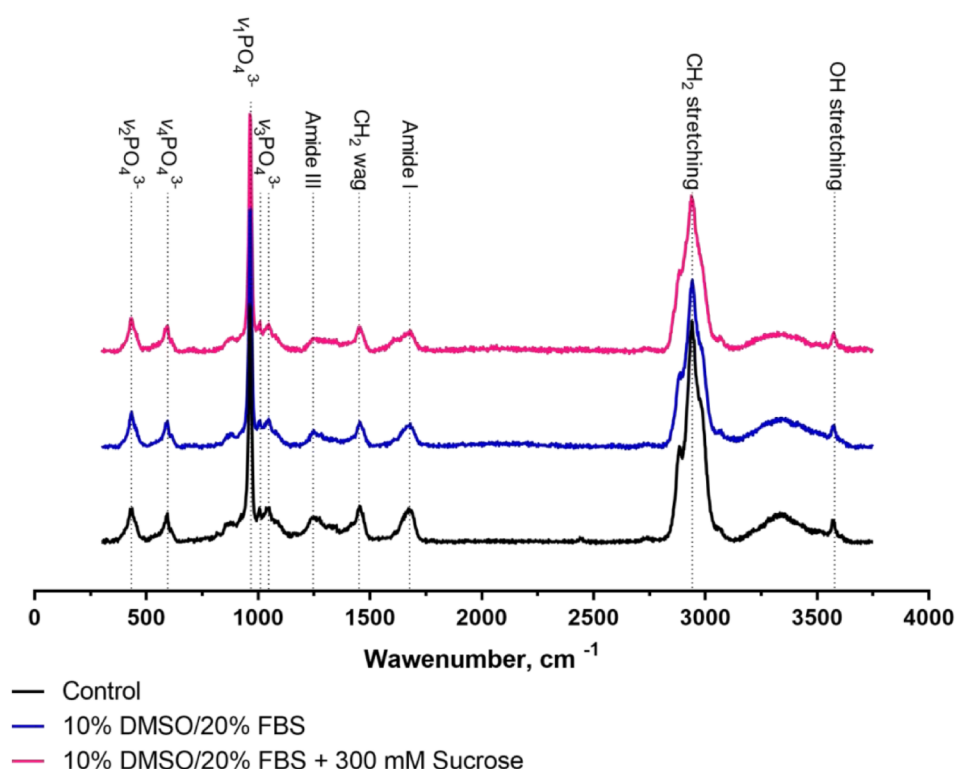


Figure 3.15 Raman analysis of scaffolds frozen vs. fresh

Typical Raman peaks for fresh and frozen samples presented in the wavenumber range 300–3700 cm^{-1} . No apparent shifts in characteristic peaks were observed after modified cryopreservation.

Table 3.2 . Raman spectral assignments for collagen and HAP.

Substance	Wavenumber cm^{-1}	Assignments (Carden and Morris, 2000)
Collagen	2840–2986	CH_2 stretching
Collagen	1595–1720	Amide I
Collagen	1243–1269	Amide III
Collagen	1447–1452	CH_2 wag
Hydroxyapatite	3572–3575	OH stretching
Hydroxyapatite	961	$\nu_1\text{PO}_4^{3-}$
Hydroxyapatite	430	$\nu_2\text{PO}_4^{3-}$
Hydroxyapatite	1006–1055	$\nu_3\text{PO}_4^{3-}$
Hydroxyapatite	1046	$\nu_3\text{PO}_4^{3-}$, triply degenerate (Khan et al., 2013)
Hydroxyapatite	590	$\nu_4\text{PO}_4^{3-}$

Next, FTIR spectroscopy was used to specifically characterize the amide-I band region of collagen (1595 – 1720 cm^{-1}) after cryopreservation. **Fig. 3.16** shows second derivative spectra of the amide-I region of collagen-HAP scaffolds prior to and after cryopreservation. Inspection of this region revealed changes in the secondary structure of collagen. These are

characterized by shifts to lower wavenumber in α -helix and a relative decrease in the absorbance of α -helix structures and an increase in the β -sheet structures in the cryopreservation group.

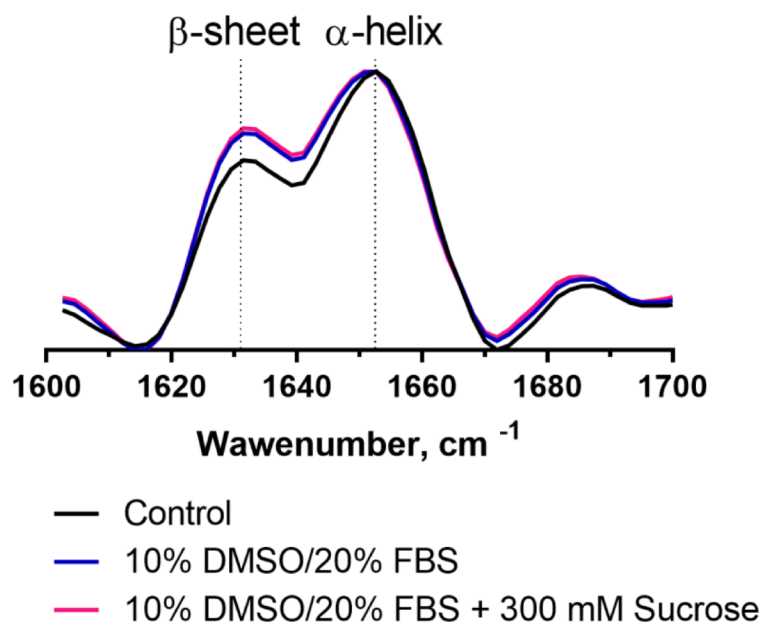


Figure 3.16 FTIR profiles of collagen-HAP scaffolds before and after cryopreservation

Normalized second derivative spectra in the $1700\text{--}1600\text{ cm}^{-1}$ region for frozen and control collagen-HAP scaffolds. Shifts in α -helix band suggest changes in a secondary structure of collagen after cryopreservation.

Mechanical properties are important for scaffolds and to study these, compression tests were performed. Analysis of data on compression of cell-free scaffolds revealed a significant reduction in compressive stress of both cryopreserved groups. Onset of plastic deformation in frozen samples was accompanied by a softening which was followed by gradual increase in compression but lagging behind control and suggesting that they were more deformable than control after preconditioning steps (**Fig. 3.17, A**). Calculation of compressive stress revealed a 25% reduction in specimens frozen with ($20.60 \pm 1.34\text{ kPa}$) and without sucrose ($20.88 \pm 1.10\text{ kPa}$) compared to control ($27.48 \pm 1.88\text{ kPa}$, **Fig. 3.17, B**). Scaffolds were frozen using the modified cryopreservation protocol.

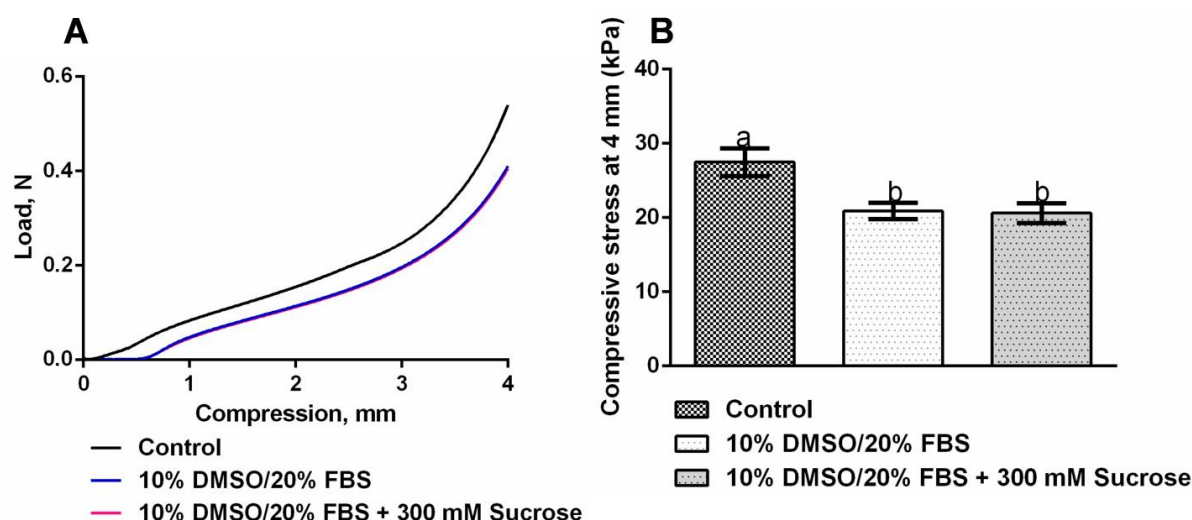


Figure 3.17 Mechanical properties of scaffolds before and after cryopreservation

The results of an uniaxial compression test utilizing control and post-thaw cell-free collagen-HAP scaffolds. Graph A shows typical load-displacement curve of the compression test and graph B represents calculated compressive stress at 50% compression. Letters indicate statistically significant differences ($n = 5$, One-way ANOVA, $p < 0.05$).

Pore size distribution analysis revealed no differences between the x10, x50, x90 and span values. There is a small reduction of values in the cryopreserved groups compared to control (e.g. the span value: 0.7 for 10% DMSO + sucrose compared to 0.84 for control). It is probably due to dehydration and ‘solution effects’ occurring upon freezing. A summary of the results is given in the **Table 3.3**. When the cumulative distribution is plotted over pore diameter it can be seen that the control has a lower slope between 20 and 60 μm compared to the frozen scaffolds (see **Fig 3.18, A**). No statistical differences in x10, x50, x90 and span values between groups were revealed. In general, the results suggest that modified cryopreservation does not adversely affect the scaffold porosity characteristics.

Table 3.3 . Summary with representative values used to characterize pore size distribution.

Comparison groups	Parameters			
	x10 [μm]	x50 [μm]	x90 [μm]	Span value
Control	20.38 \pm 6.91	37.26 \pm 5.57	50.92 \pm 4.13	0.84 \pm 0.19
10% DMSO/20% FBS	16.97 \pm 4.82	34.06 \pm 2.31	45.03 \pm 2.62	0.83 \pm 0.23
10% DMSO/20% FBS + 300 mM Sucrose	20.16 \pm 1.75	34.04 \pm 0.12	44.35 \pm 1.80	0.70 \pm 0.11

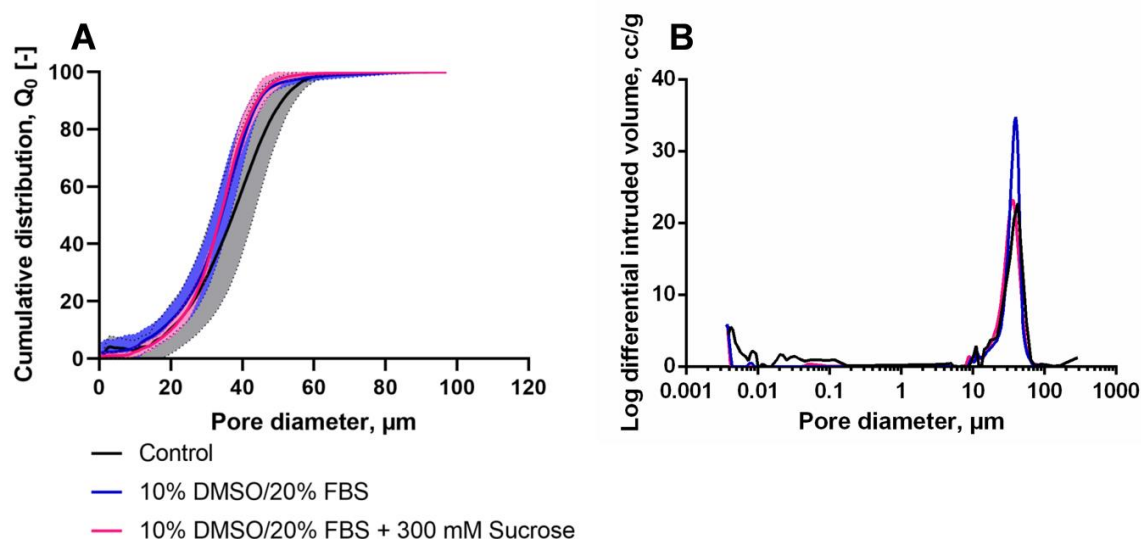


Figure 3.18 Representative pore size distribution plots

Cumulative density distribution curves with 95% confidence envelope (A) and differential intruded volume $-dV/d(\log d)$ (B) vs. pore diameter for control and frozen samples as measured by mercury intrusion porosimetry ($n = 3$). No statistical difference in pore size distribution among frozen and control samples was revealed.

Coupled with the results on pore size distribution, a swelling test showed no differences between control and frozen groups. Swelling percentage for control scaffolds was 1407.30 ± 97.90 %, for DMSO 1271.80 ± 176.70 % and DMSO supplemented with sucrose 1236 ± 109.40 %, respectively.

The specific heat capacity of dry scaffolds alone and with CPAs was measured by DSC in the range between -140 to $+20$ °C. The data are represented on the **Fig. 3.19**.

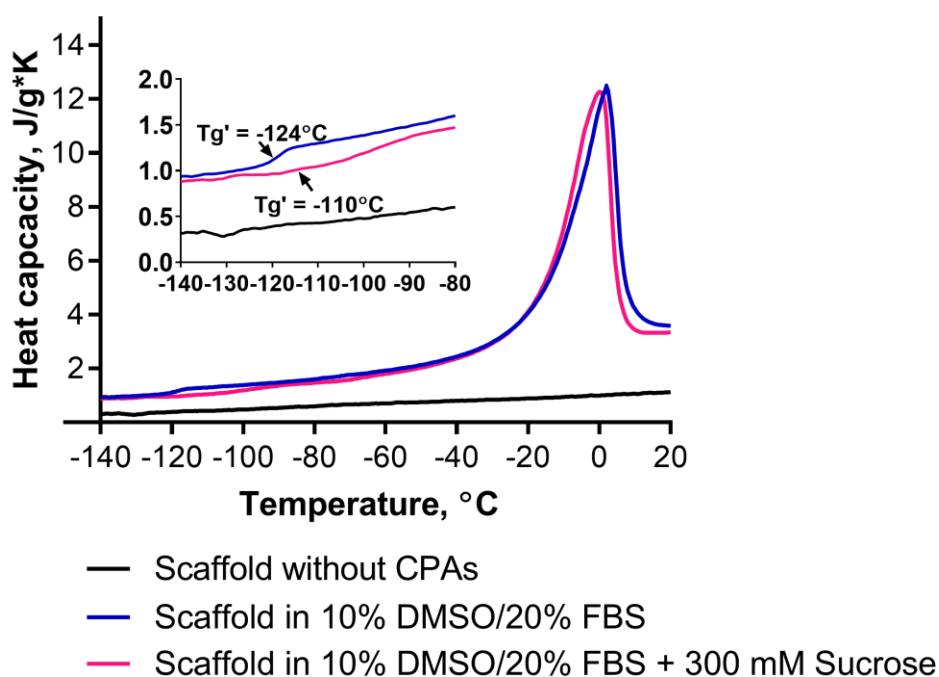


Figure 3.19 Specific heat capacity for collagen-HAP scaffolds with and without CPAs

Heat capacity of scaffolds without CPAs is much lower than that of with CPAs. The insert shows close-up region with glass transition temperatures for CPA mixtures with scaffolds. Values are calculated from DSC data.

The general trend observed was that the values for specific heat capacity of dry collagen-HAP scaffolds were lower than those with CPAs. Most biomaterials have lower specific heat capacity than water (Choi and Bischof, 2008). In all groups, changes in specific heat capacity were temperature-dependent and showed lower values with lower temperature. The reason is that ice has lower heat capacity than water and higher thermal conductivity. Upon phase change of the freeze-concentrated portion of the CPAs to liquid phase at Tg'_{onset} (-125.25 ± 1.34 °C for DMSO and -107.65 ± 1.91 °C for DMSO with sucrose) the specific heat values increased. The sharp peak on the heat capacity graph indicates melting point (2.2 ± 0.14 °C for DMSO and -0.95 ± 1.34 °C for DMSO with sucrose) again because water has higher specific heat than ice.

To compare the conventional and modified thawing protocols described in **Subsection 2.5.3**, experimental determination of thawing rate was carried out. The results of these measurements are represented in **Fig. 3.20** and in the **Table 3.4**. Several general tendencies in thawing profile can be seen as follows:

1. It takes 2 times less time to achieve +4 °C temperature (commonly associated with less DMSO toxicity) with modified thawing vs. conventional one.
2. Thawing rates in the region -180 to -110 °C in modified protocol are significantly lower than in conventional one.

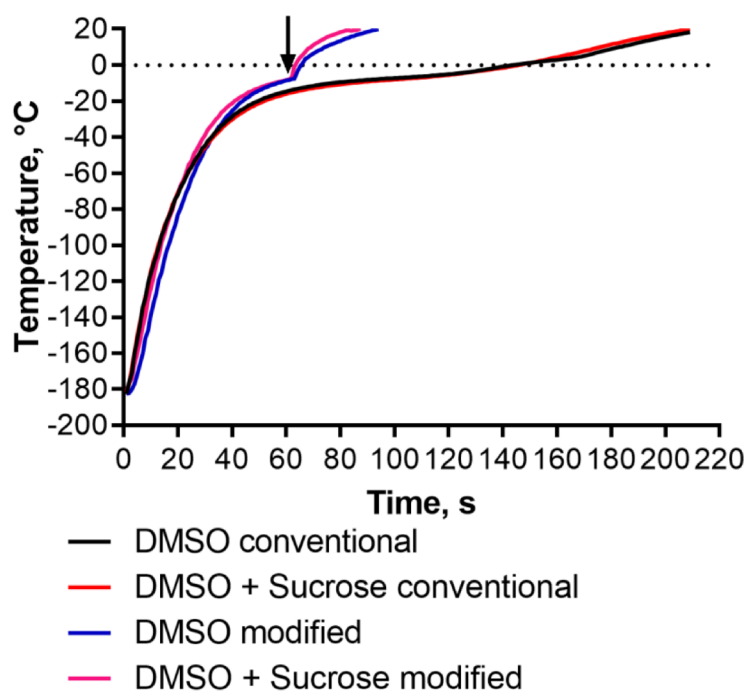


Figure 3.20 Representative warming curves for conventional and modified thawing

The arrow and corresponding increase in the temperature indicate a time point at which pre-warmed medium is added. Modified thawing in the context of ‘in air’ freezing is allowed to reach +4°C around 2 times faster than conventional one.

Table 3.4 Thawing rates and time intervals determined for conventional and modified cryopreservation.

Thawing protocol				
Parameter	DMSO conventional	DMSO modified	DMSO + Sucrose conventional	DMSO + Sucrose modified
Thawing rate from -180 to -110°C [K/min]	435.3 ± 14.6 ^{NS}	331.8 ± 9.7	445.2 ± 5.1 ^{NS}	384.1 ± 12.4
Thawing rate from -4 to 4°C [K/min]	12.6 ± 0.3 ^{NS}	192.9 ± 14.0	15.0 ± 0.8 ^{NS}	272.9 ± 8.0
Time till 4°C is reached [s]	167 ± 1	68 ± 3 ^{NS}	158 ± 4	65 ± 1 ^{NS}

* NS indicates non-significant differences between marked groups within the respective parameter sets according to one-way ANOVA, $p < 0.05$ (n = 6).

3.2.5. Impact of modified cryopreservation on viability of *cj*MSCs frozen in 3D scaffolds

Motivated by better performance of modified cryopreservation, the further logical step of this work was to test its performance on more complex system involving cells.

Of note, in *in vitro* experiments before cryopreservation cell-seeded scaffolds were incubated for 24 h in culture medium supplemented with 100 mM sucrose to enable its loading into cells. After thawing, cells were allowed to recover within 24 h under culture conditions to account for cell loss associated with apoptosis and latent cell damage. As can be seen from the **Fig. 3.21**, morphology, attachment and spreading of cells cryopreserved both in DMSO (**B**) and its combination with sucrose (**C**) were equivalent to that of control cells (**A**). These findings were encouraging and indicated that modified cryopreservation procedure has no detrimental effect on these vital functional characteristics of *cj*MSCs frozen within 3D collagen-HAP scaffolds.

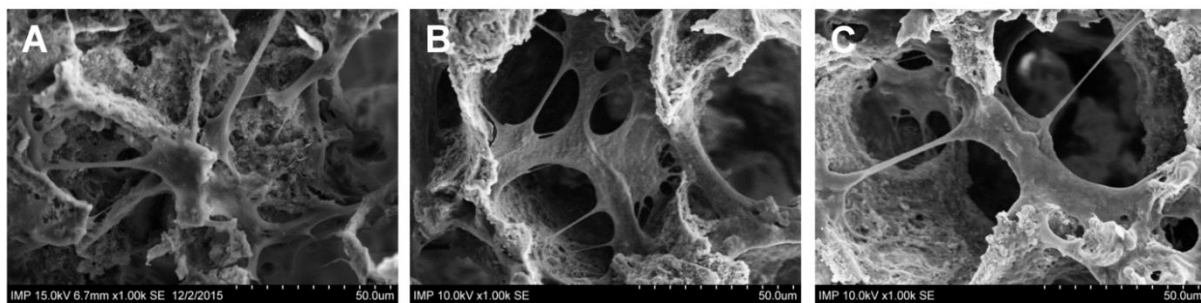


Figure 3.21 Attachment and spreading of MSCs after cryopreservation

Growth, attachment and spreading characteristics of *cj*MSCs post-thaw. SEM pictures of control *cj*MSCs (**A**) and *cj*MSCs frozen according to modified protocol without (**B**) and with sucrose (**C**) within collagen-HAP scaffolds. Cryopreserved cells demonstrate characteristic shape, preserved cell-cell and cell-substrate contacts similar to control.

Maintenance of post-thaw structure, viability and function is likely to be significant for post-thaw cell recovery and proliferation. To qualitatively assess the cell viability after modified cryopreservation, live-dead staining of *cj*MSCs within 3D collagen-HAP scaffolds was also performed 24 h after thawing as another functional test. The experimental results on cell viability are shown in **Fig. 3.22**. As a negative control cells frozen in a culture medium without any CPAs were used (**Fig. 3.22 A**). In this group massive cell loss was detected. In contrast, viability of *cj*MSCs frozen on collagen-HAP scaffolds as observed was not different qualitatively from that of control. Confocal images demonstrate high number of viable cells in control (**Fig. 3.22 B**) as well as samples that underwent modified cryopreservation under

protection of DMSO alone (**Fig. 3.22 C**) and in combination with sucrose (**Fig. 3.22 D**). Recovered cells covered porous scaffolds as in control group.

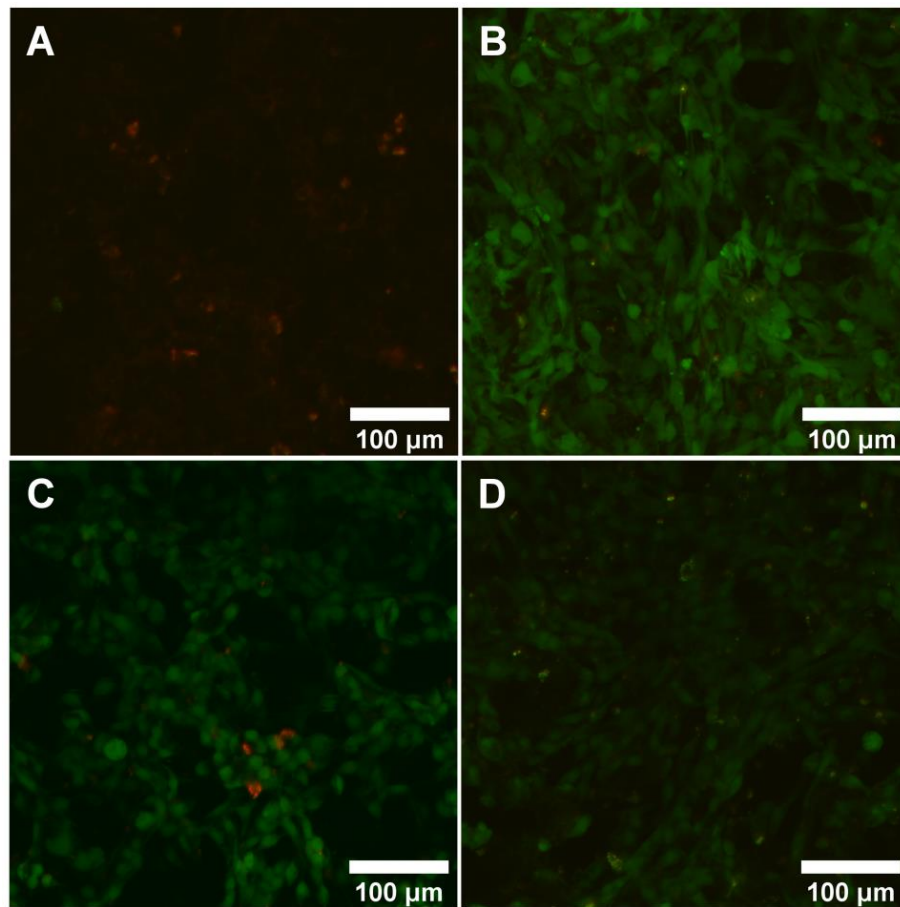


Figure 3.22 Live dead staining of cells in collagen -HAP scaffolds after cryopreservation

Comparative confocal microscopy images of *cj*MSCs 24 h after cryopreservation within collagen-HAP scaffolds. Cells were stained with Calcein AM and EthD-1 to visualize live (green) and red (dead) cells, respectively. Few live and dead in a sample frozen without CPA (A) suggest cell loss and death within recovery period. Samples frozen in DMSO (C) and DMSO with sucrose (D) demonstrate cells distributed throughout a scaffold with retained cell morphology and viability comparable to control samples (B).

In the cryopreservation of TEPs, very often decrease in the number of viable cells is accompanied by decrease in the number of attached cells as we observed in the experiments with conventional freezing. Therefore, determination of a number of viable attached cells normalized to control was regarded as giving more accurate data on cell recovery.

The viability of *cj*MSCs was evaluated by confocal cryomicroscopy and resulted in comparable viability between cryopreserved scaffolds (DMSO and sucrose) and non-frozen

scaffolds. To account for possible cell loss, the number of viable attached cells was counted from Z-stacked confocal microscopy images and normalized to non-cryopreserved group. The results of the quantification are shown in **Fig. 3.23** and indicate that addition of sucrose allowed to increase cell viability by 20% from $61.14 \pm 16.12\%$ (DMSO alone) to $82.31 \pm 25.94\%$ (combination of DMSO with sucrose), respectively.

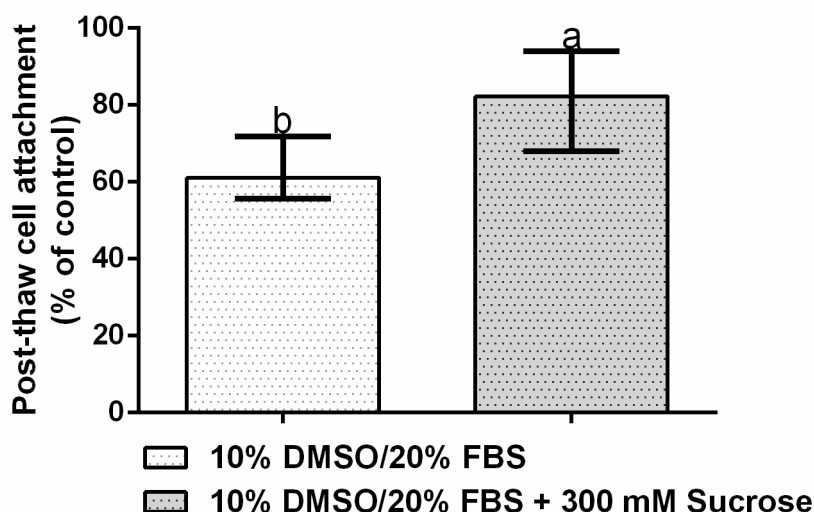


Figure 3.23 Quantitative assessment of post-thaw cryopreservation outcome

Data are presented as median \pm IQR (Kruskal-Wallis test). Letters indicate statistically significant differences ($p < 0.05$) with respect to control. Introduction of sucrose increases the number of viable c attached cells by 20%.

3.2.6. Comparison of recrystallization behavior of DMSO vs. DMSO with sucrose

As addition of sucrose to DMSO yielded better survival results in comparison with DMSO alone, it was interesting to elucidate whether it also has an impact on ice recrystallization. Separate set of experiments involved characterization of CPA samples without scaffolds and cells annealed at $-10\text{ }^{\circ}\text{C}$ (temperature close to the melting point of tested CPAs). The results of IRI assay presented on the **Fig. 3.24** show that at every step of isothermal annealing at $-10\text{ }^{\circ}\text{C}$ whether it be 10 min (**D** vs. **A**), 30 min holding (**E** vs. **B**) or secondary cooling to $-50\text{ }^{\circ}\text{C}$ (**F** vs. **C**), samples containing sucrose exhibits much smaller ice crystals. In this study, projected area of ice crystals was not quantified.

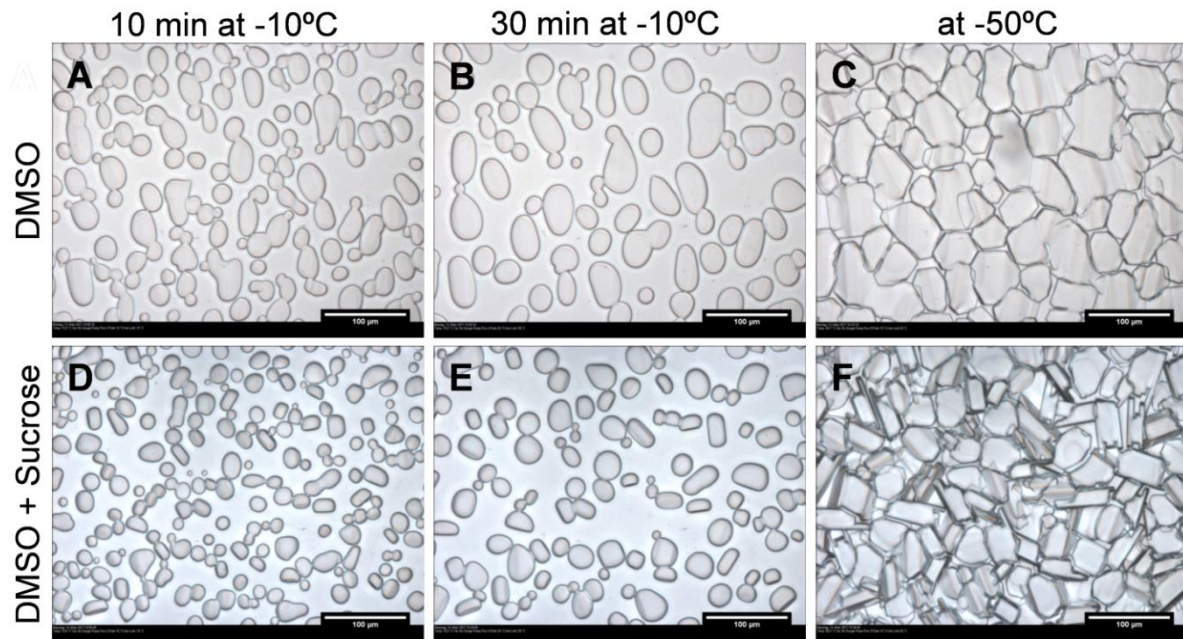


Figure 3.24 Cryomicroscopic pictures illustrating the impact of sucrose on recrystallization of DMSO solution

The upper panel demonstrates ice crystals developed in DMSO solution at 10 (A), 30 (B) min of isothermal annealing at -10°C followed by secondary cooling to -50°C (C). The lower panel shows the same conditions for 10% DMSO solution supplemented with 300 mM sucrose (D, E and F, respectively). Smaller ice crystals in presence of sucrose are clearly visible. Scale bar represents 100 μm .

Overall impact of sucrose on preservation of stem cells in 2D and 3D formats was positive. Still, the issue of DMSO toxicity and high time expenditures related to endocytotic delivery of sucrose cannot be ignored. Therefore, next experiments were related to DMSO- and serum-free cryopreservation of stem cells in suspension using electroporation-assisted loading of sucrose along with other sugars. The rationale behind and long-term goal is to establish in future DMSO- and serum-free cryopreservation of attached cells in 2D and 3D formats.

3.3. Effect of cell electroporation with sugars on cryopreservation outcome

3.3.1. Evaluation of cell permeabilization and recovery

The first parameter that had to be evaluated is if electroporation can help to transport non-penetrating sugars into cells without compromising their attachment and viability. The results from the optimization of electroporation parameters such as voltage, electroporation solutions and sugar concentrations are presented first, followed by a viability study using the optimized

parameters and their influence on cell survival after cryopreservation. Lastly, some physical properties of solutions provided the highest cell survival are shown.

Electroporation is a well-established and long used method to introduce membrane-impermeable molecules into cells and has found its application in cryopreservation. To test if the loading of cells either with sucrose, trehalose or raffinose can be achieved via electroporation, pulses with different strength of electrical field were tested. In the electroporation field, PI uptake is used to determine the efficiency of permeabilization.

In these set of experiments, it was necessary to determine the strength of electrical field which would provide effective permeabilization of hUCMSCs while not compromising their recovery. In optimization studies, all sugars were used in isotonic concentration of 250 mM. Cell recovery was evaluated by resazurin reduction assay 24 h after electroporation. Varying the electrical field in the range of 0-2.5 kV/cm, respective permeabilization *vs.* recovery curves were generated and plotted against each other (**Fig. 3.25**). In the normalization process, the maximum fluorescence intensity of the permeabilized cells was taken as 1 and the minimum intensity of the unstained cells was taken as 0. With an increasing electrical field, significantly more PI was able to get transported into the cells. The uptake of PI exponentially increased between 1.0 and 2.0 kV/cm and then reached the plateau (**Fig. 3.25 A-C**, red lines). The fluorescence intensity of PI is predictive of the concentration of sugar in the cells after electroporation. At the same time, viability linearly declined starting from 1.5 kV/cm as shown by the blue lines in **Fig 3.25 A-C**. The trend of loading efficiency and viability were similar for all three sugars with no significant reduction in cell viability.

The two parameters (viability *vs.* loading) for all sugars had their interception between 1.0 and 1.5 kV/cm. Since at about 2.0 kV/cm no further increase in PI intensity was observed and from 1.5 kV/cm cell recovery started to decrease, the latter value was regarded as the optimal.

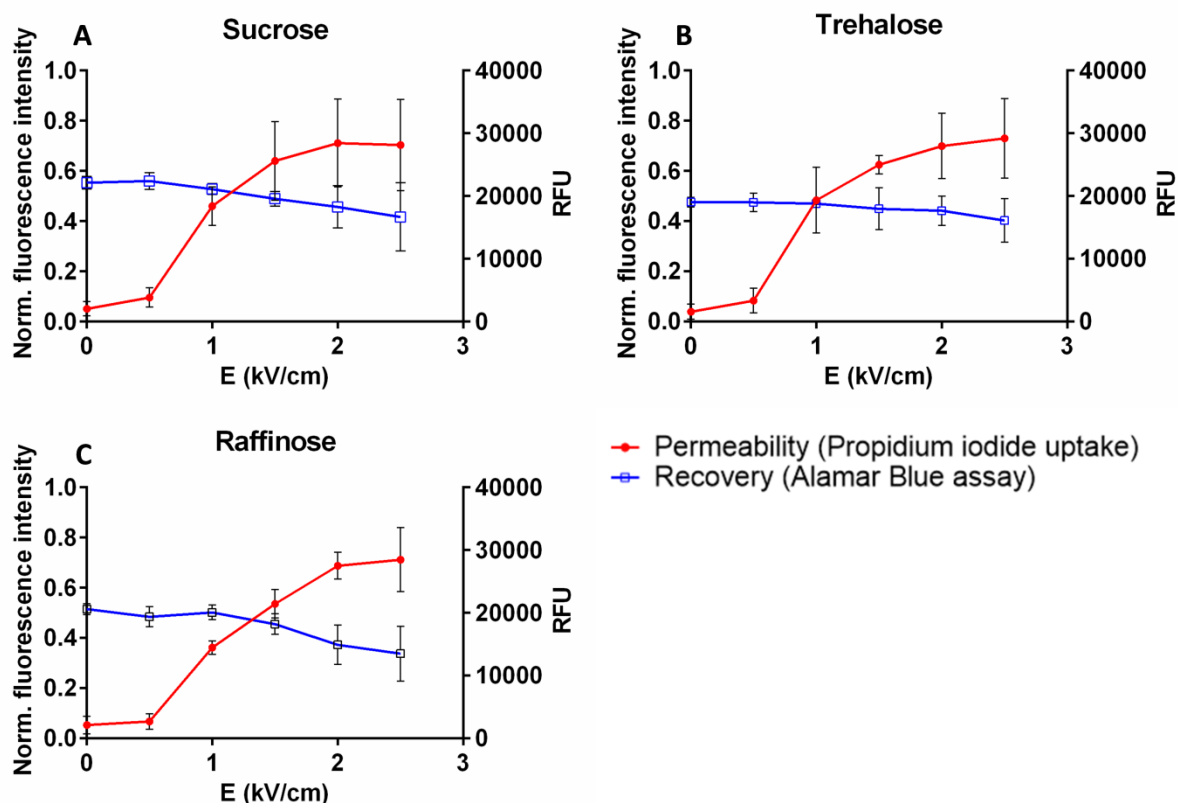


Figure 3.25 Viability and efficiency of PI uptake during electroporation

The normalized fluorescence intensity of PI and resazurin fluorescence after electroporation of hUCMSCs using (A) sucrose, (B) trehalose and (C) raffinose at 100 μ s, 1 Hz, and 8 pulses are presented. Permeabilization of PI increased, and cell recovery decreased with higher voltages. Mean values with standard deviation of at least four independent experiments are shown.

An interesting observation was, that using a high electrical field had a negative effect on cell attachment and morphology in all three sugar groups (see **Fig. 3.26 G-I**). Cells showed similar shape and attachment when an electrical field of 1.5 kV/cm (**Fig. 3.26 D-F**) was used for permeabilization in comparison to control cells (**Fig. 3.26 A-C**). At 2.5 kV/cm only a few cells were able to attach, whereas the highest amount of surviving cells was found when sucrose was used.

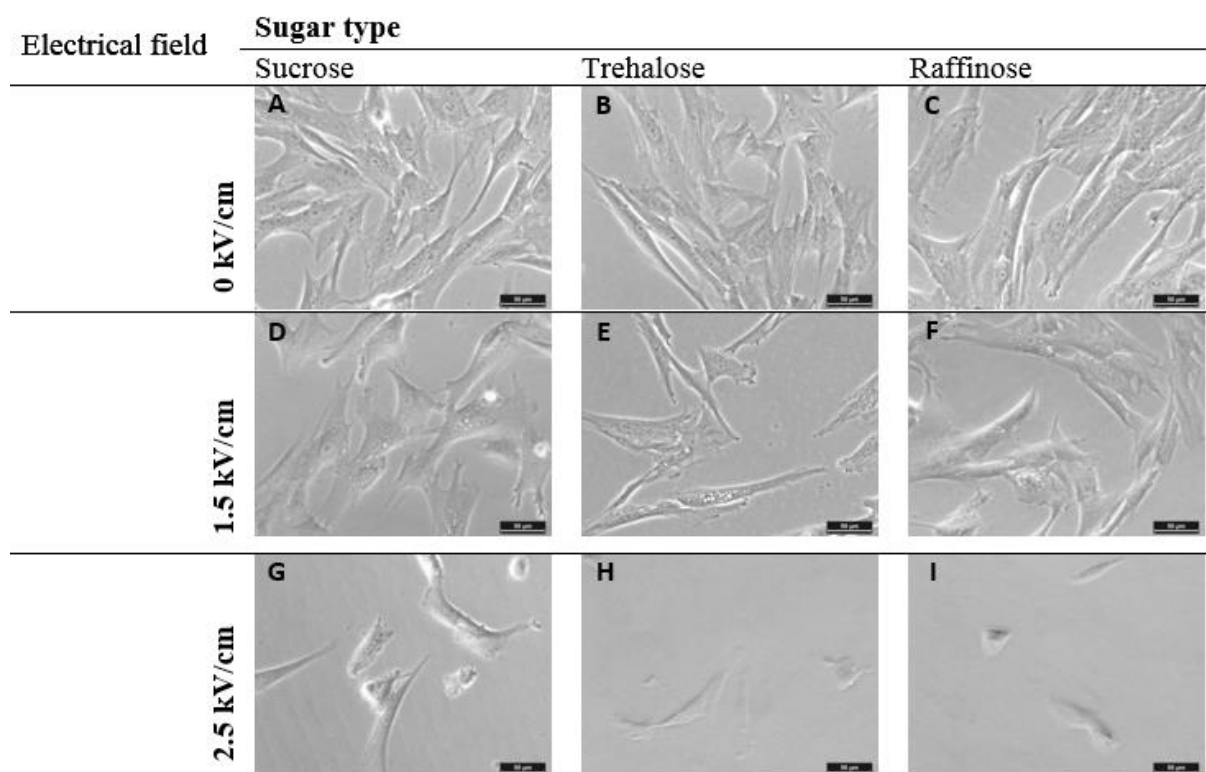


Figure 3.26 Influence of electrical field and sugar type on cell morphology

Panel of light microscopy images of hUCMSCs before and 24 h after electroporation with 250 mM sucrose, trehalose and raffinose. Control (A, B, C) and electroporated at 1.5 kV/cm (D, E, F) cells exhibit typical fibroblast-like morphology, attachment and spreading characteristics. However, cells electroporated at 2.5 kV/cm (G, H and I) demonstrate visibly altered cellular morphology and decreased cell numbers in all three groups of sugars. Scale bars represent 50 μ m.

3.3.2. Evaluation of electroporation-assisted cryopreservation on post-thaw cell survival

Since the optimal field strength and sugar solutions have been evaluated, the next step was to investigate the effect of different sugar concentrations loaded into hUCMSCs on their protective effect during freezing. For this purpose, low-conductivity electroporation buffers containing 0-400 mM of corresponding sugars were used as the sole cryoprotectants. As a positive control, the standard freezing solution containing 10% DMSO and 90% FBS was used. Cell viability before and after cryopreservation was analyzed by trypan blue exclusion assay and FACS using PI.

The effect of different sugar concentrations on post-thaw viability of hUCMSCs based on membrane integrity is shown in **Fig. 3.27**. In general, cryopreservation of hUCMSCs using 10% DMSO lead to a higher viability (94.53 ± 4.30 %) compared to the other groups using sugar as sole cryoprotectant independent of the analysis method. Using the trypan blue

exclusion assay (**Fig. 3.27 A**), a sugar concentration dependent increase in viability is shown. The highest percentage of viable cells was found to be for sucrose 76.07 ± 8.44 , trehalose 76.98 ± 7.60 and raffinose 81.73 ± 9.15 , respectively, using the highest tested concentration of 400 mM. Similar results were achieved using FACS analysis (**Fig. 3.27 B**). Again, with increasing sugar content, post-thaw viability increased and suggests a correlation between the viability of hUCMSCs and concentration of sugars used for the electroporation. In addition, FACS data corroborated that all 3 sugars are equally effective in preserving hUCMSCs without animal serum and DMSO.

The cryopreservation efficiency using 400 mM was reproducibly statistically higher than in other groups tested, therefore, this concentration was used in the further experiments.

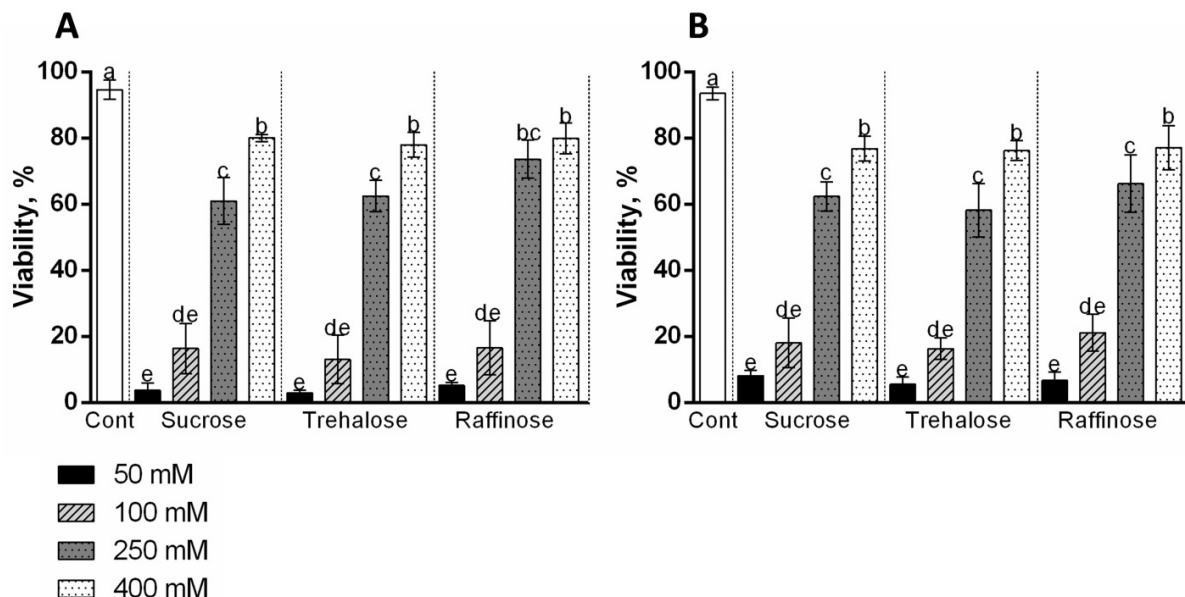


Figure 3.27 Post thaw viability of hUCMSCs using different sugar concentrations

Column charts showing the results on determination of viable cell counts using trypan blue (A) and FACS (B) after electroporation and cryopreservation using different concentrations of sugars. 10% DMSO/90% FBS served as a positive control (Cont). Data are reported as mean \pm standard deviations and different letters represent significant differences between groups ($p < 0.05$) followed by one-way ANOVA.

Since it was found that hyperosmolar pulse media are significantly more effective at protecting hUCMSCs from freezing injury than isotonic one (400 mM vs. 250 mM), the next experiment was to compare the cryosurvival of electroporated and non-electroporated cells using 400 mM sugars. First, electroporation efficiency in hyperosmolar sugar-containing media was assessed using Lucifer Yellow uptake. It is a small, polar and non-permeant fluorescent tracer with a molecular mass of 522 g/mol and a net charge of -2. In the context of

this study, LY is widely used in both electroporation and cryopreservation as a tool for detection of otherwise membrane-impermeable molecules after exposure to electric field (Towhidi et al., 2012) or freezing-induced osmotic forces (Zhang et al., 2016). **Fig. 3.28** shows, that the vast majority of electroporated hUCMSCs exhibit green fluorescence in hyperosmolar medium containing sucrose (A), trehalose (B) and raffinose (C). On the contrary, no or negligible number of cells were fluorescent in all negative control samples (D, E, F), respectively.

Lucifer yellow was homogeneously distributed throughout the cell cytoplasm, but in non-electroporated cells LY started to accumulate in endocytotic vesicles.

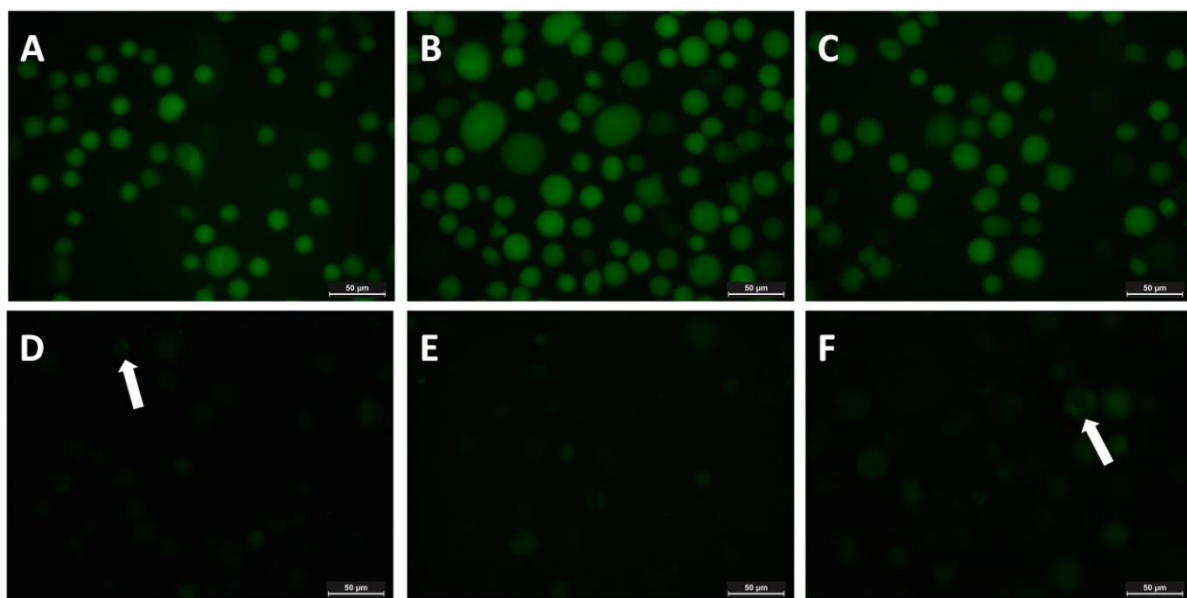


Figure 3.28 Detection of electroporation of hUCMSCs by Lucifer Yellow uptake

All fluorescent images were acquired either 10 min after incubation in LY or after applying electrical pulse. Cells electroporated with LY in sucrose- (A), trehalose- (B) and raffinose-based pulse media (C) exhibit bright green fluorescence, respectively. In some negative control cells (D, E, F) accumulation of LY in endocytotic vesicles was observed (white arrows). Scale bar represents 50 μm .

The number of LY-positive cells was calculated from fluorescent images and compared with the total number of cells determined from respective phase contrast images. High electroporation efficiency (sucrose $93.36 \pm 5.37\%$, trehalose $91.78 \pm 4.99\%$, raffinose $93.99 \pm 4.83\%$) was accompanied by high post-electroporation survival of hUCMSCs (sucrose $90.61 \pm 5.99\%$, trehalose $88.81 \pm 4.99\%$, raffinose $90.23 \pm 4.65\%$).

Since osmolality plays a key role in resealing and cryopreservation, the osmolality of the freezing solutions was determined. A 400 mM sucrose freezing medium exhibited an osmolality 497 mOsm/kg, trehalose 503 mOsm/kg and raffinose 592 mOsm/kg compared to

10% DMSO/90% FBS which has an osmolality of 2000 mOsm/kg. No significant correlation between media osmolality, electroporation efficiency and cell viability was found (see **Table 3.5**).

Table 3.5 Characteristics of hyperosmolar buffers and results after electroporation.

Parameters studied	Sugar type		
	Sucrose	Trehalose	Raffinose
Electroporation efficiency, % of LY+ cells	90.61±5.99	88.81±4.99	90.23±4.65
Cell viability after electroporation, % of viable cells	93.36±5.37	91.78±5.49	93.99±4.83
Osmolality, mOsm /kg	497± 1	503 ± 3	592 ± 5

To investigate whether the intracellular presence of sugars is needed to ensure high cryopreservation efficiency, electroporated and non-electroporated hUCMSCs were frozen in buffers containing 400 mM of each sugar as an extracellular cryoprotectant. Indeed, the presence of an intracellular sugar significantly increases the cell viability after thawing as analyzed by trypan blue exclusion assay and FACS (see **Fig. 3.29 A, B**). Trypan blue exclusion assay revealed that hUCMSCs frozen with 400 mM intracellular sucrose have a post-thaw viability of 80.70 ± 5.92 viable cells compared to non-electroporated cells ($19.09 \pm 8.23\%$, **Fig. 3.29 A**). Similar results were found for trehalose ($82.54 \pm 7.13\%$ vs. $18.80 \pm 6.92\%$) and raffinose ($89.37 \pm 4.62\%$ vs. $20.07 \pm 8.74\%$). The same trend was found also using FACS with PI (**Fig. 3.29 B**).

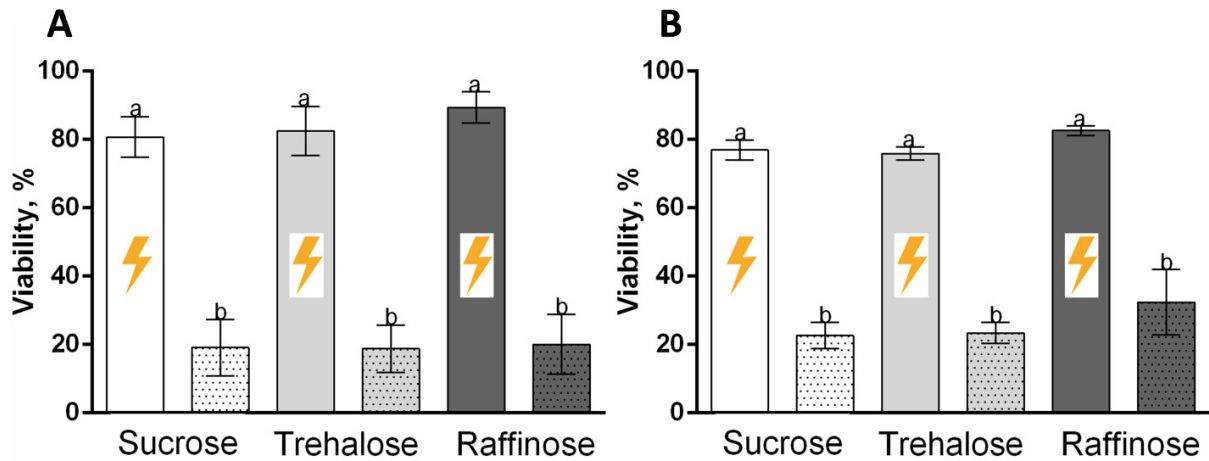


Figure 3.29 Post thaw viability of hUCMSCs after cryopreservation for loaded or non-loaded cells

Column charts showing the results on determination of viable cell counts using trypan blue (A) and FACS (B) in electroporated (symbol of current) and non-electroporated samples cryopreserved using 400 mM sugar concentration. Data are reported as mean \pm standard deviations and different letters represent significant differences between groups ($p < 0.05$) followed by one-way ANOVA.

Not only is the post-thaw viability an important parameter but also attachment and morphology of the cells. To analyze the cell shape, attachment and spreading after cryopreservation, hUCMSCs were thawed, plated and cultured for 24 h before light microscopy images were acquired.

No morphological changes were found regardless of CPA after attachment. **Fig. 3.30 A-E** presents morphological features of cells cryopreserved using sucrose (A), trehalose (B), raffinose (C) and DMSO (D) in comparison to fresh cells (E). All cryoprotectants employed preserved well the cell ability to adhere and spread as well as their typical fibroblast-like morphology. Electroporated cells frozen under the protection of sugars accumulated characteristic bright vacuoles absent in fresh and positive control cells.

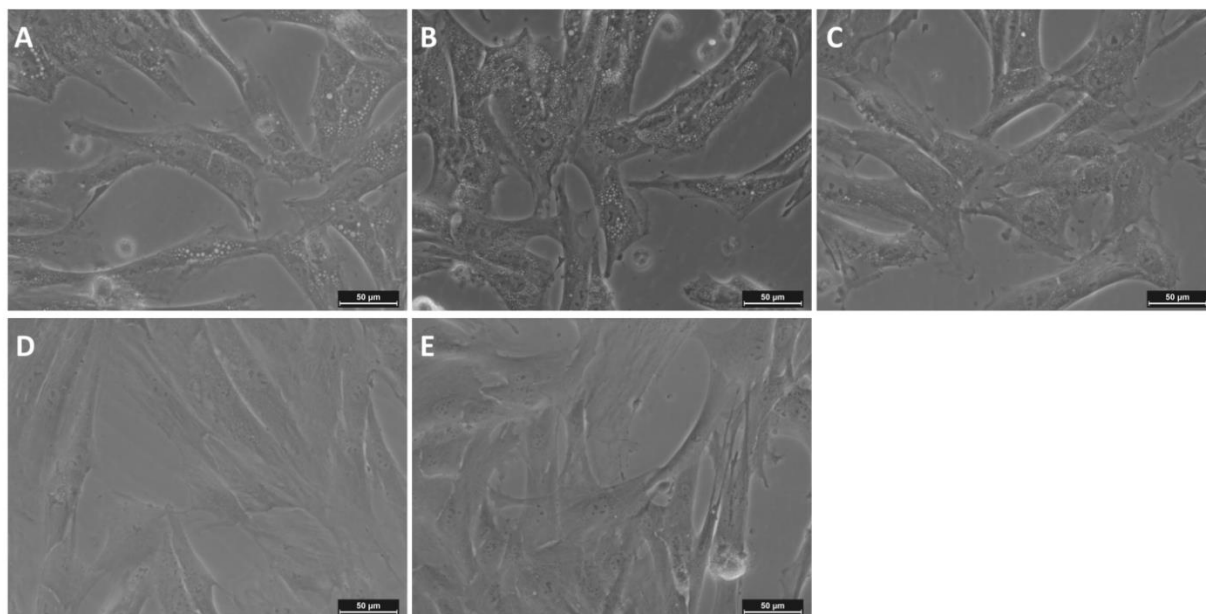


Figure 3.30 Morphology of cells 24h after cryopreservation using either sugars or DMSO compared to non-cryopreserved cells

Representative light microscopy images of *in vitro* cultures of cryopreserved vs. fresh hUCMSCs. Cells electroporated and cryopreserved using sucrose (A), trehalose (B) and raffinose (C) display comparable morphology to cells cryopreserved in DMSO (D) and fresh cells (E). No negative impact of electroporation-assisted cryopreservation on cell attachment 24 h post-thaw was observed. Scale bar represents 50 μm .

3.4. Evaluation of some physical properties of sugar-containing electroporation buffers relevant to cryopreservation

3.4.1. Determination of glass transition and melting temperatures in electroporation buffers used for cryopreservation

In order to understand the effect of different sugars on the cryopreservation process DSC and cryomicroscopy investigations were necessary.

During freezing and thawing two transitions from liquid to glass (glass transition, T_g') and the onset of ice melting for sugar-water mixtures were found. Liquid sucrose transitioned to glass at -45.23 ± 0.21 $^{\circ}\text{C}$ compared to trehalose (-39.73 ± 0.83 $^{\circ}\text{C}$), raffinose (-39.73 ± 0.83 $^{\circ}\text{C}$) and DMSO (-117.83 ± 1.70 $^{\circ}\text{C}$). The onset of melting was found to be at -32.50 ± 0.71 $^{\circ}\text{C}$ (sucrose), -29.53 ± 0.60 $^{\circ}\text{C}$ (trehalose) and -26.67 ± 0.50 $^{\circ}\text{C}$ (raffinose) compared to DMSO (-8.3 ± 0.95 $^{\circ}\text{C}$). Additionally, the melting peak was determined to be 5.78 ± 0.57 $^{\circ}\text{C}$ for sucrose, 6.23 ± 0.35 $^{\circ}\text{C}$ for trehalose and 5.47 ± 0.87 $^{\circ}\text{C}$ for raffinose. The melting peak of DMSO was significantly smaller (0.70 ± 1.18 $^{\circ}\text{C}$) compared to the analyzed sugars. **Fig. 3.31**

demonstrates representative DSC scans for all three sugar-containing freezing solutions whereas **Table 3.6** is an overview of the quantitative data.

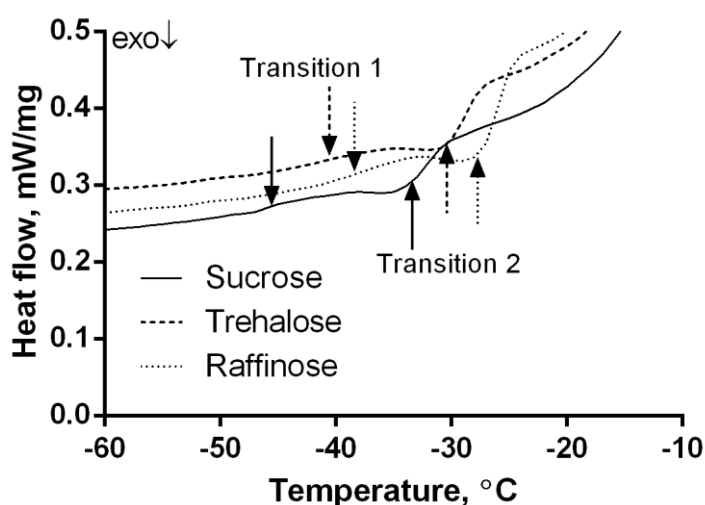


Figure 3.31 Thermogram of different sugars analyzed with DSC

A typical DSC thermogram of sugar-containing pulse media measured at heating rate of 10 °C/min. Two endothermic events representing glass transition points (Transition 1) and onset of melting (Transition 2) for sucrose (solid line and arrows), trehalose (dashed line and arrow) and raffinose (dotted line and arrow) are shown on the DSC curves.

Table 3.6 Characteristics of hyperosmolar electroporation buffers.

Parameters studied	Sugar type		
	Sucrose	Trehalose	Raffinose
Glass transition temperature (T _g ' midpoint), °C	-45.23 ± 0.21	-39.73 ± 0.83	-37.97 ± 0.40
T _{onset} of melting, °C	-32.50 ± 0.71	-29.53 ± 0.60	-26.67 ± 0.50
Melting peak (T _m), °C	5.78 ± 0.57	6.23 ± 0.35	5.47 ± 0.87

3.4.2. Ice formation and recrystallization behavior

Ice crystallization and recrystallization are typical processes occurring during freezing/thawing. Crystallization temperatures determined using cryomicroscope for 400 mM sucrose, trehalose and raffinose were -19.67 ± 2.90 °C, -18.57 ± 1.70 °C and -17.20 ± 0.40 °C, respectively. Much lower values were obtained for 10 % DMSO/90% FBS group: -24.83 ± 0.60 °C.

The next logical step was on assessing the IRI activity of sugars and DMSO compared to a positive control (fish type III antifreeze protein, AFPIII). Samples were subjected to isothermal annealing at the temperatures close to their corresponding melting points determined using DSC (**Table 3.7**). All known types of recrystallization processes were revealed in sugar and DMSO solutions as opposed to AFPIII which completely suppressed recrystallization. **Fig. 3.32** shows crystals formed in freezing solutions at 5 and 30 min during isothermal annealing when crystals were fairly separated from each other. Isomass recrystallization which refers to changes in ice crystal shape in a way that a crystal with irregular-shape tends to become smoother due to minimization of energy is exemplified by sucrose (**A** vs. **B**). Migratory recrystallization or so-called *Ostwald* ripening is based on the growth of larger crystals at the expense of smaller ones. Larger ice crystals have higher specific surface energy in virtue of what water molecules tend to diffuse from the surface of smaller ice crystal to that of larger ones (**I** vs. **J**, example of raffinose). However, in our studies the most prominent was accretive recrystallization which occurs when two adjacent ice crystals fuse together to form a single larger crystal (**F** vs. **E**, example of trehalose).

ImageJ software was used for quantification of mean projected crystal area as a measure of IRI activity. At least 10 separated ice crystals were randomly selected on every image and all experiments were repeated 3 times. The most pronounced IRI activity showed 0.1 mM AFPIII (**K**, **L**) in 30% sucrose as compared to 30% sucrose reference sample (**G**, **H**). In this sample, no changes in ice crystal size were observed over 30 min which reflects complete inhibition of ice recrystallization by AFPIII. Among all other CPA tested, the smallest ice crystals were detected in DMSO, with data on sugars increasing in the order raffinose < trehalose < sucrose (summarized in **Table 3.7**).

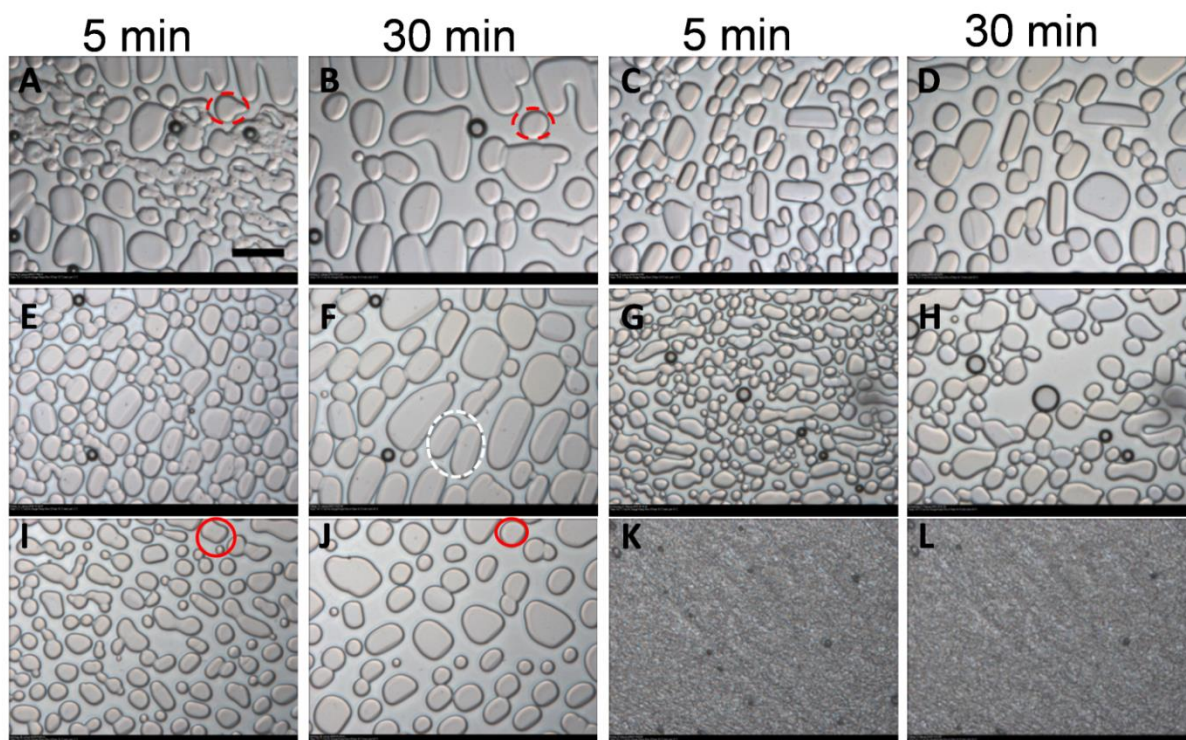


Figure 3.32 Cryomicroscopic analysis of ice recrystallization

Cryomicroscopy images showing dynamics of ice crystal growth in the presence of electroporation buffers containing 400 mM sucrose (A, B), trehalose (E, F), raffinose (I, J), 10% DMSO/90% FBS (C, D), 30% sucrose (G, H) and 30% sucrose with 0.1 mM of AFP III (K, L). Isomass (red dashed circles), accretive (white dashed circle) and migratory (red solid circles) types of recrystallization are shown in sucrose, trehalose and raffinose, respectively. Scale bar represents 50 μm .

Table 3.7 Mean projected area of ice crystals during isothermal annealing.

CPA	Annealing temperature, $^{\circ}\text{C}$	Mean projected area of ice crystals, μm^2	
		5 min	30 min
Sucrose	-3	654.43 ± 138.47	1358.15 ± 229.05
Trehalose	-3	408.82 ± 46.05	1117.33 ± 32.56
Raffinose	-3	241.82 ± 4.53	670.87 ± 128.61
DMSO	-10	288 ± 52.50	569.94 ± 139.64
AFPIII	-6	-	-

4. Discussion

The effect of sucrose on cell viability and its influence on cryopreservation on adherent cells was studied. Additionally, a translation of the sucrose-based protocol to 3D constructs such as collagen-HAP scaffolds was established. For this purpose, a modified freezing/thawing protocol was developed and its effect on cell viability and physicochemical properties of the scaffolds was evaluated. Lastly, a different approach to induce large molecules such as sugars into the cell using electroporation and its influence on cell survival after cryopreservation was analyzed to establish DMSO- and serum-free cryopreservation of stem cells in suspension. The long-standing goal of this research is to establish safe and stable cryopreservation of stem cells within 3D constructs.

4.1. Cryopreservation of cells on 2D carriers and the effect of sucrose on *cj*MSCs

To insure safe and feasible cryopreservation, many factors have to be considered. One of the most important is the cytotoxicity of the used cryopreservation solution and the use of animal compounds such as FBS (Germann et al., 2011; Shimazu et al., 2015). The gold standard for cell freezing is a combination of 10% DMSO and FBS in different concentrations. This mixture has been used for several decades and no more effective solution has been found (for review see Luetzkendorf et al., 2015). Additionally, a cell dependent cryopreservation protocol, CPA solution and washing have to be developed to ensure high cell survival and low or no adverse effect when the cell product is transfused/transplanted into the recipient (Watts and Linch, 2016).

In recent years sugars such as trehalose and sucrose have found their application in cryopreservation (Huang et al., 2017; Martinetti et al., 2017; Pan et al., 2017). One of the major drawbacks of using these perspective sugars is that they cannot readily pass the cell membrane and either need longer time to get inside or special treatment (e.g. electroporation (Zhou et al., 2010), freezing (Zhang et al., 2016) and many more (Acker et al., 2003; Sharp et al., 2013; Zhang et al., 2009).

In this study, first strategy used for sucrose loading was fluid-phase endocytosis. At low concentrations (up to 100 mM) no significant changes were found, but above that, cell viability declined rapidly. A broad range of sucrose concentrations (0 – 250 mM) was tested

for cytotoxicity with *cj*MSCs to reveal the optimal concentration to preload the cells in preparation for cryopreservation.

Similar tendency was observed in the studies by Petrenko et al., 2014 and Rogulska et al., 2017 on human dermal MSCs and adipose-derived MSCs, respectively, with the only difference that hMSCs could tolerate as high as 200 mM sucrose. This indicates that such difference could be species-related and that *cj*MSCs are more sensitive towards increased osmotic pressure.

Although 50 mM sucrose did not inhibit cell metabolic activity or adversely affect the cell morphology, for cryopreservation purposes preference was given to 100 mM taking into account limited endocytotic uptake of membrane-impermeable disaccharides and their concentration-dependent cryoprotective effect (Eroglu et al., 2000). In addition, 100 mM of sucrose is routinely used concentration for sucrosome induction which was also evaluated in the study by Karageorgos et al., 1997. In this work, 100 mM of sucrose was found to be an optimal concentration that stimulated increase in the amount of sucrosomes. Moreover, actin cytoskeleton of *cj*MSCs was not affected by pre-treatment with 100 mM sucrose and no cell detachment was observed (**Fig 3.3**) suggesting the steady-state adaptation dynamics of cells subjected to mild osmotic stress within 24 h. This may have direct implications for induction of cell tolerance to more severe osmotic stress cells undergo during cryopreservation in adherent state (Xu et al., 2012).

Mammalian cells are devoid of enzymes cleaving disaccharides with cryoprotective properties such as trehalose and sucrose. Intracellular sucrose can be rapidly eliminated from the cells by the treatment with an invertase (Ferris et al., 1987; Jahraus et al., 1994). This enzyme converts sucrose into fructose and glucose and requires low pH for its activity. Receptor-mediated endocytotic uptake of an invertase into lysosomes and its subsequent proteolytic digestion was, for example, shown in hepatocytes (Tolleshaug et al., 1986).

In our experiments, treatment of sucrose-loaded *cj*MSCs with an invertase for 24 h resulted in complete disappearance of sucrosomes (**Fig. 3.4 D vs. B**, respectively) whereas in the control culture media group sucrosomes were still noticeable (**Fig. 3.4 C vs. A**, respectively).

This may imply that for complete elimination of sucrose from cells via autophagy (Higuchi et al., 2014) more prolonged cell cultivation in sucrose-free medium might be necessary after loading. Although a number of methods for loading of disaccharides into mammalian cells for cryopreservation purposes have been already established and disputed (Stewart and He,

2018), the key factor limiting their clinical utility is the development of methods suitable for their routine unloading (Lynch and Slater, 2011). Application of invertase for sucrose unloading is coupled with immunogenicity and cost-efficiency issues, nevertheless, it could be considered as a good reference method. Future work would therefore attempt to establish the strategies for effective sucrose unloading post-thaw.

Cellular delivery of membrane-impermeable disaccharides such as sucrose and trehalose could be indirectly investigated through the endocytotic uptake of LY. Using this method it was previously shown that LY and consequently trehalose could be successfully incorporated into hMSCs by clathrin-dependent fluid-phase endocytotic mechanism (Oliver et al., 2004). After 24 h incubation with LY in the presence or absence of sucrose revealed that 90% of cells are LY-positive with or without sucrose-inducible LY introduction, but showed different uptake pattern as shown in **Fig. 3.5**.

Sucrose-inducible LY uptake was also studied by DeCourcy and Storrie, 1991 on CHO and Vero cells cultured on 30 to 50 mM sucrose for 1-3 days. Despite the differences in the methodology and cell types, the general tendency observed was similar to the results in this work. The only difference was that no enhanced fluorescent staining of sucrosomes was observed because samples were not recultured in LY-free media to clear early endocytic compartments but they were fixed immediately instead.

Such observed perinuclear localization of sucrose may influence the character of intracellular ice propagation and was investigated using cryomicroscopy. Pretreated suspension cells are more resistant to IIF than non-pretreated cells (see **Fig. 3.6**). The intracellular ice propagation in sucrose-loaded cells (**3.6 B** and **D**) was rather different from that of seen in control cells (**3.6 A** and **C**). The majority of sucrose-loaded cells exhibited intracellular ice at the cell periphery and did not advance further. In contrast, in the control cells ice formation was more observed in the central part of a cell. This may indicate that intracellular sucrose blocks the advancement of ice further throughout a cell which needs more in-depth investigations to clarify this impact on adherent cell cryopreservation with the presence of extracellular sucrose. The results obtained partly support this hypothesis.

The volume measurements using the Coulter counter showed a volume increase of 30% when cells were treated with 100 mM sucrose compared to control cells (from was $3222 \pm 692.0 \mu\text{m}^3$ to $4830 \pm 649.9 \mu\text{m}^3$, Fig. 2.8.). Referring to the above observations, the different pattern of IIF in sucrose-treated and non-treated cells could also be related to the fact that treated cells

are less tolerant to cell volume excursions. In the study by Prickett et al., 2015, it was shown that the incidence of IIF was higher in cells treated in the isotonic solution compared to hypertonic one at any given degree of supercooling. Since cells in hypertonic solution shrink due to water efflux it was hypothesized that the difference in IIF behavior could be attributed to the decreased volume of cells and water content when present in the hypertonic solution. In our case, on the contrary, cells increased in volume but apparently at the expense of intracellular sucrose forming strong hydrogen bonds with water thereby mitigating IIF (Shiraga et al., 2017).

We could assume that the first cell response to hyperosmolar challenge would be shrinkage due to exoosmosis. Progressive accumulation of sucrose promotes water influx inside cells with subsequent recovery of cell volume back to the isotonic volume and increase during long term culture. As a consequence of sucrose uptake, osmotic gradient as the ratio of extracellular to intracellular osmolality decreases which could make a cell more resistant to freezing stresses and ‘solution effects’.

Such volumetric changes, in turn, may influence cell cryosurvival as it was shown by Lynch and Slater, 2011b for trehalose-loaded erythrocytes. In this study, the post-thaw survival of human erythrocytes frozen at high cooling rates was shown to increase approximately linearly with pre-freeze cell volume, suggesting that osmotically inactive cell volume may act as a barrier to damaging levels of cell shrinkage during rapid freezing. In the case of slow cooling used in this study, a cell has enough time to dehydrate and the role of increased pre-freeze volume in cell cryosurvival is not completely clear and worth further investigating. However, we cannot exclude that intracellular sucrose could modulate and buffer the reduction in intracellular water content during dehydration induced by concentrated CPA addition and extracellular ice formation.

To elucidate the impact of sucrose loading on general cellular stress response, the activation of MAPK-kinase p38 by phosphorylation was analyzed. Samples were collected at each selected time point (0, 1, 6 and 24 h) and western blotting was performed to specifically detect phosphorylated p38 upon mild osmotic stress and cell volume changes. MAPK-kinase p38 kinase regulates various physiological functions including cell proliferation and apoptosis (for review, Cuadrado and Nebreda, 2010) and is involved in response to different physical stimuli including changes in the temperature, osmolarity, pH and freezing-related challenges

(Omori et al., 2007). The mechanism of p38 MAPK activation is dual phosphorylation at the Thr-Gly-Tyr motif.

Although pP38 was still visible 6 h after activation, its activity returned to basal levels following 24 h after challenging with sucrose (**Fig. 3.8**). These dynamics could be related to changes in cell volume and intracellular osmolality induced by sucrose uptake. When cells reach equilibrium volume and system stabilizes indicating adaptation of a cell to osmotic shock the activity of p38 returns to its basal levels even in the continuous presence of stress stimuli as a compensatory reaction.

Time-dependent activation of p38 after treatment of *Xenopus* oocytes with hyperosmolar (400 mM) or intermediate (200, 300 mM) sorbitol concentrations was observed in the study by Messaoud et al., 2015. The authors drew the conclusion that hyperosmotic shock activates the p38 signaling pathway with an ultrasensitive and bimodal response. It would be interesting to investigate the mechanisms and down-stream events responsible for observed transient activation of p38 after sucrose treatment with possible implications to freezing of adherent cells. In this context it is noteworthy to mention the work by Fong et al., 2007 who described p38 MAPK activation in mouse preimplantation embryos following exposure to hyperosmotic treatment using compounds and their concentrations with direct relevance to cryopreservation such as 10% glycerol, 1.4 M sucrose or 0.2 M sorbitol.

Cryopreservation of adherent cells is a hot topic and has many challenges (Bahari et al., 2018; Batnyam et al., 2017). One of these is the propagation of ice inside the cells. Here, the detailed analysis of IIF in adherent *cj*MSCs was not possible due to low camera recording speed. However, we were able to observe IIF in all tested groups with and without CPAs. The studies on the visualization of IIF using high-speed video cryomicroscopy by Stott and Karlsson, 2009 comparing adherent and suspended bovine pulmonary artery endothelial cells showed different ice initiation sites in both cell configurations. Specifically, in adherent cultures IIF started at ice initiation centers that were preferentially located either at the distal edge of the spreading cell or near a paracellular ice dendrite. On the contrary, in the suspended cells sites of intracellular ice crystallization were located in the interior zone of cells. The latter study was also corroborated by Yang et al., 2011 showing that the initial site of IIF in adherent HUVECs and MCF-7 cells was found to be located on the cell plasma membrane. Moreover, it was demonstrated that ice seeding has a significant impact on the dynamics of intracellular ice propagation. Upon freezing with active ice seeding the velocity

of intracellular crystal growth is fifteen folds slower than that of stochastic nucleation and upon thawing recrystallization only appears in the cells frozen without ice seeding. The probability of IIF was shown to be higher in MCF-7 cells than that in HUVECs suggesting cell-type specific differences. Among critical factors worth mentioning with relevance to freezing of adherent cells are paracellular ice penetration (Higgins and Karlsson, 2013), higher incidence of IIF with lower extracellular ice nucleation temperature and higher incidence of IIF (via cell-to-cell contacts) in adherent cells compared to suspended cells (Zhurova et al., 2010). However, multiple publications demonstrated that IIF is not necessarily damaging to adherent cells (Acker and McGann, 2003).

When adherent cells were frozen the viability was very low in the presence of DMSO alone (15.85%) and linearly increased with the addition of increasing sucrose (up to 53% using 300 mM). The observed reduction in cells survival using higher sucrose concentrations could be attributed to detrimental effects of excessive osmotic stress upon exposure to CPA before crystallization and freezing injury due to 'solution effects'. During slow cooling prolonged exposure to hyperosmolar freeze-concentrated CPAs may result in cell toxicity.

As a rule, monolayer cryopreservation protocols are more complex than protocols developed for cell suspensions and are based on different combinations of approaches and CPAs. Viability data reported in the literature for post-thaw recovery of cells frozen in adherent state considerably vary among research groups. This is because cryopreservation is a cell-specific multi-parameter process and any subtle change in individual process parameters could bring about different results. Fan et al., 2008 reported on vitrification of bovine corneal endothelial cells in a monolayer using 25% (w/w) 1,2-propanediol and 35% (w/w) trehalose as cryoprotective agents using cryomicroscopy. Approximately, 61.3% of the cells were shown to be viable after vitrification. Stevenson et al., 2004 demonstrated the positive impact of increasing serum concentration in DMSO-based freezing solutions for slow cooling cryopreservation of primary rat hepatocyte monolayers attached to collagen coated culture dishes. The combination of 10% DMSO and 90% FBS allowed to preserve 79.7 % of hepatocytes in monolayers. Coating of substrates with different compliant biomolecules such as polylysine, fibronectin or collagen is used as a strategy to avoid cell detachment and breakage of cell-cell interactions due to increased thermal stresses and cell loss after washing out of CPAs. For example, in the study by Xu et al., 2012 coverslips were covered with 0.1% gelatin but still a significant decrease in hMSCs viability by around 30% after

cryopreservation at all cooling rates tested (1, 5 and 10 K/min) in adherent state in comparison to the cells in suspension. (Ji et al., 2004). A recent study by Eskandari et al., 2018 has shown considerable promise in cryopreservation of adherent cells, even though the proposed protocol is very complex. It includes freezing using slow cooling with rates 0.2 or 1 K/min, combination of 5% DMSO, 2% chondroitin sulfate and 6% HES as CPA and application of fibronectin-covered glass or *Rinzl* coverslips made of vinyl plastic with a coefficient of thermal expansion similar to that of ice. High survival of HUVECs ($97.3 \pm 3.2\%$) and porcine corneal endothelial cells ($95.9 \pm 3.7\%$) has been demonstrated. Such combinatory strategies based on interdisciplinary research raise great expectations since successful cryopreservation of adherent cells would make feasible clinical and commercial availability of cell-based products for tissue engineering and regenerative medicine and there is still room for further improvements.

4.2. Effect freezing on cells seeded into collagen-HAP scaffolds

A great variety of biomaterials and techniques are used in manufacturing of 3D scaffolds for tissue engineering and regenerative medicine applications. Collagen-based biomaterials has gained widespread use in research and clinical settings because of their numerous advantages such as biocompatibility, biodegradability and low immunogenicity (for review see Parenteau-Bareil et al., 2010). Current state of the research shows the great promise of tissue engineering of biomimetic scaffolds bearing inherent characteristics facilitating their cryopreservation and increasing their storage potential. Incorporation of ice-nucleating agents into scaffolds at the stage of their preparation to actively control the temperature of ice formation and provide homogeneous temperature distribution upon cooling and thawing is an innovative paradigm in cryopreservation. This might have a beneficial impact on scaffold freezing/thawing profile which in turn may preserve their original shape and maintain mechanical properties as well as high viability of stem cells.

In the present study, 3D scaffolds having cylindrical shape with well-interconnected pores were designed using mineralization of collagen suspension (**Fig. 3.11**). As was shown by Gelinsky et al., 2008 mineralization of collagen increases the thermal stability of collagen molecules and mechanical stability of collagen scaffolds which has direct relevance to cryopreservation. Apart from that, such surface topography with incorporated hydroxyapatite nanoparticles providing multiple sites where ice embryos could nucleate and grow to crystals, might contribute to prevention of supercooling of the system. Another interesting aspect is that

in our preliminary experiments, we observed much lower heat capacity in collagen-HAP scaffolds than that of made of pure collagen (data not shown) suggesting that less energy would be required to warm them. On the other side, HAP crystals apparently may confer higher thermal conductivity to mineralized collagen scaffolds compared to ones made of pure collagen. Thermal conductivity of pure collagen at room temperature is 0.56 W/mK and that of pure HAP is 2.0 W/mK.

Therefore, prepared collagen-HAP scaffolds *per se* are interesting cryobiological models and in the next step their cytocompatibility with *cj*MSCs was investigated to prepare TEP for cryopreservation purposes.

When seeded with cells, 3D constructs resemble tissue or organ structures, hence they can be used as cryopreservation models to optimize conditions for efficient cryopreservation of tissues and organs. Cells accepted the scaffolds without cytotoxic effects and spread normally through the porous structure (**Fig. 3.12**).

Seeded scaffolds were frozen using conventional freezing (in bulk medium) and resulted in partly destroyed scaffolds and low viability after thawing (**Fig. 3.13**). Scaffold damage and cell detachment could be explained by thermal expansion of ice leading to disruption of scaffold interconnectivity and the cell-matrix contacts. In this context, it was also shown that cell-specific cytoskeletal mechanics *per se* and mechanical interactions between cells and matrix in engineered tissues may govern cell response to freezing-induced dehydration (Ghosh et al., 2016).

To understand the mechanisms behind the scaffold destruction, cryomicroscopy of sectioned scaffolds was used. Although simplified model system represented by scaffold sections frozen in small amount of CPAs on glass coverslips cannot be readily extrapolated to 3D format, it can be used for visualization of crystallization and recrystallization processes and sample behavior at LN temperatures. For recrystallization study, scaffold sections were subjected to isothermal annealing at -10°C (onset of melting of 10% DMSO) and time-lapse imaging of whole freezing-hold-thawing event was performed. It showed, that several phenomena observed may contribute to the loss of scaffold integrity: 1) ice cracking in a scaffold in DMSO and PBS after passing the temperature around -120°C, presumably due to difference in thermal expansion of ice and stiff glass substrate (Rabin et al., 2006); 2) accelerated ice recrystallization (**Fig. 3.14**). Ice recrystallization has an adverse effect on biological materials being stored in freezers at isothermal conditions and using compounds capable of controlling

ice recrystallization in CPAs solutions could potentially increase the post-thaw integrity and function of 3D TEPs (Capicciotti et al., 2015).

At the next stage, conventional cryopreservation protocol was modified to cope with observed challenges and as quality assurance parameters analysis of the physicochemical and mechanical properties of the scaffolds was conducted.

At first, Raman microscopy was performed to evaluate the impact of cryopreservation procedure on general composition of scaffolds. DMSO is known to be a strong organic solvent therefore it is crucial to study its impact on structure of biomolecules. Raman microscopy is a potent tool to investigate cryopreservation-induced biochemical transformations. For instance, with the aid of Raman microscopy in the study by Rusciano et al., 2017 vitrification-induced changes in protein secondary structure manifested by α -helices loss were observed suggesting cold protein denaturation. No noticeable changes were found when using Raman (**Fig. 3.15**) but FTIR revealed increase in the β -sheet structures of collagen (**Fig. 3.16**). Small changes in collagen secondary structure induced by freezing-thawing procedure were observed in the study by Ozcelikkale and Han, 2016 in hydrogel environment presumably due to freezing-induced expansion of extrafibrillar fluid which were alleviated by DMSO. Additional experiments to enable a more detailed assessment of observed changes in amide-I region of collagen-HAP scaffolds are required.

Preserved mechanical properties of tissue-engineered constructs during long-term storage is one of the most crucial quality assurance parameters for their successful use in transplantation. A number of publications have addressed this issue highlighting the general tendency toward increased stiffness of collagen-based biomaterials after cold storage with (Elder et al., 2005) or without (Chow and Zhang, 2011; Oswald et al., 2017) CPAs presumably due to changes in collagen characteristics. However, the response of tissue-engineered construct to mechanical stresses is determined not only by its composition but also the structure as well as CPAs and freezing-thawing procedure which could influence their thermal expansion characteristics (Xu et al., 2013). Other studies show no increase in biomaterial stiffness after cryopreservation with DMSO (Delgadillo et al., 2010; Lam et al., 2011).

Compression tests of cryopreserved scaffolds showed a significant reduction of compression stress from 27.48 ± 1.88 kPa (control) compared scaffolds frozen with (20.60 ± 1.34 kPa) and without sucrose (20.88 ± 1.10 kPa, see **Fig. 3.17**). In reported data on the impact of

cryopreservation on mechanical properties of TEPs there is still much controversy. For instance, Bissoyi et al., 2014 in the paper on cryopreservation of hMSCs seeded silk nanofibers compare effect of 10% DMSO or combination of 2.5% DMSO and natural osmolytes. The study shows that elongation at breakage of non-cryopreserved TECs was significantly higher compared to the cryopreserved ones whereas no difference in tensile strength between groups was found regardless of CPA used. Similar results reports Chen et al., 2011 for chitosan-gelatin membranes seeded with keratinocytes frozen either with 10% DMSO/50% FBS or the same with 0.4 M trehalose: significantly lower from control elongation at breakage in frozen samples; no differences in tensile strengths; fine cracks in membranes frozen with DMSO alone. Repanas et al., 2016 show no impact of cryopreservation in PBS on mechanical properties of polycaprolactone or polycaprolactone-chitosan fiber mats, although slight increase in the values of Young's modulus in frozen group was noticed. In the study by Popa et al., 2013 assessing the stability of κ -carrageenan hydrogels laden with human adipose derived stem cells upon cryopreservation with 10% DMSO more prominent increase in loss factor and no changes in elastic modulus with increasing frequency was shown by dynamic mechanical analysis. Critical role in preserving mechanical properties of TEPs also plays end freezing temperature as suggested by (Neidert et al., 2004) where collagen-based tissue equivalents frozen with 0.5-1 M DMSO or glycerol stored at -80 and -160°C had intact or compromised mechanical properties, respectively. It is also important to note that thermal expansion during water-ice phase transitions and thermal expansion of a given biomaterial are important determinants of preserved mechanical properties (for review see Stańczyk and Telega, 2003). Finally, in the development of thermo-mechanical stresses also important role play the characteristics of the freezing container such as stiffness and location of 3D TEP in it (Steif et al., 2007). Although 'in air' freezing clearly better preserves integrity of scaffolds than conventional one, we cannot exclude the contribution of expanding ice in scaffold pores from remaining CPAs which may led to formation of microcracks and subsequent alterations of scaffold mechanical properties. Therefore, further research is needed to look into plausible mechanisms behind observed affected mechanical properties and to further improve cryopreservation protocol.

In order to investigate the influence of the cryopreservation procedure on the pore size of scaffolds, mercury intrusion porosimetry measurements were conducted. Preservation of porosity and interconnectivity of scaffolds is of great importance not only for their mechanical properties but also for cells residing inside or outside pores. In general, porous

materials would promote better diffusion, retaining and removal of CPAs as compared with nonporous materials. Interestingly, as shown by Costa et al., 2012, porous scaffolds with higher average porosity provided better cell cryoprotection than nonporous discs and using conventional cryopreservation scaffold average porosity was preserved. On the other hand, propagating ice front and thermo-mechanical stresses induced by differential ice expansion could have detrimental impact on scaffold interconnectivity and cell attachment. In terms of modified thawing using pre-warmed medium, porous structure is preferable due to fast diffusion into scaffold and more homogeneous heat transfer than it would be expected in a compact scaffold with lower porosity. Other important aspect to consider is that water or otherwise CPAs in porous constructs would freeze gradually from big pores to small ones because water confined in nanopores crystalizes only partially and with supercooling effect compared to bulk water (Findenegg et al., 2008). Although a tendency to shrinkage of constructs was observed in the studies on pore size distribution as summarized in the **Table 3.3** and depicted on the **Fig.3.17**, the differences were negligible. Somewhat lower swelling percentage values for frozen samples could be related to changes in water absorption properties of collagen because no reduction in dry weight of scaffolds after cryopreservation was revealed. Altogether, changes in collagen secondary structure revealed by FTIR and swelling behavior as well as partial construct shrinkage could collectively contribute to observed changes in mechanical properties of scaffolds.

As the next step, specific heat capacity of collagen-HAP scaffolds was analyzed using DSCs. For successful cryopreservation of TEPs, the investigation of thermal properties of biomaterials in the course of cryopreservation is of utmost importance (reviewed in Choi and Bischof, 2010). These properties are highly dependent on temperature, CPAs and phase changes. Among important parameters influencing thermal history of a biomaterial determining role play their thermal conductivity, heat capacity and density as classical Pennes' bioheat equation suggests:

$$\rho c_p \frac{\partial T}{\partial t} = \frac{\partial}{\partial x} \left(k \frac{\partial T}{\partial x} \right) + \dot{q}_m + \dot{q}_p, \quad (4.1)$$

where ρ , c_p , T , k and \dot{q}_m are the tissue density, specific heat capacity, temperature, thermal conductivity and metabolic heat generation per unit volume (Pennes, 1948).

Much lower specific heat capacity values were obtained for dry collagen-HAP scaffolds than for scaffolds frozen with CPAs. Most biomaterials biological tissues have relatively low

thermal conductivity and high specific heat still lower than both of water (Baust et al., 2009). In all groups changes in specific heat capacity were temperature-dependent and showed lower values with lower temperature owing to the fact that ice has lower heat capacity than water and higher thermal conductivity. In general, the specific heat in the system DMSO/sucrose + scaffold was lower than that of DMSO + scaffold. In terms of optimizing a warming procedure, it must be taken into account that for CPAs with higher specific heat more energy would be required for the rapid thawing.

A major component of biological materials and CPAs is water, which undergoes phase change from liquid to ice or glass. It is also known that the latent heat of biological tissues is quite different from that of pure water but most frequently is calculated as the product of the total water content of tissue and the latent heat of CPA (He, 2011). Additional experiments on latent heat evolution in 3D porous TEPs would be essential to optimize cryopreservation protocols.

Determination of thawing rate is very important in cryopreservation studies especially for TEPs to optimize thawing procedure. Uniform heating is needed to reduce the thermal stresses. Conventional thawing on a water bath is often suboptimal due to increased temperature gradients and related cracking. Much more research has been focused on developing warming procedures for vitrified samples including ultra-rapid warming with infra-red laser (Jin and Mazur, 2015), in magnetic field using nanoparticles (Manuchehrabadi et al., 2017) or combination of electromagnetic and conductive rewarming (Pan et al., 2018). In this context, Eisenberg et al., 2014 demonstrate that reducing initial rewarming rate and a temperature hold near glass transition temperature are coupled with reduced mechanical stresses; rigid containers (like cryovials) are more suitable for slow cooling since with vitrification they drastically increase mechanical stress in which case cryobags might be a better option (Solanki et al., 2017). Some modifications have also been introduced to conventional thawing of samples being frozen with slow cooling rates. For example, Campbell and Brockbank, 2014 developed the two stage thawing procedure with particular focus on cells frozen in an adherent state. First stage includes slow-warming to a transient temperature of around -30 °C stage before rapid thawing at 37°C using a water bath.

Thawing rate depends on CPAs and their concentration, size, type and shape of container as well as a sample being frozen and thawing strategy used (Pan et al., 2018). In turn, thermal properties of CPAs influence heat transfer (Han and Bischof, 2002). Heat conduction rate

depends on the ratio of thermal conductivity to specific heat capacity and density related with each other over thermal diffusivity according to the equation:

$$\alpha = \frac{\kappa}{\rho c_p}, \quad (4.2)$$

where κ is thermal conductivity (W/(m*K)), C_p is specific heat capacity (J/(kg*K)) and ρ is density (kg/m³).

In this respect, increasing publications about thermal properties of CPAs at ultra-low temperature such as viscosity (Kilbride and Morris, 2017) or thermal conductivity (Li et al., 2017) have invaluable cryobiological significance which could help to better understand heat transfer within CPAs and CPA-loaded TEPs to establish effective thawing procedures. Interestingly, Ehrlich et al., 2015 showed that thermal conductivity of crystalline or vitrified DMSO samples which is a key component of the most CPA solutions changes differently with decreasing temperature: vitrified samples showed decreased while crystalline samples showed increased thermal conductivity.

Inspired by state-of-the-art publications, a modified cryopreservation protocol was established.

To compare the conventional and modified thawing protocols described in **Subsection 2.5.3**, experimental determination of thawing rate was carried out. The results of these measurements are represented on the **Fig. 3.20** and in the **Table 3.4**. Four major differences were found between the two protocols:

1. Thawing rates in the region -180 to -110 °C in modified protocol are significantly lower than in conventional one. This apparently because of lower thermal conductivity of air compared to ice and less area of contact with a sample. Thermal conductivity of air is considered to be temperature-independent and corresponds to around 0.02 W/m*K at standard atmospheric pressure whereas thermal conductivity of pure water ice at -180°C corresponds to around 6 W/m*K and thermal conductivity of crystallized 2 M DMSO is around 2.5 W/m*K and decreases with increasing temperature (Ehrlich et al., 2015).
2. Thawing rates in the region -4 to 4°C are significantly higher for modified thawing because introduction of pre-warmed medium at around -7 °C when melting starts will significantly accelerate heat transfer and melting of the rest amount of CPA absorbed

by a sample. In contrast, at this temperature a sample frozen in 1 ml of CPAs will slowly reach equilibrium state and would require more time for melting taking into account high heat capacity of both ice and melted CPA.

3. In both protocols higher thawing rates were revealed for DMSO-sucrose mixtures compared with DMSO alone probably due to lower heat capacity as measured with DSCs.
4. As a result, it takes 2 times less time to achieve +4 °C temperature with modified thawing.

The proposed two-step thawing protocol discussed above was developed based on simulation studies (data not shown) from the following practical assumptions: 1) to slow down a thawing rate in the region comprising glass transition and mitigate thermal stresses by implementing ‘in air’ approach and 2) to reduce the likelihood of ice recrystallization by adding pre-warmed medium at the onset of CPA melting. Further experimental and simulation studies would be necessary to measure CPA thermal properties at subzero temperatures and predict heat transfer for ‘in air’ cryopreservation system.

Limitations of temperature measurements with a thermocouple within 3D sample have to be considered. First of all, it is difficult if at all possible to place it consistently in a middle of a sample; second, a thermocouple could promote heat transfer itself. In this regard, additional non-invasive methods, *e.g.*, infrared video thermography could give an additional valuable information on temperature distribution within multiple samples (Zaragotas et al., 2016).

Further work was focused on the applicability of modified cryopreservation obtained for cell-free scaffolds on *cj*MSCs seeded onto 3D collagen-HAP scaffolds.

When scaffolds were frozen/thawed using the modified protocol cell attachment and viability considerably improved and qualitatively did not differ from control in DMSO and DMSO plus sucrose group (**Fig. 3.21** and **3.22**). Cryopreservation of complex tissues is very often associated with dramatic cell loss due to detachment (Halberstadt et al., 2003) which could be caused by freezing-induced tissue deformation via volumetric expansion (Han et al., 2013). The results of the quantification are shown on the **Fig. 3.23** and indicate that combination of 100 mM sucrose used for cell pre-treatment and 300 mM used in CPA with 10% DMSO/20% FBS increases cell viability by 20% from 61.14 ± 16.12 to 82.31 ± 25.94 , respectively. In general, obtained viability values are well comparable with other studies as was shown in the **Table 1.1**.

Relating these data to much lower survival obtained in 2D studies using the same combination of CPA as presented on the **Fig. 2.9**, the plausible key explanation might lie in the material properties. Glass is rigid, brittle and non-porous substrate compared to compliant porous collagen-HAP scaffolds developed in this study, and could cause deformation of monolayer and cell cytoskeleton due to bigger mismatch between thermal expansion coefficients of ice and glass compared to ice and biological material (Rutt et al., 2018). Moreover, 2D system with a thin layer of CPA has much higher probability of development of thermal stresses than 3D samples frozen according to modified protocol having an air layer between the walls of freezing container and the sample boundary. The observed differences could also be attributed to different thawing procedures used: constant thawing rate 100 °C/min in the 2D system and two-step thawing in 3D system.

The results on viability using sucrose obtained for 3D constructs are in somewhat contrast with findings from the study by Gurruchaga et al., 2017 in which introduction of 0.2 M sucrose to 10% DMSO freezing solution in fact did not provide additional benefits for survival of hMSCs frozen within 3D bioscaffolds made of platelet rich plasma and synovial fluid. For both CPA mixtures, the same viability levels of around 70% were reported. In another study by (Umehura et al., 2011) much higher concentrations of sucrose (1 M) in combination with 10% EG and 0.00075 M PVP were used. Post-thaw survival of dental pulp stem cells frozen within alginate bioconstructs exceeded 90%.

It is believed that the observed positive contribution of extracellular sucrose to enhanced post-thaw cell survival could be only partially explained by dehydration which decreases the probability of IIF. On the other hand, cryomicroscopy studies on cell suspension allowed us to conclude that there presumably is a cooperative effect of intra- and extracellular sucrose on decreased IIF. We observed that the occurrence of IIF was much more pronounced in sucrose-loaded cells frozen without extracellular sucrose than in its presence (data not shown). Raman studies by Yu et al., 2017 revealed that trehalose and dextran form a thin protective layer between the cell membrane and extracellular ice and the occurrence of IIF is lower when this distance is bigger. The decisive role, however, in cell post-thaw fate plays not the presence of IIF itself but its amount and crystal size. Hence, we can assume that the other possible mechanism of sucrose protection is inhibition of IIF by cell dehydration and membrane protection. Another study from the same group (Yu et al., 2018) shows that indeed non-frozen sucrose forms a thin layer at the interface between the cell and extracellular ice and around

10% from extracellular sucrose was detected within cells highlighting the freezing-induced uptake of sucrose similarly to that of trehalose recently shown (Zhang et al., 2016). We cannot also exclude the complex interplay between sucrose, DMSO and water involving hydrogen bonding and contribution of each component to overall cryopreservation outcome is very difficult to assess since CPAs in combination behave differently from being used separately.

In the context of ‘in air’ freezing, one important aspect to consider is a supercoiling phenomenon. Obviously, the probability of heterogeneous ice nucleation is much higher in a bulk solution compared to ‘in air’ situation. The effect of supercoiling on cells frozen in TEPs is difficult to predict but to test the effect of ice seeding on the performance of ‘in air’ approach seems to be very interesting alternative. In support of this assumption, the study by Pravdyuk et al., 2013 indicates that the highest viabilities and metabolic rates were obtained following cryopreservation of hMSCs in alginate bioconstructs by protocol involving controlled ice nucleation step.

On warming, isothermal storage at not cryogenic temperatures, temperature fluctuations during sample shipment, recrystallization of both intracellular and extracellular ice may occur which is lethal to cells and damaging to a scaffold, respectively (Seki and Mazur, 2011). The results of recrystallization analysis shown on the **Fig. 3.24** suggest that addition of 300 mM sucrose to 10% DMSO/20% FBS does reduce ice crystals during annealing and secondary cooling. We could further assume that in the second step of modified thawing smaller ice crystals with higher surface energy induced by sucrose would melt faster and result in reduced freeze damage. However, this is unlikely to be a single mechanism by which sucrose could contribute to higher cryopreservation efficiency. Sucrose has far more prominent protein stabilization, glass forming and osmotic buffering properties making this non-toxic sugar ubiquitous component of diverse cryoprotective cocktails (Elliott et al., 2017). For example, Kuleshova et al., 1999 showed that sugars contribute the most to the vitrification properties of ethylene glycol-based vitrification solutions and have low toxicity to human embryos and oocytes.

4.3. Evaluation of electroporation for the delivery of cell impermeable sugars and their effect on cryopreservation outcome

To study sucrose and other sugar uptake, PI was used due to its similar molecular mass. The molecular mass of PI corresponds to 668 g/mol, however a recent study has shown that also propidium ions (molecular mass, 542 g/mol) are detected by this method (Napotnik and Miklavčič, 2018). The sugars used in this study have a similar molecular weight as PI. It is a non-permeant and non-permeable fluorescent molecule widely used for electroporation detection. Sucrose has a molecular weight of 342 g/mol, trehalose dihydrate 378 g/mol and raffinose pentahydrate 594 g/mol. All sugars were delivered into the cells using 1.5 kV/cm as an optimal electric field, but above this value, the viability began to decrease (**Fig. 3.25**). The cell morphology was not altered when using 1.5 kV/cm compared to control cells (**Fig. 3.26**).

For cryopreservation properties cells were loaded with sucrose, trehalose and raffinose in 50-400 mM concentration range and were frozen in the same sugar concentrations to mitigate osmotic stress. Non-loaded cells cryopreserved with 10% DMSO/90% FBS were used as a positive control. Among all sugars and concentration tested, the highest percentage of viable cells around 80% was obtained using corresponding sugar in 400 mM concentration. Still the viability in positive control group was by around 15% higher as determined by trypan blue exclusion test and FACS (see **Fig. 3.27**). Although it was expected that hyperosmolar concentrations would not provide additional benefits as it was shown by Dovgan et al., 2017 for human adipose-derived stem cells, the cryopreservation efficiency using 400 mM of sugars in this study was significantly higher. This might imply cell-type specific differences *e.g.* in osmotic and membrane permeability characteristics that must be taken into account to establish effective consensus protocols for xeno-free cryopreservation of different clinically relevant stem cells.

The next question was whether cryoprotective action of intra- and extracellular sugars is additive or solely depends on extracellular presence. To this end, permeabilization efficiency in hyperosmolar media was first confirmed using Lucifer Yellow followed by cryopreservation studies involving two comparison groups for respective sugars: cells frozen solely in extracellular sugar solutions and cells frozen employing both intracellular (introduced by electroporation) and extracellular sugars.

Fluorescence imaging revealed higher than 90% efficiency of LY incorporation and cell viability after electroporation in all groups tested (see **Table 3.5** and **Fig. 3.28**). After cryopreservation using extracellular sugars alone the viability levels were around 60% lower than that of in the group with intra- and extracellular sugars used in combination.

All cryoprotectants employed preserved well the cell ability to adhere and spread and their typical fibroblast-like morphology (**Fig. 3.30**). Electroporated cells frozen under the protection of sugars accumulated characteristic bright vacuoles as we observe in the case of endocytosis-mediated introduction of sucrose (see **Fig. 3.2** and **3.4**). Such inclusions were absent in fresh and positive control cells. Campbell and Brockbank, 2012 also refer to development of vacuoles in cells exposed to trehalose overnight. We believe that after electroporation sugars are initially homogeneously distributed within the cell cytoplasm and organelles as was demonstrated by LY delivery and then after prolonged cell culture they are sequestered in lysosomes. Additional experiments are needed to prove this assumption and to determine the intracellular content of sugars providing the highest cryopreservation outcome. Although trehalose is the most widely used and investigated sugar with respect to its intracellular delivery for cryopreservation purposes, this study clearly demonstrates that sucrose and raffinose are as effective as trehalose. Our study is consistent with the previous work by Petrenko et al., 2014 in which no difference between sucrose, trehalose and raffinose was found in DMSO- and xeno-free cryopreservation of hMSCs. Some studies suggest that sucrose, trehalose and raffinose when internalized promote autophagy in mammalian cells (Chen et al., 2016; Higuchi et al., 2014; Hosseinpour-Moghaddam et al., 2018; Seglen et al., 2009). Other studies showed that non-reducing disaccharides could block autophagy (Yoon et al., 2017). The overall role of autophagy in cryopreservation-induced stresses is disputable and largely unexplored. Gallardo Bolaños et al., 2012 showed that autophagy acts as a pro-survival mechanism in stallion spermatozoa stored at refrigeration temperatures. Some more information is available regarding the important role of autophagy as an adaptive response to cold stress in the ovarian cryopreservation by vitrification (Yang et al., 2016). However, in the context of our studies, it is not clear what contribution would have autophagy induced by cold stress or internalized sugars to overall cryopreservation outcome and its cross-talk with the apoptosis. Further investigations are needed to address these questions. The issue of sugar elimination from cells is scarcely addressed in the literature and was beyond the scope of these investigations. Eroglu et al., 2005 revealed rapid elimination of microinjected trehalose from developing mouse embryos presumably occurred by exocytosis. Zhang et al., 2016

showed that intracellular trehalose washes progressively out of cells during cell culture at a somewhat slower rate compared to endocytic uptake. In case of electroporated cells, further studies would be of great value to determine the kinetics of sugar efflux from cells.

Being used as sole extracellular CPAs, sugars produce multiple cryoprotective actions. According to the most accepted ‘water replacement hypothesis’ formulated by Carpenter and Crowe, 1989, trehalose stabilizes lipid membranes through direct interaction with polar groups of membrane lipids and proteins by hydrogen bonding. The more frequently used strategy of sugar-based cryopreservation relies on combining of sugars with other penetrating and/or non-penetrating cryoprotective agents in part to reduce overall toxicity of a freezing solution. For instance, Eroglu, 2010 reports on successful cryopreservation of mammalian oocytes using intra- and extracellular raffinose and low concentrations of DMSO. The other strategy to decrease toxic concentrations of penetrating CPAs is to use ice recrystallization inhibitors (Capicciotti et al., 2015).

It is generally admitted that for stable long-term storage frozen samples must be stored well below the glass transition point (T_g) of CPA when no or limited molecular mobility takes place. Sugars are known to possess excellent glass forming properties which is a major advantage in terms of storage stability. In view of an emerging interest in the use of -80°C freezers for storage of cells and tissues in biobanks or, importantly, safe specimens shipment on dry ice, some recent studies address the feasibility of cell storage at -80°C by elevating the T_g of cryoprotective medium using for instance sucrose (Sydykov et al., 2018). Yuan et al., 2016 show that the cryoprotective medium comprised of Ficoll 70 and DMSO provides reliable cryopreservation of various kinds of human and porcine pluripotent stem cells at -80°C via increased devitrification temperature of the CPA (-67°C). In our DSC studies, we observed two transitions differently interpreted in the literature. Schawe, 2006 reports that the transition 1 at lower temperature (at around -44°C) is T_g' (glass transition of freeze-concentrated solution when glass transforms to liquid) and the transition 2 (at around -34°C) represents the onset of ice melting for sucrose-water mixtures. Hauptmann et al., 2018 determined T_g' in sucrose-containing samples at -35°C and revealed no second glass transition in DSC scans near -42°C .

Since the measured T_g 's of all the sugar solutions used for electroporation and introduction to freezing solutions are much lower -80°C (see **Fig. 3.31** and **Table 3.6**), we hypothesize that samples frozen with sugars might potentially be long term stored at this temperature in

ordinary laboratory freezers. This would reduce high maintenance costs associated with liquid nitrogen handling and risk of contamination through liquid nitrogen. However long-term storage stability studies are needed to prove this hypothesis.

IRI activity of sugars was studied and compared to 10% DMSO/90% FBS and positive control 1 mM of AFP III. Ice recrystallization is one of the key mechanisms of cryodamage during transient warming and thawing and in particular at multiple freeze-thaw cycles and is manifested by enlargement of ice crystals. The results on IRI activity are presented on the **Fig. 3.32** and summarized in the **Table 3.7**. As expected, among all CPAs tested, the strongest inhibition was observed with the AFP III. This protein belongs to the class of naturally-derived IBPs with very potent IRI activity (for review see (Bar Dolev et al., 2016). Despite their evident cryoprotective potential, IBPs still are not commonly used in routine cryopreservation practice because their action is mostly limited to extracellular ice management as they cannot readily penetrate across cellular membrane. We anticipate that using electroporation these proteins could be also delivered into mammalian cells and inhibit IIF and recrystallization upon rewarming. This would facilitate the further advancement of IBPs in cryobiological practice.

The size of crystals developed in 10% DMSO at isothermal annealing was smaller than in sucrose and trehalose but bigger than in raffinose group. Comparing the sugar group alone, the same order was revealed as with crystallization and glass transition temperatures: raffinose < trehalose < sucrose. Although not statistically significant, electroporation with raffinose showed a trend towards higher cryopreservation efficiency as compared to sucrose and trehalose.

The study by Chaytor et al., 2012 on IRI activity of diverse sugars showed that disaccharides inhibit ice recrystallization better than monosaccharides and that 200 mM galactose provided the best cell viability after cryopreservation at the level comparable to 5% DMSO. The authors also demonstrated that the cryoprotective benefits of galactose were a result of its internalization and ability to mitigate osmotic stress, prevent IIF and/or inhibit ice recrystallization. Moreover, introduction of ice recrystallization inhibitors into cells is a novel approach to modulate intracellular ice growth as has recently been shown by Poisson et al., 2018.

In contrast to endocytosis used to introduce sucrose into cells cultured in 2D and 3D systems, electroporation mediates faster delivery and more homogeneous distribution of sugars within

cells and is intended to be used in future studies for the development of DMSO- and serum-free cryopreservation strategies for 3D tissue-like structures. Electroporation with optimized parameters seems to be a cell-friendly method for intracellular sugar delivery for cryopreservation purposes and stimulates new scientific ideas to cover wider range of applications in the field of cryobiology. However, further studies are needed to shed light on the intracellular sugar content providing improved cryopreservation outcome and overall long-term stability and safety of electroporation-assisted cryopreservation.

5. Summary

Cryopreservation is a powerful tool for the rapid translation and commercialization of regenerative medicine research through efficient supply of stem cells on demand. Using cryopreservation, stem cells could be stored not only in suspension but also in tissue-engineered scaffolds which greatly reduces storage processing time and improves logistics management. In this work, several methodological strategies were employed to address the challenges associated with cryopreservation of stem cells attached to 2D and 3D substrates and DMSO- and serum-free cryopreservation of suspended cells. Here, brief summary with the main conclusions from each subchapter is presented underlying the novel contributions of the current work.

Freezing of cells in a monolayer

In this study, the cumulative impact of sucrose used for pre-treatment and addition into DMSO-containing freezing solution on post-thaw survival of *cj*MSCs frozen in adherent state was investigated. First, optimal sucrose concentrations for cell pre-treatment were selected from the 0-250 mM concentration range via analyzing of cell attachment and viability. Second, optimal sucrose concentrations for cryopreservation together with DMSO were selected from 0-500 mM concentration range based on survival data.

It was shown that the cell pretreatment with sucrose (optimal concentration 100 mM) does not negatively affect the cell attachment and viability, causes 30% increase in cell volume and activates MAPK-kinase p38 by phosphorylation in time-dependent manner as an adaptive mechanism to mild osmotic stress. Cryopreservation with 10% DMSO resulted in $95.00 \pm 1.85\%$ survival of *cj*MSCs in suspension. However, under the same conditions survival of the adherent cells dramatically decreased to $15.8 \pm 5.8\%$. After sucrose pretreatment and subsequent cryopreservation with 10% DMSO and 300 mM sucrose the survival of cells significantly increased to $53.0 \pm 8.2\%$. Thus, although the obtained results still leave much room for further improvements, the first hypothesis as outlined in the **Subsection 1.4** stating that combined application of sucrose improves the efficiency of DMSO-based cryopreservation of attached cells has been proven by the current results. The results obtained may facilitate the further development of cryopreservation protocols for adherent stem cells frozen in 2D and 3D formats.

Freezing of cells in a 3D scaffold

Conventional slow-freezing using DMSO and thawing in a water bath developed for suspended cells do not provide sufficient protection of stem cells frozen in 3D scaffolds. The current thesis reports on successful cryopreservation of stem cells on porous 3D collagen-HAP scaffolds achieved by adopting ‘in air’ cryopreservation approach, translating sucrose-pretreatment protocol to adherent cells, modifying thawing protocol and combining penetrating and non-penetrating cryoprotectants. The scaffolds were fabricated using freeze-drying of mineralized collagen. Scaffolds were seeded with *cj*MSCs and subjected to 24 h pre-shrinking in 100 mM sucrose and slow freezing in 10% DMSO/20% FBS alone or supplemented with 300 mM sucrose. Concentrations of sucrose were pre-selected using cell monolayers as a model. Diverse analytical methods were used for the interpretation of cryopreservation outcome such as Raman, cLSM and SEM microscopy, FTIR spectroscopy, compression testing, cryomicroscopy and DSC. No alterations in overall chemical structure of ‘in air’ cryopreserved scaffolds were revealed. Compressive stress of frozen scaffolds was significantly lower than in the control group presumably due to microdamages caused by ice crystals. In both groups, cells exhibited typical shape and well-preserved cell-cell and cell-matrix contacts after thawing. Moreover, viability test 24 h post-thaw demonstrated that application of sucrose in cryoprotective solution preserves significantly bigger portion of sucrose-pretreated cells (more than 80%) in comparison to DMSO alone (60%). Scaffolds *per se* showed very low heat capacity compared to that of pre-saturated with tested cryoprotectants. In conclusion, while many factors may contribute to this success, the second hypothesis to improve and optimize conventional cryopreservation by implementing ‘in air’ freezing, modified thawing protocol and combined application of sucrose has also been confirmed by the experimental results. In summary to this part of the project, cryopreservation of ‘ready-to-use’ TEPs is a promising strategy facilitating their future clinical application.

Electroporation of cells with sugars for xeno-free cryopreservation

Cryopreservation is the universal technology enabling continuous availability of cell aliquots to meet regenerative medicine demands. However, safety concerns over DMSO-induced side effects and immunogenicity of animal serum (main components of standard freezing media), support their replacement with non-toxic substances. Due to multiple cryoprotective properties, selected disaccharides, such as sucrose and trehalose, are widely used as additives

to various freezing solutions. Conceptually, combined introduction of sugars into cryopreservation media and their pre-freeze loading into cells serves as a novel alternative to conventional cryopreservation workflow. Among diverse techniques for sugar loading (e.g. fluid-phase endocytosis, genetically engineered proteins or nanoparticle-mediated delivery) electroporation is a preferred method in cryopreservation owing to its high-performance speed, safety and accuracy.

In this part of research work, the effect of electroporation-assisted delivery of sucrose, trehalose and raffinose into hUCMSCs on their post-thaw survival was investigated. The optimal strength of electrical field 1.5 kV/cm was determined from permeabilization (propidium iodide uptake) vs. cell survival data (resazurin reduction assay). After sugar loading (0-400mM), cells were allowed to reseal for 10 min and subjected to slow cooling followed by storage for 24 h in liquid nitrogen. Cell survival was evaluated using trypan blue assay and FACS. Using sugars as sole cryoprotectants, concentration-dependent increase in cell survival was observed. Irrespective of sugar type, the highest cell survival (up to 80%) was achieved at 400 mM concentration. Cell freezing without electroporation yielded significantly lower survival rates. In the optimal scenario, cells were able to attach 24 h after thawing demonstrating characteristic shape and sugar-loaded vacuoles. Application of 10% DMSO/90% FBS as a positive control provided cell survival exceeding 90%. Next, high glass transition temperatures determined for all sugars by DSC suggest the possibility to store samples at -80°C. To summarize this part of the work, electroporation with sugars is an effective strategy towards DMSO- and serum-free cryopreservation of stem cells confirming the third hypothesis formulated in this thesis.

In conclusion, the results of this dissertation work may pave the way for further progress in the establishing clinically safe biopreservation strategies for efficient long-term biobanking of 'ready-to-use' tissue-engineered constructs.

6. Outlook

6.1. Sucrose, antifreeze proteins and directional freezing as means to improve the cryopreservation outcome of adherent cells

The first part of ongoing work deals with determination of intracellular sucrose content using invertase and anthrone colorimetric methods and cell osmotic inactive volume using Coulter Counter. The main goal of this research is to determine intracellular sucrose concentration required for effective cryoprotection of adherent cells.

Other optimization steps include work directed towards optimization of sugar loading procedure into adherent cells using electroporation.

The further 2D cryopreservation work is being carried out in collaboration with Prof. Ido Braslavsky from the Institute of Biochemistry, Food Science and Nutrition, Robert H. Smith Faculty of Agriculture, Food and Environment, The Hebrew University of Jerusalem, Israel. This work includes establishing of the protocols for cryopreservation of adherent cells on flat electrospun scaffolds using directional freezing technique which involves ice seeding step. The directional freezing of HeLa cells attached to fiber mats prepared of polycaprolactone (PCL; 200 mg/ml, PCL200) and poly-L-lactic acid (PLA; 100 mg/ml, PLA100) using electrospinning method has shown a great promise as an innovative approach to successful cryopreservation of tissue-like structures. The post-thaw viability of cells was higher than 80% and the overall fiber mats integrity was found to be preserved. Further work is focused on the improvement of conventional cryopreservation by application of antifreeze proteins to reduce DMSO-mediated cellular toxicity. **Fig. 5.1** shows some promising results of the ongoing collaborative work.

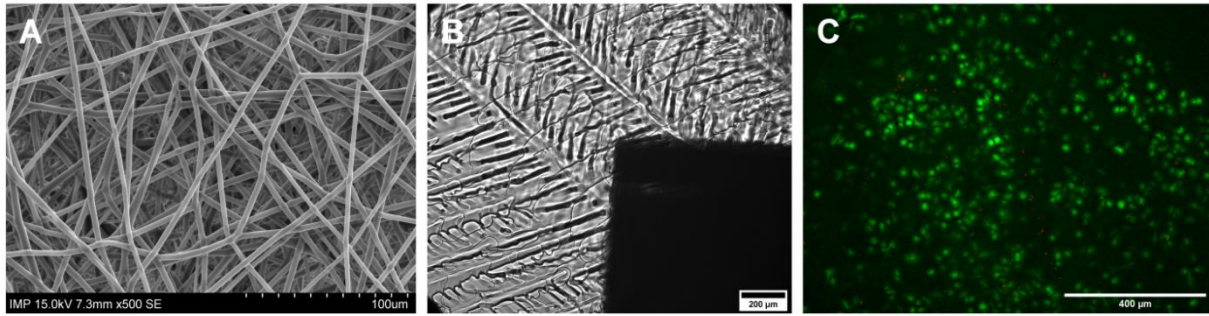


Figure 6.1 Results on design and cryopreservation of PCL200/PLA100 electrospun fiber mats seeded with HeLa cells

Typical SEM picture of a fiber mat with intricate fiber assemblies and interconnected pores (A), bright field picture of the process of ice formation during directional freezing of a fiber mat in 10% DMSO (B) and fluorescent picture showing the results of live-dead staining after freezing. Live cells are stained with fluorescein diacetate (FDA) in green and dead cells are stained in red with PI. The prevailing number of FDA-positive cells and small number of PI-stained cells reflects high cell viability after directional freezing.

6.2. Optimization and further characterization of ‘in air’ freezing and translation to other TEPs and cell types

Although ‘in air’ approach has not yet been optimized for more cryosensitive TEPs, preliminary translation of the developed protocol to freezing of coaxial alginate macrospheres laden with complex 3D structures formed by *cj*MSCs shows that it is superior to conventional cryopreservation. It must be noted that such intricate 3D constructs contain a fluid core and an alginate shell and are fairly difficult objects to cryopreserve because fluid contained in a core could contribute to enhanced thermal expansion and impairment of alginate visco-elastic properties. However, comparative pictures on the **Fig. 5.2** demonstrate that modified cryopreservation provided visibly better cryoprotection manifested by preserved construct integrity (C) and high viability of *cj*MSCs 3D assemblies (F) comparably with a control (A and D, respectively). At the same time, conventional protocol produced damages to structure of coaxial beads (B) and was characterized by much lower cell viability (E).

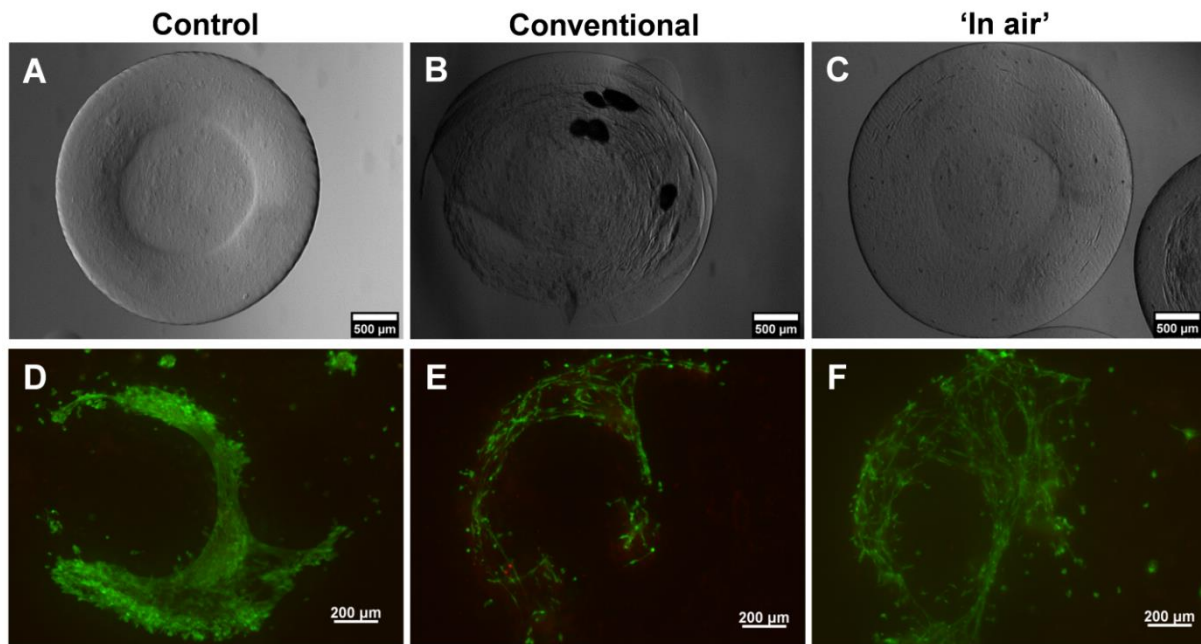


Figure 6.2 Results on translation of modified protocol to cryopreservation of tissue-like structures formed by *cJMSCs* within coaxial alginate beads.

The upper panel demonstrates optical microscopy pictures showing the state of alginate coaxial beads prior (A), after standard (B) and modified cryopreservation developed in the present work. On the lower panel, fluorescence microscopy pictures show the viability results for *cJMSCs* 7 days after modified (F) and standard (E) freezing against non-frozen cells (D). Much better preserved structure of 3D constructs and viability of *cJMSCs* building 3D tissue structures by modified cryopreservation suggest its further practical utility.

Thus, the following steps will further be elaborated to enhance the cryopreservation outcome:

1. Translation of modified protocol a to broader spectrum of cells and scaffolds;
2. Evaluation of controlled rate freezing with an active control over ice nucleation and vitrification for protection of scaffold mechanical properties;
3. Increase loading efficiency of natural CPAs using electroporation to assess DMSO-free cryopreservation of TEPs
4. Cryopreservation of stem cells in pre-differentiated state on 3D scaffolds;
5. Cryopreservation of 3D scaffolds in cryobags with improved heat transfer and thermal expansion properties;
6. Investigate the consequences of modified cryopreservation to immunological and epigenetic response of cells.

Another part of the ongoing work in collaboration with Prof. Anastassopoulos from the TEI Thessaly, Greece is related to monitoring the freezing/thawing dynamics within 3D TEPs using differential thermal analysis. This method together with thermocouples provides more complete picture of heat distribution upon for ‘in air’ system. **Fig. 5.3** illustrates visualization

of latent heat release within in house prepared collagen-HAP scaffolds frozen ‘in air’ (A) or bulk medium (B). For comparison purposes, measurements with thermocouples (C) have also been performed.

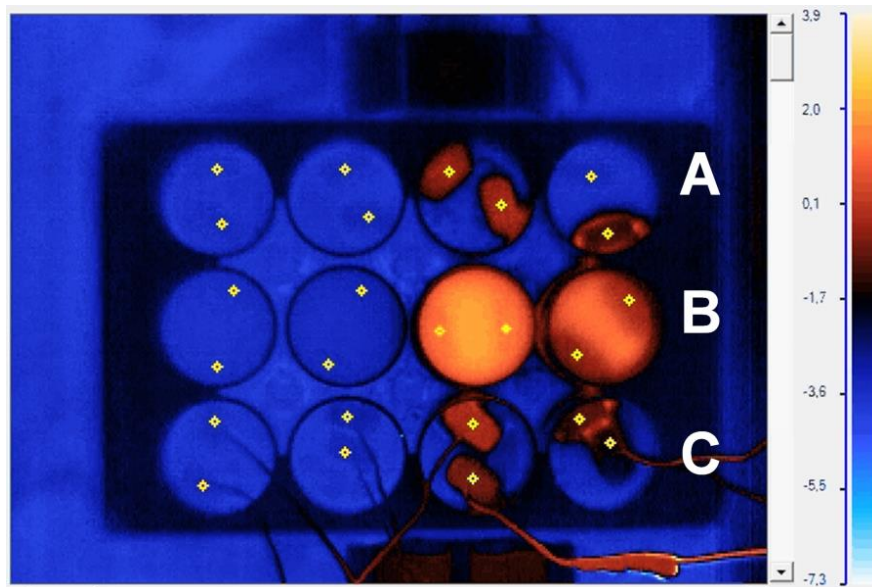


Figure 6.3 Still frame from a thermal video recorded by μ -Thermalyzer software.

The picture shows latent heat release in 3D collagen-HAP scaffolds frozen ‘in air’ (A) and in bulk solution with antifreeze proteins (fish AFPIII) (B). Color scale indicates difference in temperatures. Latent heat at different stages of its evolution is clearly seen by higher temperatures in gradations of red.

6.3. Electroporation of stem cells in TEPs to establish their DMSO- and serum-free cryopreservation

Furthermore, the work on electroporation presented in this thesis is integrated into a broader ongoing international research project with Ljubljana University, Slovenia with the ultimate goal to introduce non-permeant natural CPAs of interest (sugars, AFPs) into stem cell-seeded tissue-engineered 3D scaffolds and tissue sections for efficient cryopreservation. The first results obtained on electrospun fiber mats are promising and stimulate further in-depth research. **Fig. 5.4** presents the designed electrodes (A) used for electroporation of Chinese hamster ovary cells (CHO). Before electroporation cells were stained with viability dye CellTracker Green giving green fluorescence. PI with red fluorescence was used for staining of both dead and permeabilized cells. A control sample (B) and a sample electroporated at 1.5 kV/cm (C) are shown. Increased number of PI-positive cells simultaneously stained with

CellTracker Green in the electroporated sample suggests efficient electroporation of attached cells.

In the future studies the following points are intended to be addressed:

1. Test different pulse parameters;
2. Determine intracellular sugar content providing highest cell viability;
3. Increase storage time;
4. Perform more detailed study of cell recovery after electroporation and cryopreservation;
5. transfer the technology on adherent cells and cells to 3D scaffolds

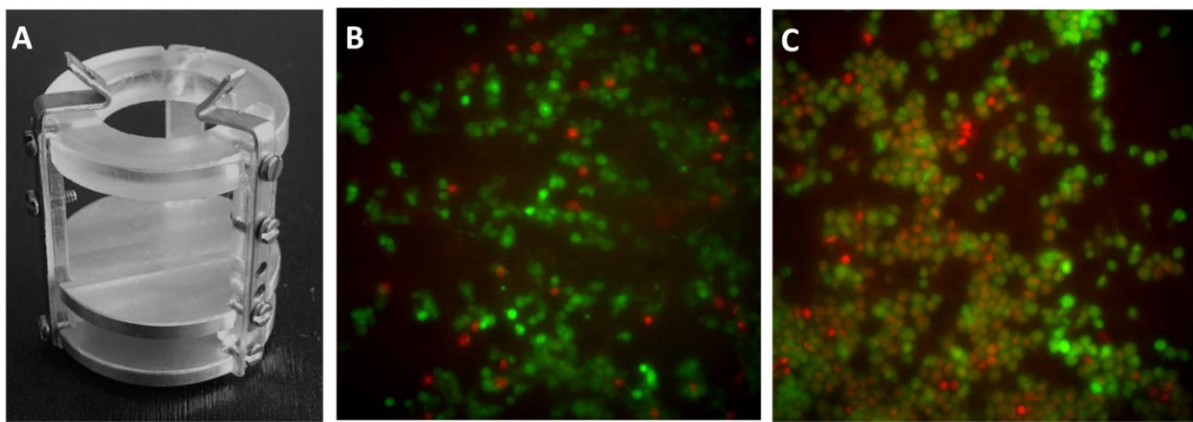


Figure 6.4 Electrode assembly for electroporation of electrospun fiber mats (A).

CHO cells on fiber mats before (B) and after (C) electroporation with PI in sucrose-based buffer. Cells with green fluorescence represent viable cells, red cells represent dead cells. Colocalized images with cells exhibiting green and red fluorescence simultaneously being permeabilized (image courtesy by Tobias Pfister).

7. References

- Acker JP, Lu XM, et al. Measurement of trehalose loading of mammalian cells porated with a metal-actuated switchable pore. *Biotechnol Bioeng*. 2003;82(5):525–32.
- Acker JP, McGann LE. Protective effect of intracellular ice during freezing? *Cryobiology*. 2003;46(2):197–202.
- Bahari L, Bein A, et al. Directional freezing for the cryopreservation of adherent mammalian cells on a substrate. *PLoS One*. 2018;13(2):e0192265.
- Bailey TL, Wang M, et al. Protective effects of osmolytes in cryopreserving adherent neuroblastoma (Neuro-2a) cells. *Cryobiology*. 2015;71(3):472–80.
- Bakken AM. Cryopreserving human peripheral blood progenitor cells. *Curr Stem Cell Res Ther*. 2006;1(1):47–54.
- Batista Napotnik T, Miklavčič D. Bioelectrochemistry In vitro electroporation detection methods – An overview. *Bioelectrochemistry*. 2018;120:166–182.
- Batnyam O, Suye SI, Fujita S. Direct cryopreservation of adherent cells on an elastic nanofiber sheet featuring a low glass-transition temperature. *RSC Advances*. 2017;7(81):51264–51271.
- Baust JG, Gao D, Baust JM. Cryopreservation: An emerging paradigm change. *Organogenesis*. 2009;5(3):90–6.
- Beier AFJ, Schulz JC, et al. Effective surface-based cryopreservation of human embryonic stem cells by vitrification. *Cryobiology*. 2011;63(3):175–85.
- Ben Messaoud N, Katarova I, López JM. Basic properties of the p38 signaling pathway in response to hyperosmotic shock. *PLoS One*. 2015;10(9):e0135249.
- Best BP. Cryoprotectant toxicity: facts, issues, and questions. *Rejuvenation Res*. 2015;18(5):422–36.
- Bieback K. Platelet lysate as replacement for fetal bovine serum in mesenchymal stromal cell cultures. *Transfus Med Hemother*. 2013; 40(5): 326–335.
- Bissoyi A, Bit A, et al. Enhanced cryopreservation of MSCs in microfluidic bioreactor by regulated shear flow. *Sci. Rep*. 2016;6:1–13.
- Bissoyi A, Pramanik K, et al. Cryopreservation of hMSCs seeded silk nanofibers based tissue engineered constructs. *Cryobiology*. 2014;68(3):332–42.
- Bright NA, Davis LJ, et al. Endolysosomes are the principal intracellular sites of acid hydrolase activity. *Curr Biol*. 2016;26(17):2233–45.
- Bright NA, Reaves BJ, et al. Dense core lysosomes can fuse with late endosomes and are re-formed from the resultant hybrid organelles. *J Cell Sci*. 1997;110(Pt17):2027–40.
- Campbell LH, Brockbank KGM. Comparison of electroporation and ChariotTM for delivery of β -galactosidase into mammalian cells: strategies to use trehalose in cell preservation. *Vitr Cell Dev Biol - Anim*. 2011;47(3):195–199.
- Capicciotti CJ, Kurach JDR, et al. Small molecule ice recrystallization inhibitors enable

- freezing of human red blood cells with reduced glycerol concentrations. *Sci Rep*. 2015;5:9692.
- Carden A, Morris MD. Application of vibrational spectroscopy to the study of mineralized tissues (review). *J Biomed Opt*. 2000;5(3):259–68.
- Cardoso LMDF, Pinto MA, et al. Cryopreservation of rat hepatocytes with disaccharides for cell therapy. *Cryobiology*. 2017;78:15–21.
- Carpenter JF, Crowe JH. An infrared spectroscopic study of the interactions of carbohydrates with dried proteins. *Biochemistry*. 1989;28(9):3916–22.
- Charoo NA, Rahman Z, et al. Electroporation: an avenue for transdermal drug delivery. *Curr Drug Deliv*. 2010;7(2):125–36.
- Chatterjee A, Saha D, et al. Effects of cryopreservation on the epigenetic profile of cells. *Cryobiology*. 2017;74:1–7.
- Chaytor JL, Tokarew JM, et al. Inhibiting ice recrystallization and optimization of cell viability after cryopreservation. *Glycobiology*. 2012;22(1):123–33.
- Chen A, Mercado SA, Slater NK. Antioxidant modified amphiphilic polymer improves intracellular cryoprotectant delivery and alleviates oxidative stress in HeLa cells. *Adv Mater Sci*. 2017; 2(4):1–7.
- Chen F, Zhang W, et al. Cryopreservation of tissue-engineered epithelial sheets in trehalose. *Biomaterials*. 2011;32(33):8426–35.
- Chen G, Yue A, et al. Comparison of the effects of different cryoprotectants on stem cells from umbilical cord blood. *Stem Cells Int*. 2016;2016:1396783–1396790.
- Chen X, Li M, et al. Trehalose, sucrose and raffinose are novel activators of autophagy in human keratinocytes through an mTOR-independent pathway. *Sci Rep*. 2016;22;6:28423.
- Chinnadurai R, Copland IB, et al. Cryopreserved mesenchymal stromal cells are susceptible to T-cell mediated apoptosis which is partly rescued by ifn γ licensing. *Stem Cells*. 2016;34(9):2429–42.
- Cho HJ, Lee SH, et al. Evaluation of cell viability and apoptosis in human amniotic fluid-derived stem cells with natural cryoprotectants. *Cryobiology*. 2014;68(2):244–50.
- Choi J, Bischof JC. Review of biomaterial thermal property measurements in the cryogenic regime and their use for prediction of equilibrium and non-equilibrium freezing applications in cryobiology. *Cryobiology*. 2010;60(1):52–70.
- Chow MJ, Zhang Y. Changes in the mechanical and biochemical properties of aortic tissue due to cold storage. *J Surg Res*. 2011;171(2):434–42.
- Pan C, Yu S, et al. Effect of sucrose on cryopreservation of pig spermatogonial stem cells. *J Integr Agric*. 2017;16(5):1120–1129.
- Costa PF, Dias AF, et al. Cryopreservation of cell/scaffold tissue-engineered constructs. *Tissue Eng Part C Methods*. 2012;18(11):852–8.
- Costanzo JP, Lee RE. Avoidance and tolerance of freezing in ectothermic vertebrates. *J Exp Biol*. 2013;216(Pt 11):1961–7.
- Cuadrado A, Nebreda AR. Mechanisms and functions of p38 MAPK signalling. *Biochem J*.

- 2010;429(3):403–17.
- Daniele N, Zinno F. Quality controls of cryopreserved hematopoietic stem cells. *Acta Haematol. Pol.* 2015;46(5):347–52.
- De Sousa PA, Steeg R, et al. Rapid establishment of the european bank for induced pluripotent stem cells (EBiSC) - the hot start experience. *Stem Cell Res.* 2017;20:105–114.
- DeCoursey K, Storrie B. Osmotic swelling of endocytic compartments induced by internalized sucrose is restricted to mature lysosomes in cultured mammalian cells. *Exp Cell Res.* 1991;192(1):52–60.
- Delgadillo JOV, Delorme S, et al. Effect of freezing on the passive mechanical properties of arterial samples. *J Biomed Sci Eng.* 2010;3:645–652
- Dolev MB, Braslavsky I, Davies PL. Ice-binding proteins and their function. *Annu Rev Biochem.* 2016;85:515–42.
- Dovgan B, Barlič A, et al. Cryopreservation of human adipose-derived stem cells in combination with trehalose and reversible electroporation. *J Membr Biol.* 2017;250(1):1–9.
- Ehrlich LE, Feig JSG, et al. Large thermal conductivity differences between the crystalline and vitrified states of DMSO with applications to cryopreservation. *PLoS One.* 2015;10(5):e0125862.
- Eisenberg DP, Steif PS, Rabin Y. On the effects of thermal history on the development and relaxation of thermo-mechanical stress in cryopreservation. *Cryogenics.* 2014;64:86–94.
- Elder E, Chen Z, et al. Enhanced tissue strength in cryopreserved, collagen-based blood vessel constructs. *Transplant Proc.* 2005;37(10):4625–9.
- Elliott GD, Wang S, Fuller BJ. Cryoprotectants: A review of the actions and applications of cryoprotective solutes that modulate cell recovery from ultra-low temperatures. *Cryobiology.* 2017;76:74–91.
- Elliott GD, Wang S, et al. Cryoprotectants: A review of the actions and applications of cryoprotective solutes that modulate cell recovery from ultra-low temperatures. *Cryobiology.* 2017;76:74–91.
- Erdag G, Eroglu A, et al. Cryopreservation of fetal skin is improved by trehalose, *Cryobiology.* 2002;44(3):218–28.
- Eroglu A, Elliott G, et al. Progressive elimination of microinjected trehalose during mouse embryonic development. *Reprod Biomed Online.* 2005;10(4):503–10.
- Eroglu A, Russo MJ, et al. Intracellular trehalose improves the survival of cryopreserved mammalian cells. *Nat Biotechnol.* 2000;18(2):163–7.
- Eroglu A. Cryopreservation of mammalian oocytes by using sugars: Intra- and extracellular raffinose with small amounts of dimethylsulfoxide yields high cryosurvival, fertilization, and development rates. *Cryobiology.* 2010;60(3 Suppl):54–9.
- Eskandari N, Marquez-Curtis LA, et al. Cryopreservation of human umbilical vein and porcine corneal endothelial cell monolayers. *Cryobiology.* 2018. pii: S0011–2240(18)30250–5.
- Everatt MJ, Convey P, et al. Responses of invertebrates to temperature and water stress: A

- polar perspective. *J Therm Biol.* 2015;54:118–32.
- Fahy GM, MacFarlane DR, et al. Vitricification as an approach to cryopreservation. *Cryobiology.* 1984;21(4):407–26.
- Fahy GM, Wowk B, Wu J. Cryopreservation of Complex Systems: The Missing Link in the Regenerative Medicine Supply Chain. *Rejuvenation Res.* 2006;9(2):279–91.
- Fahy GM, Wowk B. Principles of Cryopreservation by Vitricification. *Methods Mol Biol.* 2015;1257:21–82.
- Fan WX, Ma XH, et al. Vitricification of corneal endothelial cells in a monolayer. *J Biosci Bioeng.* 2008;106(6):610–3.
- Farooque TM, Chen Z, et al. Protocol development for vitricification of tissue-engineered cartilage. *Bioprocessing (Williamsbg Va).* 2009;8(4):29–36.
- Ferris AL, Brown JC, et al. Chinese hamster ovary cell lysosomes rapidly exchange contents. *J Cell Biol.* 1987;105(6 Pt 1):2703–12.
- Findenegg GH, Jähnert S, et al. Freezing and melting of water confined in silica nanopores. *Chemphyschem.* 2008;9(18):2651–9.
- Fong B, Watson PH, Watson AJ. Mouse preimplantation embryo responses to culture medium osmolarity include increased expression of CCM2 and p38 MAPK activation. *BMC Dev Biol.* 2007;7:2.
- Fong LP, Hunt CJ, Pegg DE. Cryopreservation of the rabbit cornea: freezing with dimethyl sulphoxide in air or in medium. *Curr Eye Res.* 1987;6(4):569–77.
- François M, Copland IB, et al. Cryopreserved mesenchymal stromal cells display impaired immunosuppressive properties as a result of heat-shock response and impaired interferon- γ licensing. *Cytotherapy.* 2012;14(2):147–152.
- Gallardo BJM, Miró MÁ, et al. Autophagy and apoptosis have a role in the survival or death of stallion spermatozoa during conservation in refrigeration. *PLoS One.* 2012;7(1):e30688.
- Gelinsky M, König U, et al. Poröse Scaffolds aus mineralisiertem Kollagen – ein biomimetisches Knochenersatzmaterial. *Materwiss. Werkstofftech.* 2004;35(4):229–233.
- Gelinsky M, Welzel PB, et al. Porous three-dimensional scaffolds made of mineralised collagen: Preparation and properties of a biomimetic nanocomposite material for tissue engineering of bone. *Chem Eng J.* 2008;137(1):84–96.
- Gelinskya M, Welzelb PB, et al. Porous three-dimensional scaffolds made of mineralised collagen: Preparation and properties of a biomimetic nanocomposite material for tissue engineering of bone. *Chem Eng J.* 2008;137(1):84–96.
- Germann A, Schulz JC, et al. Standardized serum-free cryomedia maintain peripheral blood mononuclear cell viability, recovery, and antigen-specific T-cell response compared to fetal calf serum-based medium. *Biopreserv Biobank.* 2011;9(3):229–236.
- Ghosh S, Ozcelikkale A, et al. Role of intracellular poroelasticity on freezing-induced deformation of cells in engineered tissues. *J R Soc Interface.* 2016;13(123). pii: 20160480.
- Giwa S, Lewis JK, et al. The promise of organ and tissue preservation to transform medicine. *Nat Biotechnol.* 2017;35(6):530–542.

- Goecke T, Theodoridis K, et al. In vivo performance of freeze-dried decellularized pulmonary heart valve allo- and xenografts orthotopically implanted into juvenile sheep. *Acta Biomaterialia*. 2018;68:41–52.
- Gordon PB, Tolleshaug H, Seglen PO. Autophagic sequestration of [^{14}C]sucrose introduced into isolated rat hepatocytes by electrical and non-electrical methods. *Exp Cell Res*. 1985;160(2):449–58.
- Graham B, Bailey TL, et al. Polyproline as a minimal antifreeze protein mimic that enhances the cryopreservation of cell monolayers. *Angew Chem Int Ed Engl*. 2017;56(50):15941–15944.
- Gryshkov O, Hofmann N, et al. Multipotent stromal cells derived from common marmoset *Callithrix jacchus* within alginate 3D environment: Effect of cryopreservation procedures. *Cryobiology*. 2015;71(1):103–11.
- Gryshkov O, Hofmann N, et al. Multipotent stromal cells derived from common marmoset *Callithrix jacchus* within alginate 3D environment: Effect of cryopreservation procedures. *Cryobiology*. 2015;71(1):103–11.
- Gryshkov O, Pogozhykh D, et al. Encapsulating non-human primate multipotent stromal cells in alginate via high voltage for cell-based therapies and cryopreservation. *PLoS One*. 2014;9(9):e107911.
- Gurruchaga H, Saenz Del Burgo L, et al. Cryopreservation of human mesenchymal stem cells in an allogeneic bioscaffold based on platelet rich plasma and synovial fluid. *Sci Rep*. 2017;7:15733.
- Halberstadt M, Böhnke M, et al. Cryopreservation of human donor corneas with dextran. *Invest Ophthalmol Vis Sci*. 2003;44(12):5110–5.
- Han B, Bischof JC. Effect of thermal properties on heat transfer in cryopreservation and cryosurgery. ASME 2002 International Mechanical Engineering Congress and Exposition. Advances in Heat and Mass Transfer in Biotechnology, New Orleans, Louisiana, USA, November 17–22, 2002.
- Han B, Teo KY, et al. Thermomechanical analysis of freezing-induced cell-fluid-matrix interactions in engineered tissues. *J Mech Behav Biomed Mater*. 2013;18:67–80.
- Hauptmann A, Podgor K, et al. Impact of buffer, protein concentration and sucrose addition on the aggregation and particle formation during freezing and thawing. *Pharm Res*. 2018;35(5):101.
- He X. Thermostability of biological systems: fundamentals, challenges, and quantification. *Open Biomed Eng J*. 2011;5:47–73.
- Helip-Wooley A, Thoene JG. Sucrose-induced vacuolation results in increased expression of cholesterol biosynthesis and lysosomal genes. *Exp Cell Res*. 2004;292(1):89–100.
- Heng BC, Yu YJH, Ng SC. Slow-cooling protocols for microcapsule cryopreservation. *J Microencapsul*. 2004;21(4):455–67.
- Higgins AZ, Karlsson JOM. Effects of intercellular junction protein expression on intracellular ice formation in mouse insulinoma cells. *Biophys J*. 2013;105(9):2006–15.
- Higuchi T, Nishikawa J, Inoue H. Sucrose induces vesicle accumulation and autophagy. *J*

- Cell Biochem.* 2015;116(4):609–17.
- Holm S. Biobanking human embryonic stem cell lines: policy, ethics and efficiency. *Monash Bioeth Rev.* 2015;33(4):265–76.
- Huang H, Zhao G, et al. Predehydration and ice seeding in the presence of trehalose enable cell cryopreservation. *ACS Biomater Sci Eng.* 2017;3(8):1758–1768.
- Huang YT, Yan H, et al. Cryopreserved cell monolayers for rapid detection of herpes simplex virus and influenza virus. *J Clin Microbiol.* 2002;40(11):4301–4303.
- Hunt CJ. Cryopreservation of human stem cells for clinical application: a review. *Transfus Med Hemother.* 2011; 38(2): 107–123.
- Iwatani M, Ikegami K, et al. Dimethyl sulfoxide has an impact on epigenetic profile in mouse embryoid body. *Stem Cells.* 2006;24(11):2549–56.
- Jahraus A, Storrie B, et al. Evidence for retrograde traffic between terminal lysosomes and the prelysosomal/late endosome compartment. *J Cell Sci.* 1994;107(Pt1):145–57.
- Jang TH, Park SC, et al. Cryopreservation and its clinical applications. *Integr Med Res.* 2017;6(1):12–18.
- Ji L, de Pablo JJ, Palecek SP. Cryopreservation of adherent human embryonic stem cells. *Biotechnol Bioeng.* 2004;88(3):299–312.
- Jin B, Mazur P. High survival of mouse oocytes/embryos after vitrification without permeating cryoprotectants followed by ultra-rapid warming with an IR laser pulse. *Sci Rep.* 2015;5:9271.
- Karageorgos LE, Isaac EL, et al. Lysosomal biogenesis in lysosomal storage disorders. *Exp Cell Res.* 1997;234(1):85–97.
- Katzen E, Wolfgang F, et al. Cryopreservation of primary human hepatocytes : the benefit of trehalose as an additional cryoprotective agent. *Liver Transpl.* 2007;13(1):38–45.
- Katkov I. Electroporation of cells in applications to cryobiology: summary of 20-year experience. *Problems of Cryobiology.* 2002;2:3–8.
- Katkov II, Kan NG, et al. DMSO-free programmed cryopreservation of fully dissociated and adherent human induced pluripotent stem cells. *Stem Cells Int.* 2011;2011:981606.
- Katkov II, Kim MS, et al. Cryopreservation by slow cooling with DMSO diminished production of Oct-4 pluripotency marker in human embryonic stem cells. *Cryobiology.* 2006;53(2):194–205.
- Katsen-Globa A, Meiser I, et al. Towards ready-to-use 3-D scaffolds for regenerative medicine: Adhesion-based cryopreservation of human mesenchymal stem cells attached and spread within alginate-gelatin cryogel scaffolds. *J Mater Sci Mater Med.* 2014;25(3):857–71.
- Khan AF, Awais M, et al. Raman spectroscopy of natural bone and synthetic apatites. *Appl Spectrosc Rev.* 2013;48(4):329–355.
- Kilbride P, Mahbubani K, et al. Cryopreservation of adherent cells in 96 well plates. 2nd IIR Workshop on cold applications in life sciences, Germany, 2016.09.8–9.
- Kilbride P, Morris GJ. Viscosities encountered during the cryopreservation of dimethyl

- sulphoxide systems. *Cryobiology*. 2017;76:92–97.
- Kinosita K Jr, Tsong TY. Survival of sucrose-loaded erythrocytes in the circulation. *Nature*. 1978;272(5650):258–60.
- Kofron MD, Opsitnick NC, et al. Cryopreservation of tissue engineered constructs for bone. *J Orthop Res*. 2003;21(6):1005–10.
- Koshimoto C, Mazur P. The effect of the osmolality of sugar-containing media, the type of sugar, and the mass and molar concentration of sugar on the survival of frozen-thawed mouse sperm. *Cryobiology*. 2002;45(1):80–90.
- Kubo K, Kuroyanagi Y. Development of a cultured dermal substitute composed of a spongy matrix of hyaluronic acid and atelo-collagen combined with fibroblasts: cryopreservation. *J Biomater Sci Polym Ed*. 2003;14(7):625–41.
- Kuleshova LL, Gouk SS, Hutmacher DW. Vitrification as a prospect for cryopreservation of tissue-engineered constructs. *Biomaterials*. 2007;28(9):1585–96.
- Lam SKL, Chan SCW, et al. The role of cryopreservation in the biomechanical properties of the intervertebral disc. *Eur Cell Mater*. 2011;22:393–402.
- Lauterboeck L, Saha D, et al. Xeno-free cryopreservation of bone marrow-derived multipotent stromal cells from *Callithrix jacchus*. *Biopreserv Biobank*. 2016;14(6):530–538.
- Lee JC, Timasheff SN. The stabilization of proteins by sucrose. *J Biol Chem*. 1981;256(14):7193–201.
- Lee Y, Kim Y, et al. Effect of sugar molecules on the cryopreservation of mouse spermatogonial stem cells. *Fertil Steril*. 2014;101(4):1165–75.e5.
- Levin RL, Cravalho EG, Huggins CE. A membrane model describing the effect of temperature on the water conductivity of erythrocyte membranes at subzero temperatures. *Cryobiology*. 1976;13(4):415–29.
- Li Y, Zhao G, et al. Measurement of thermal conductivities of two cryoprotective agent solutions for vitreous cryopreservation of organs at the temperature range of 77 k–300 k using a thermal sensor made of microscale enamel copper wire. *Biopreserv Biobank*. 2017;15(3):228–233.
- Lia H. Campbell and Kelvin G.M. Brockbank (July 25th 2014). Cryopreservation of adherent cells on a fixed substrate, Recent advances in cryopreservation, Hideaki Yamashiro, IntechOpen.
- Lia H. Campbell and Kelvin G.M. Brockbank (March 14th 2012). Cryopreservation of adherent smooth muscle and endothelial cells with disaccharides, Current frontiers in cryopreservation, Igor I. Katkov, IntechOpen.
- Lippens E, Cornelissen M. Slow cooling cryopreservation of cell-microcarrier constructs. *Cells Tissues Organs*. 2010;192(3):177–86.
- Liu BL, McGrath JJ. Effects of freezing on the cytoskeleton, focal adhesions and gap-junctions in murine osteoblast cultures. *Conf Proc IEEE Eng Med Biol Soc*. 2005;5:4896–9.
- Liu Y, Xu X, et al. Effect of various freezing solutions on cryopreservation of mesenchymal stem cells from different animal species. *Cryo Letters*. 2011;32(5):425–35.

- Lovelock JE, Bishop MW. Prevention of freezing damage to living cells by dimethyl sulphoxide. *Nature*. 1959;183(4672):1394–5.
- Luetzkendorf J, Nerger K, et al. Cryopreservation does not alter main characteristics of Good Manufacturing Process e grade human multipotent mesenchymal stromal cells including immunomodulating potential and lack of malignant transformation. *Cytotherapy*. 2015;17(2):186–98.
- Lynch AL, Slater NKH. Mediated trehalose un-loading for reduced erythrocyte osmotic fragility and phosphatidylserine translocation. *Cryo Letters*. 2011;32(5):415–24.
- Malpique R, Ehrhart F, et al. Cryopreservation of adherent cells: strategies to improve cell viability and function after thawing. *Tissue Eng Part C Methods*. 2009;15(3):373–86.
- Mantri S, Kanungo S, Mohapatra PC. Cryoprotective effect of disaccharides on cord blood stem cells with minimal use of DMSO. *Indian J Hematol Blood Transfus*. 2015;31(2):206–12.
- Manuchehrabadi N, Gao Z, et al. Improved tissue cryopreservation using inductive heating of magnetic nanoparticles. *Sci Transl Med*. 2017;9(379). pii: eaah4586.
- Martinetti D, Colarossi C, et al. Effect of trehalose on cryopreservation of pure peripheral blood stem cells. *Biomed Rep*. 2017;6(3):314–318.
- Matsumura K, Kawamoto K, et al. Cryopreservation of a two-dimensional monolayer using a slow vitrification method with polyampholyte to inhibit ice crystal formation. *ACS Biomater Sci Eng*. 2016;2(6):1023–1029.
- Mazur P, Leibo SP, Chu EH. A two-factor hypothesis of freezing injury. Evidence from Chinese hamster tissue-culture cells. *Exp Cell Res*. 1972;71(2):345–55.
- Mazur P. Freezing of living cells: mechanisms and implications. *Am J Physiol*. 1984;247(3 Pt 1):C125–42.
- Mensink MA, Frijlink HW, et al. How sugars protect proteins in the solid state and during drying (review): Mechanisms of stabilization in relation to stress conditions. *Eur J Pharm Biopharm*. 2017;114:288–295.
- Meryman HT, Williams RJ, Douglas MSJ. Freezing injury from “solution effects” and its prevention by natural or artificial cryoprotection. *Cryobiology*. 1977;14(3):287–302.
- Meryman HT. Osmotic stress as a mechanism of freezing injury. *Cryobiology*. 1971;8(5):489–500.
- Michele KH, Amirhossein C. Autophagy induction by trehalose : Molecular mechanisms and therapeutic impacts. *J Cell Physiol*. 2018;233(9):6524–6543.
- Miklavčič D, Mali B, et al. Electrochemotherapy: From the drawing board into medical practice. *Biomed Eng Online*. 2014;13(1):29.
- Mitrus I, Smagur A, et al. Reduction of DMSO concentration in cryopreservation mixture from 10% to 7.5% and 5% has no impact on engraftment after autologous peripheral blood stem cell transplantation: results of a prospective, randomized study. *Bone Marrow Transplant*. 2018;53(3):274–280.
- Miyamoto Y, Enosawa S, et al. Cryopreservation in situ of cell monolayers on collagen vitrigel membrane culture substrata: Ready-to-use preparation of primary hepatocytes and

- ES cells. *Cell Transplant*. 2009;18(5):619–26.
- Miyoshi H, Ehashi T, et al. Cryopreservation of fibroblasts immobilized within a porous scaffold: effects of preculture and collagen coating of scaffold on performance of three-dimensional cryopreservation. *Artif Organs*. 2010;34(7):609–14.
- Moll G, Alm JJ, et al. Do cryopreserved mesenchymal stromal cells display impaired immunomodulatory and therapeutic properties? *Stem Cells*. 2014;32(9):2430–42.
- Moll G, Geißler S, et al. Cryopreserved or fresh mesenchymal stromal cells: only a matter of taste or key to unleash the full clinical potential of msc therapy? *Adv Exp Med Biol*. 2016;951:77–98.
- Morris C, de Wreede L, et al. Should the standard dimethyl sulfoxide concentration be reduced? Results of a European Group for Blood and Marrow Transplantation prospective noninterventional study on usage and side effects of dimethyl sulfoxide. *Transfusion*. 2014;54(10):2514–22.
- Mutsenko V, Gryshkov O, et al. The impact of sucrose pretreatment on survival of mesenchymal stromal cells, cryopreserved in suspension and adherent state. *Cryobiology*. 2016;73(3):402.
- Mutsenko VV, Gryshkov O, et al. Novel chitin scaffolds derived from marine sponge *Ianthella basta* for tissue engineering approaches based on human mesenchymal stromal cells: Biocompatibility and cryopreservation. *Int J Biol Macromol*. 2017;104(Pt B):1955–1965.
- Neidert MR, Devireddy RV, et al. Improved freezing in the presence of cryoprotective agents. *Tissue Eng*. 2004;10(1-2):23–32.
- Neves LS, Rodrigues MT, et al. Current approaches and future perspectives on strategies for the development of personalized tissue engineering therapies. *Expert Rev Precis Med Drug Dev*. 2016;1(1): 93–108.
- Ntai A, Baronchelli S, et al. A review of research-grade human induced pluripotent stem cells qualification and biobanking processes. *Biopreserv Biobank*. 2017;15(4):384–392.
- Ohkawara H, Miyagawa S, et al. Development of a vitrification method for preserving human myoblast cell sheets for myocardial regeneration therapy. *BMC Biotechnol*. 2018;18(1):56.
- Oliver AE, Jamil K, et al. Loading human mesenchymal stem cells with trehalose by fluid-phase endocytosis. *Cell Preserv Technol*. 2004;2(1):35–49.
- Omori K, Valiente L, et al. Improvement of human islet cryopreservation by a p38 MAPK inhibitor. *Am J Transplant*. 2007;7(5):1224–32.
- Oswald I, Rickert M, et al. The influence of cryopreservation and quick-freezing on the mechanical properties. *J Biomech*. 2017;64:226–230.
- Ozawa M, Ozawa Y, et al. A simple improvement of the conventional cryopreservation for human ES and iPS cells. *Protocol Exchange* (2014).
- Ozcelikkale A, Han B. Thermal destabilization of collagen matrix hierarchical structure by freeze/thaw. *PLoS One*. 2016;11(1):e0146660.
- Pan J, Shu Z, et al. Towards uniform and fast rewarming for cryopreservation with electromagnetic resonance cavity: numerical simulation and experimental investigation.

- Appl Therm Eng.* 2018;140:787–798.
- Parenteau-Bareil R, Gauvin R, Berthod F. Collagen-based biomaterials for tissue engineering applications. *Materials (Basel)*. 2010;3(3):1863–1887.
- Park BW, Jang SJ, et al. Cryopreservation of human dental follicle tissue for use as a resource of autologous mesenchymal stem cells. *J Tissue Eng Regen Med.* 2017;11(2):489–500.
- Pasch J, Schiefer A, et al. Variation of the HES concentration for the cryopreservation of keratinocytes in suspensions and in monolayers. *Cryobiology.* 41(2):89–96
- Pegg DE. Cryopreservation of vascular endothelial cells as isolated cells and as monolayers. *Cryobiology.* 2002;44(1):46–53.
- Pennes HH. Analysis of tissue and arterial blood temperatures in the resting human forearm. *J Appl Physiol (1985)*. 1998;85(1):5–34.
- Peters JH, Preijers FW, et al. Clinical Grade Treg : GMP isolation , improvement of purity by CD127 pos depletion, treg expansion, and treg cryopreservation. *PLoS One.* 2008;3(9):e3161.
- Petrenko YA, Jones DRE, Petrenko AY. Cryopreservation of human fetal liver hematopoietic stem/progenitor cells using sucrose as an additive to the cryoprotective medium. *Cryobiology.* 2008;57(3):195–200.
- Petrenko YA, Petrenko AY, et al. Perfusion bioreactor-based cryopreservation of 3D human mesenchymal stromal cell tissue grafts. *Cryobiology.* 2017;76:150–153.
- Petrenko YA, Rogulska OY, et al. A sugar pretreatment as a new approach to the me2so- and xeno-free cryopreservation of human mesenchymal stromal cells. *Cryo Letters.* 2014;35(3):239–46.
- Pless-Petig G, Knoop S, Rauhen U. Serum- and albumin-free cryopreservation of endothelial monolayers with a new solution. *Organogenesis.* 2018;14(2):107–121.
- Pogozhykh O, Prokopyuk V, et al. Towards biobanking technologies for natural and bioengineered multicellular placental constructs. *Biomaterials.* 2018;185:39–50.
- Poisson JS, Acker JP, et al. modulating intracellular ice growth with cell permeating small molecule ice recrystallization inhibitors. *Langmuir.* 2018.
- Pollock K, Samsonraj RM, et al. improved post-thaw function and epigenetic changes in mesenchymal stromal cells cryopreserved using multicomponent osmolyte solutions. *Stem Cells Dev.* 2017;26(11):828–842.
- Popa EG, Rodrigues MT, et al. Cryopreservation of cell laden natural origin hydrogels for cartilage regeneration strategies. *Soft Matter.* 2013;9:875–885.
- Pravdyuk AI, Petrenko YA et al. Cryopreservation of alginate encapsulated mesenchymal stromal cells. *Cryobiology.* 2013;66(3):215–22.
- Prickett RC, Marquez-Curtis LA, et al. Effect of supercooling and cell volume on intracellular ice formation. *Cryobiology.* 2015;70(2):156–163.
- Rabin Y, Steif PS, et al. Fracture formation in vitrified thin films of cryoprotectants. *Cryobiology.* 2006;53(1):75–95.
- Rao W, Huang H, et al. nanoparticle-mediated intracellular delivery enables cryopreservation

- of human adipose-derived stem cells using trehalose as the sole cryoprotectant. *ACS Appl Mater Interfaces*. 2015;7(8):5017–28.
- Repanas A, Lauterböck L, et al. The effect of freezing on PCL and PCL/ CS electrospun scaffolds for tissue engineering applications. *Sch Acad J Biosci*. 2016;4(10A):818–821.
- Robinson CH. cold adaptation in arctic and antarctic fungi. *New Phytologist*. 2001;151(2):341–353.
- Rodrigues JP, Paraguassú-Braga FH, et al. Evaluation of trehalose and sucrose as cryoprotectants for hematopoietic stem cells of umbilical cord blood. *Cryobiology*. 2008;56(2):144–51.
- Rogulska O, Petrenko Y, Petrenko A. DMSO-free cryopreservation of adipose-derived mesenchymal stromal cells: expansion medium affects post-thaw survival. *Cytotechnology*. 2017;69(2):265–276.
- Rols MP. (2017) Gene delivery by electroporation in vitro: Mechanisms. In: Miklavčič D. (eds) *Handbook of Electroporation*. Springer, Cham.
- Routledge C, Armitage WJ. Cryopreservation of cornea: A low cooling rate improves functional survival of endothelium after freezing and thawing. *Cryobiology*. 2003;46(3):277–83.
- Rusciano G, De Canditiis C, et al. Raman-microscopy investigation of vitrification-induced structural damages in mature bovine oocytes. *PLoS One*. 2017;12(5):e0177677.
- Russo MJ, Bayley H, Toner M. Reversible permeabilization of plasma membranes with an engineered switchable pore. *Nat Biotechnol*. 1997;15(3):278–82.
- Rutt T, Eskandari N, et al. Thermal expansion of substrate may affect adhesion of Chinese hamster fibroblasts to surfaces during freezing. *Cryobiology*. 2018. pii: S0011-2240(18)30249-9.
- Sarangi SK, Pramanik K. Cryopreservation in tissue engineering: challenges & prospects. *Adv Technol Enhancing Qual Life*. 2010.
- Sardesai NY, Weiner DB. Electroporation delivery of DNA vaccines: prospects for success. *Curr Opin Immunol*. 2011;23(3):421–9.
- Schawe JEK. A quantitative DSC analysis of the metastable phase behavior of the sucrose – water system. *Thermochimica Acta*. 2006;451(1-2):115–125.
- Seglen PO, Sætre F. Sequestration assays for mammalian autophagy. *Methods Enzymol*. 2009;452:63–83.
- Seki S, Mazur P. Stability of mouse oocytes at -80°C: the role of the recrystallization of intracellular ice. *Reproduction*. 2011;141(1):407–415.
- Sharp DMC, Picken A, et al. Amphipathic polymer-mediated uptake of trehalose for dimethyl sulfoxide-free human cell cryopreservation. *Cryobiology*. 2013;67(3):305–311.
- Shimazu T, Mori Y, et al. Serum- and xeno-free cryopreservation of human umbilical cord tissue as mesenchymal stromal cell source. *Cytotherapy*. 2015;17(5):593–600.
- Shiraga K, Adachi A, et al. Characterization of the hydrogen-bond network of water around sucrose and trehalose: Microwave and terahertz spectroscopic study. *J Chem Phys*.

- 2017;146(10):105102.
- Shirakashi R, Köstner CM, et al. Intracellular delivery of trehalose into mammalian cells by electroporation. *J Membr Biol*. 2002;189(1):45–54.
- Shu Z, Heimfeld S, et al. Hematopoietic SCT with cryopreserved grafts: adverse reactions after transplantation and cryoprotectant removal before infusion. *Bone Marrow Transplant*. 2014;49(4):469–76.
- Silber S. Ovarian tissue cryopreservation and transplantation : scientific implications. *J Assist Reprod Genet*. 2016;33(12):1595–1603.
- Solanki PK, Bischof JC, Rabin Y. Thermo-mechanical stress analysis of cryopreservation in cryobags and the potential benefit of nanowarming. *Cryobiology*. 2017;76:129–139.
- Solocinski J, Osgood Q, et al. Effect of trehalose as an additive to dimethyl sulfoxide solutions on ice formation, cellular viability, and metabolism. *Cryobiology*. 2017;75:134–143.
- Soltanizadeh N, Mirmoghtadaie L, et al. Solid-state protein-carbohydrate interactions and their application in the food industry. *Compr Rev Food Sci Food Saf*. 2014;13(5):860–870.
- Stańczyk M, Telega JJ. Thermal problems in biomechanics – a review. Part III. Cryosurgery, cryopreservation. *Acta Bioeng Biomech*. 2013;5(2):3–22.
- Steif PS, Palastro MC, et al. The effect of temperature gradients on stress development during cryopreservation via vitrification. *Cell Preserv Technol*. 2007;5(2):104–115.
- Stevenson DJ, Morgan C, et al. Cryopreservation of viable hepatocyte monolayers in cryoprotectant media with high serum content: metabolism of testosterone and kaempferol post-cryopreservation. *Cryobiology*. 2004;49(2):97–113.
- Stewart MP, Langer R, Jensen KF. Intracellular delivery by membrane disruption: Mechanisms, strategies, and concepts. *Chem Rev*. 2018;118(16):7409–7531.
- Stewart S, He X. Intracellular delivery of trehalose for cell banking. *Langmuir*. 2018.
- Stokich B, Osgood Q, et al. Cryopreservation of hepatocyte (HepG2) cell monolayers: Impact of trehalose. *Cryobiology*. 2014;69(2):281–90.
- Stott SL, Karlsson JOM. Visualization of intracellular ice formation using high-speed video cryomicroscopy. *Cryobiology*. 2009;58(1):84–95.
- Sydykov B, Oldenhof H, et al. Storage stability of liposomes stored at elevated subzero temperatures in DMSO/sucrose mixtures. *PLoS One*. 2018;13(7):e0199867.
- Tarkowski ŁP, Van den Ende W. Cold tolerance triggered by soluble sugars: a multifaceted countermeasure. *Front Plant Sci*. 2015;6:203.
- Tolleshaug H, Blomhoff R, et al. (1986) Receptor-mediated endocytosis of mannose-terminated glycoproteins in hepatocytes. In: Greten H., Windler E., Beisiegel U. (eds) Receptor-mediated uptake in the liver. Springer, Berlin, Heidelberg.
- Tolosa L, Bonora-Centelles A, et al. Influence of platelet lysate on the recovery and metabolic performance of cryopreserved human hepatocytes upon thawing. *Transplantation*. 2011;91(12):1340–6.
- Towhidi L, Firoozabadi SMP, et al. Lucifer Yellow uptake by CHO cells exposed to magnetic

- and electric pulses. *Radiol Oncol*. 2012;46(2):119–125.
- Trounson A, McDonald C. Review Stem cell therapies in clinical trials: progress and challenges. *Cell Stem Cell*. 2015;17(1):11–22.
- Umemura E, Yamada Y, Nakamura S. Viable cryopreserving tissue-engineered cell-biomaterial for cell banking therapy in an effective cryoprotectant. *Tissue Eng Part C Methods*. 2011;17(8):799–807.
- Vásquez-Rivera A, Oldenhof H, et al. Use of sucrose to diminish pore formation in freeze-dried heart valves. *Scientific Reports*. 2018;8(1):1–12.
- Vásquez-Rivera A, Oldenhof H, et al. Use of sucrose to diminish pore formation in freeze-dried heart valves. *Sci Rep*. 2018;8:12982.
- Wang C, Xiao R, et al. Evaluation of human platelet lysate and dimethyl sulfoxide as cryoprotectants for the cryopreservation of human adipose-derived stem cells. *Biochem Biophys Res Commun*. 2017;491(1):198–203.
- Wang S, Elliott GD. Synergistic development of biochips and cell preservation methodologies: a tale of converging technologies. *Curr Stem Cell Rep*. 2017;3(1):45–53.
- Wang X, Hua TC, et al. Metabolic activity and functional evaluation of cryopreserved dermal equivalent. *Cell Preservation Tech*. 2004;2(2):125–132.
- Wang Z, Ting-Wu Q. Review: vitreous cryopreservation of tissue-engineered compositions for tissue repair. *J Med Biol Eng*. 2012;33(2):125–132.
- Watts MJ, Linch DC. Optimisation and quality control of cell processing for autologous stem cell transplantation. *Br J Haematol*. 2016;175(5):771–783.
- Wen F, Magalhães R, et al. Vitreous cryopreservation of nanofibrous tissue-engineered constructs generated using mesenchymal stromal cells. *Tissue Eng Part C Methods*. 2009;15(1):105–14.
- Wu Y, Wen F, et al. Cryopreservation strategy for tissue engineering constructs consisting of human mesenchymal stem cells and hydrogel biomaterials. *Cryo Letters*. 2015;36(5):325–35.
- Xu X, Liu Y, Cui Z. Effects of cryopreservation on human mesenchymal stem cells attached to different substrates. *J Tissue Eng Regen Med*. 2014;8(8):664–72.
- Xu X, Liu Y, et al. Effects of osmotic and cold shock on adherent human mesenchymal stem cells during cryopreservation. *J Biotechnol*. 2012;162(2-3):224–31.
- Xu Y, Sun HJ, et al. Effects of freezing rates and cryoprotectant on thermal expansion of articular cartilage during freezing process. *Cryo Letters*. 2013;34(4):313–23.
- Yang G, Zhang A, Xu LX. Intracellular ice formation and growth in MCF-7 cancer cells. *Cryobiology*. 2011;63(1):38–45.
- Yang Y, Cheung HH, et al. New insights into the role of autophagy in ovarian cryopreservation by vitrification. *Biol Reprod*. 2016;94(6):137.
- Yokoyama A, Gelinsky M, et al. Biomimetic porous scaffolds with high elasticity made from mineralized collagen – An animal study. *J Biomed Mater Res B Appl Biomater*. 2005;75(2):464–72.

- Yong KW, Choi JR, Wan Safwani WKZ. Biobanking of human mesenchymal stem cells: future strategy to facilitate clinical applications. *Adv Exp Med Biol*. 2016;951:99–110.
- Yoon Y, Cho E, et al. Is trehalose an autophagic inducer? Unraveling the roles of non-reducing disaccharides on autophagic flux and alpha-synuclein aggregation. *Cell Death Dis*. 2017; 8(10): e3091.
- Younis A, Carnovale D, et al. Application of intra- and extracellular sugars and dimethylsulfoxide to human oocyte cryopreservation. *J Assist Reprod Genet*. 2009;26(6):341–5.
- Yu G, Li R, Hubel A. interfacial interactions of sucrose during cryopreservation detected by raman spectroscopy. *Langmuir* (2018).
- Yu G, Yap YR, et al. Characterizing intracellular ice formation of lymphoblasts using low-temperature raman spectroscopy. *Biophys J*. 2017;112(12):2653–2663.
- Yu J, Liu JH, et al. Freeze-drying of human red blood cells: influence of carbohydrates and their concentrations. *Cell Preserv Technol*. 2004;2(4):270–275.
- Yuan Y, Yang Y, et al. Efficient long-term cryopreservation of pluripotent stem cells at -80°C. *Sci Rep*. 2016;6:34476.
- Zaragotas D, Liolios NT, Anastassopoulos E. Supercooling, ice nucleation and crystal growth: A systematic study in plant samples. *Cryobiology*. 2016;72(3):239–43.
- Zatloukal K, Stumptner C, et al. Biobanks in personalized medicine. *Expert Rev Precis Med Drug Dev*. 2018;3(4):265–273.
- Zhang A, Cheng S, et al. Thermal stress study of two different artery cryopreservation methods. *Cryo Letters*. 2005;26(2):113–20.
- Zhang M, Oldenhof H, Sieme H. Combining endocytic and freezing-induced trehalose uptake for cryopreservation of mammalian cells. *Biotechnol Prog*. 2017;33(1):229–235.
- Zhang M, Oldenhof H, et al. Freezing-induced uptake of trehalose into mammalian cells facilitates cryopreservation. *Biochim Biophys Acta*. 2016;1858(6):1400–9.
- Zhang W, Rong J, et al. The encapsulation and intracellular delivery of trehalose using a thermally responsive nanocapsule. *Nanotechnology*. 2009;20(27):275101.
- Zhou X, Yuan J, et al. Loading trehalose into red blood cells by electroporation and its application in freeze-drying. *Cryo Letters*. 2010;31(2):147–56.
- Zhou XL, Zhu H, et al. Freeze-drying of human platelets: Influence of saccharide, freezing rate and cell concentration. *Cryo Letters*. 2007;28(3):187–96.
- Zhurova M, Woods EJ, Acker JP. Intracellular ice formation in confluent monolayers of human dental stem cells and membrane damage. *Cryobiology*. 2010;61(1):133–141.

Acknowledgments

I avail this opportunity to express my deep gratitude to Prof. Prof. h.c. Dr.-Ing. Birgit Glasmacher and Dr. Oleksandr Gryshkov for excellent supervision and guidance to successfully complete this work. I would like to extend special thanks to my co-supervisors Prof. Dr. rer. nat. Thomas Illig and Prof. Dr.-Ing. Stephan Kabelac for their dedicated co-supervision of my project and stimulating discussions during the co-supervisor meetings.

I am also very grateful to Dr. Gerald Dräger and the programme IP@Leibniz for funding my exchange scientific visits to Greece and Slovenia as well as the Minerva Foundation for supporting the exchange project with Israel. Never will I forget the time spent in mentioned countries and it has been my great pleasure working with Prof. Dr. Damijan Miklavčič (Hvala!), Prof. Elias Anastasopoulos (Ευχαριστώ!) and Prof. Ido Braslavsky (ברט, הודות!). I consider myself extremely lucky to work with our collaboration partners Prof. Dr. rer. nat. habil. Hermann Ehrlich, Prof. Dr. rer. nat. Michael Gelinsky and Prof. Alexander Petrenko. I am very thankful to them for continued constructive work together, writing joint manuscripts and their contribution to my scientific growth.

Very special thanks to the laboratory technicians Dr. rer. nat. Katerina Zelena and Mrs. Julia Guewa for their extensive assistance and support at various phases of my experimental work. My special thanks to the former REBIRTH students Dr. Lothar Lauterböck and Dr. Bulat Sydykov for introducing me to diverse cryobiological methods, fruitful discussions, inspiration and constant support and encouragement. I would also like to thank the visiting scientist and my dear friend Dr. Dmytro Tarusin from the Institute for Problems of Cryobiology and Cryomedicine, Ukraine, for his dedication and contribution to joint scientific work and having a lot of fun.

And it goes without saying, that I am indebted to my parents Mutsenko Kateryna and Victor, my wife Anastasiia who had always been very supportive and caring, and special thanks goes to the new generation of scientists - my son Myroslav for his moral support with his smile. This dissertation work is devoted to my family and church community 'New Generation'.

List of own publications

Peer-reviewed publications

Mutsenko, V. V., Gryshkov, O., Lauterboeck, L., Rogulska, O., Tarusin, D.N., Bazhenov, V. V., Schütz, K., Brüggemeier, S., Gossila, E., Akkineni, A.R., Meißner, H., Lode, A., Meshke, S., Fromont, J., Stelling, A.L., Tabachnik, K.R., Gelinsky, M., Nikulin, S., Rodin, S., Tonevitsky, A.G., Petrenko, A.Y., Glasmacher, B., Schupp, P.J., Ehrlich, H., 2017. Novel chitin scaffolds derived from marine sponge *Ianthella basta* for tissue engineering approaches based on human mesenchymal stromal cells: Biocompatibility and cryopreservation. *Int. J. Biol. Macromol.* 104B, 1955–1965.

Mutsenko, V.V., Bazhenov, V.V., Rogulska, O., Tarusin, D.N., Schütz, K., Brüggemeier, S., Gossila, E., Akkineni, A.R., Meißner, H., Lode, A., Meschke, S., Ehrlich, A., Petović, S., Martinović, R., Djurović, M., Stelling, A.L., Nikulin, S., Rodin, S., Tonevitsky, A., Gelinsky, M., Petrenko, A.Y., Glasmacher, B., Ehrlich, H., 2017. 3D chitinous scaffolds derived from cultivated marine demosponge *Aplysina aerophoba* for tissue engineering approaches based on human mesenchymal stromal cells. *Int. J. Biol. Macromol.* 104B, 1966–1974.

Prykhodko M.V., Tymkovych M.Y., Avrunin O.G., **Mutsenko V.V.**, Gryshkov O., Glasmacher B. Image processing for automated microscopic analysis of ice recrystallization process during isothermal annealing. *Int J Bioelectromagnetism* 2018;20(1): 72-75.

Mutsenko, V., Barlič, A., Pezić, T., Dermol-Černe, J., Sydykov, B., Wolkers, W.F., Katkov, I., Miklavčič, D., Glasmacher, B., Gryshkov, O. Me₂SO- and serum-free cryopreservation of mesenchymal stromal cells using electroporation of sugars. *Cryobiology (in preparation)*.

Mutsenko, V., Tarusin, D., Sydykov, B., Beck, A., Dipresa, D., Lode, A., Khassawna, T. El., Petrenko, A., Korossis, S., Wolkers, W.F., Gelinsky, M., Glasmacher, B., Gryshkov, O. ‘In air’ cryopreservation of mesenchymal stromal cells on 3D collagen-hydroxyapatite-scaffolds. *Cryobiology (in preparation)*.

Book chapter

Mutsenko, V., Gryshkov, O., Rogulska, O., Lode, A., Petrenko, A. Yu., Gelinsky, M., Glasmacher, B. and Ehrlich, H. Chitinous Scaffolds from Marine Sponges for Tissue Engineering. In: A.H. Choi, B. Ben-Nissan (eds.) (2018). Marine-Derived Biomaterials for Tissue Engineering Applications, Springer Series in Biomaterials Science and Engineering (SSBSE) (submitted).

Abstracts

Mutsenko, V.V., Gryshkov, O.P., Petrenko, Yu.A., Grischuk, V.P., Kotlyarov, A., Schupp, P., Ehrlich, H., Glasmacher, B., Petrenko, A.Yu. The impact of sucrose pretreatment on survival of mesenchymal stromal cells, cryopreserved in suspension and adherent state. Cryobiology 2016;73(3): 402.

Mutsenko, V.V., Gryshkov, O., Knaack, S., Gelinsky, M., Petrenko, A.Yu., Glasmacher, B. Cryopreservation of biomimetic bone matrix with non-human primate mesenchymal stromal cells. Cryobiology 2016;73(3): 433.

Mutsenko, V., Barlič, A., Pezić, T., Dermol-Černe, J., Sydykov, B., Gryshkov, O., Wolkers, W.F., Miklavčič, D., Glasmacher, B. Me₂SO- and serum-free cryopreservation of mesenchymal stromal cells using electroporation of sugars. Cryobiology – **in press**.

Mutsenko, V., Gryshkov, O., Sydykov, B., Beck, A., Dipresa, D., Lode, A., Khassawna, T. El, Petrenko, A., Korossis, S., Wolkers, W.F., Gelinsky, M., Glasmacher, B. ‘In air’ cryopreservation of mesenchymal stromal cells on 3D collagen-hydroxyapatite-scaffolds. Cryobiology – **in press**.

Mutsenko, V., Tarusin, D., Sydykov, B., Zaragotas, D., Simaioforidou, A., Rozanski, C., Gryshkov, O., Wolkers, W.F., Braslavsky, I., Anastassopoulos, E., Glasmacher, B. Study of natural cryoprotective agents for cryopreservation of 3D tissue-engineered scaffolds. Cryobiology – **in press**.

Gryshkov, O., **Mutsenko, V.**, Tymkovych, M., Tarusin, D., Sirotinskaya, V., Braslavsky, I., Avrunin, O., Glasmacher, B. Advances in cryopreservation of alginate-encapsulated stem cells and analysis of cryopreservation outcome. Cryobiology – **in press**.

Mutsenko, V., Gryshkov, O., Glasmacher, B. Effective solutions for cryostorage of specific tissue types. Annual conference of the German Society of Refrigeration, 22-24 November 2017, Bremen, Germany.

Mutsenko, V., Gryshkov, O., Glasmacher, B. Cryopreservation of amnion-derived multipotent stem cells within alginate- and collagen-based polymeric matrices. SLTB Science Meeting 2017 Cambridge, 19-20th September, United Kingdom.

Mutsenko, V., Tarusin, D., Zaragotas, D., Simaioforidou, A., Rozanski, C., Sydykov, B., Ivnev, D., Gryshkov, O., Anastassopoulos, E., Glasmacher, B. Application of infrared video thermography for monitoring of freezing/thawing events within 3D collagen-hydroxyapatite scaffolds. SLTB 2018, Prague, September 06-07, Czech Republic.

Curriculum Vitae

Name	Mutsenko Vitalii
Date of Birth	28.12.1982
Place of Birth	Adamivka, Ukraine
Marital Status	Married
Nationality	Ukrainian

Education

2010-2011	M.Sc. Biochemistry V.N. Karazin Kharkiv National University, Kharkiv, Ukraine
2006-2010	B.Sc. Biology V.N. Karazin Kharkiv National University, Kharkiv, Ukraine
1989-1999	Secondary education Adamivka secondary general school, Adamivka, Ukraine

Research experience

2016-present	PhD Program ‘Regenerative Sciences’ Leibniz University Hannover, Hannover Medical School, Hannover, Germany
2012-2015	Research Assistant in Cryobiology Institute for Problems of Cryobiology and Cryomedicine, Kharkiv, Ukraine
2011-2012	Research Fellow Institute of Pharmacology, University of Bern, Bern, Switzerland

Awards

2018	Finalist of the PhD Thesis Presentation Contest The Annual Meeting of the German-Ukrainian Academic Society, Dresden, Germany
-------------	---

IP@Leibniz Scholarship Awardee

Research stays in the Laboratory of Biocybernetics, Faculty of Electrical Engineering, University of Ljubljana, Slovenia and in the Department of Agricultural Engineering Technologists, Technological Educational Institute of Thessaly, Larissa, Greece

Minerva short-Term Research Grant

Research stay in the Institute of Biochemistry, Food Science and Nutrition, Robert H. Smith Faculty of Agriculture, Food and Environment, The Hebrew University of Jerusalem, Rehovot, Israel

2018**John K. Critser Student Travel Award**

The 55th Annual Meeting of the Society for Cryobiology, Madrid, Spain

2016**Student Travel Award**

The 53rd Annual Meeting of the Society for Cryobiology, Ottawa, Canada

Presentations**Oral****2018**

V. Mutsenko, O. Gryshkov, B. Sydykov, A. Beck, D. Dipresa, A. Lode, T. El Khassawna, A. Petrenko, S. Korossis, W.F. Wolkers, M. Gelinsky, B. Glasmacher. 'In air' cryopreservation of mesenchymal stromal cells on 3D collagen-hydroxyapatite-scaffolds. The 55th Annual Meeting of the Society for Cryobiology – CRYO 2018, 10-13 July 2018, Madrid, Spain

V. Mutsenko, A. Barlič, T. Pezić, J. Dermol-Černe, B. Sydykov, O. Gryshkov, W.F. Wolkers, D. Miklavčič, B. Glasmacher. Me₂SO- and serum-free cryopreservation of mesenchymal stromal cells using electroporation of sugars. The 55th Annual Meeting of the Society for Cryobiology – CRYO 2018, 10-13 July 2018, Madrid, Spain

2016

V.V. Mutsenko, O. Gryshkov, S. Knaack, M. Gelinsky, A.Yu. Petrenko, B. Cryosensitivity of tissue-engineered collagen constructs based on multipotent stromal cells. SLTB Meeting 2016, 07 September 2016, Dresden, Germany

Poster**2016**

V.V. Mutsenko, O. Gryshkov, S. Knaack, M. Gelinsky, A.Yu. Petrenko, B. Glasmacher. Cryopreservation of biomimetic bone matrix with non-human primate mesenchymal stromal cells. The 53rd Annual Meeting of the Society for Cryobiology – CRYO 2016, 23-27 July 2016, Ottawa, Canada

2018

V. Mutsenko, D. Tarusin, B. Sydykov, D. Zaragotas, A. Simaioforidou, C. Rozanski, O. Gryshkov, W.F. Wolkers, I. Braslavsky, E. Anastassopoulos, B. Glasmacher. Study of natural cryoprotective agents for cryopreservation of 3D tissue-engineered scaffolds. The 55th Annual Meeting of the Society for Cryobiology – CRYO 2018, 10-13 July 2018, Madrid, Spain

Languages

Ukrainian

Russian

English

German

Statement of Contribution

I, Vitalii Mutsenko, hereby confirm that I personally have done all the measurements and data analysis, if not stated otherwise, and wrote the thesis.

The contributions included in this dissertation work are indicated below.

1) Co-supervision together with Dr. Oleksandr Gryshkov:

2 thesis-relevant exchange projects funded by the programme IP@Leibniz (Dr. Dmytro Tarusin from the Institute of Cryobiology and Cryomedicine of the National Academy of Sciences of Ukraine, Kharkiv).

Relevant experiments: preparation of collagen-hydroxyapatite scaffolds, Resazurin reduction assay, cell volume measurements, Lucifer Yellow uptake in adherent cells.

the student project by Tobias Pfister with the title: ‘Validation of plate electrodes for electroporation of cell-seeded electrospun fiber mats’ (pictures on electroporation included in the ‘Outlook’ of my thesis).

2) Western blotting was performed in the Institute of Cell Biochemistry, Medical School Hannover under the supervision of Alexey Kotlyarov, MD, Natalia Ronkina, PhD and laboratory assistant Juri Lafera.

3) Collagen-hydroxyapatite scaffolds were prepared in the Centre for translational bone, joint and soft tissue research, the Medical Faculty Carl Gustav Carus of Dresden University of Technology by the technical assistant Ortrud Zieschang within the established collaboration with Prof. Michael Gelinsky and Dr. rer. nat. Anja Lode.

4) SEM, confocal and Raman microscopy as well as experiments on ‘in air’ cryopreservation of coaxial alginate microspheres were performed under the supervision of Dr. Oleksandr Gryshkov.

5) FTIR and DSC measurements as well as data analysis were performed by me with the help of PhD Student Andrés Vásquez and Dr. Bulat Sydykov, respectively.

6) Histological sectioning and staining of scaffolds was performed in Niedersächsisches Zentrum für Biomedizintechnik, Implantatforschung und Entwicklung (NIFE) with the help of laboratory assistant Annemarie Beck, AG Rode.

7) Mercury intrusion porosimetry has been performed by Ramon Cabisco i Martinoli, Research Associate at the Institute for Particle Technology, TU Braunschweig (only authorized personnel was allowed to use the device).

8) Compression test has been performed under the supervision of Postdoctoral Research Fellow Dr. Daniele Dipresa, PhD, in NIFE, AG Korrosion.

9) All work on electroporation was performed in the Laboratory for Biocybernetics at the Faculty of Electrical Engineering of the University of Ljubljana in the framework of exchange visit funded by IP@Leibniz:

i) Prof. Damijan Miklavčič participated in the development of general concept of the electroporation studies;

ii) Assistance with FACS – junior researcher Tamara Pezić;

iii) Assistance with fluorescent microscopy during electroporation – research assistant Dr. Janja Dermol-Černe;

iiii) Help in cell permeabilization and recovery assays – research assistants Duša Hodžić and Lea Vukanović.

10) Dr. rer. nat. Lothar Lauterboeck (Postdoctoral fellow at the Cardiovascular Center of Excellence, Louisiana State University Health Sciences Center New Orleans, USA) was involved in the revising of the thesis.

Declaration

Herewith, I confirm that I have written the present PhD thesis myself and independently, in compliance with 'the policy of Hannover Medical School on the safeguarding of good scientific practice and procedural rules for dealing with scientific misconduct', and that I have not submitted it or parts thereof at any other university worldwide.

Herewith, I agree that MHH can check my thesis by plagiarism detection software as well as randomly check the primary data. I am aware that in case of suspicion, ombudsman proceedings according to § 9 of MHH's 'Policy of Hannover Medical School on the safeguarding of good scientific practice and procedural rules for dealing with scientific misconduct' will be initiated. During such proceedings, the PhD process is paused.

Hannover, 16 April 2019

A handwritten signature in blue ink is written over a horizontal line. The signature is stylized and appears to be 'Vitalii Mutsenko'.